REVIEW AND TEST OF PARAMETERIZATIONS

OF ATMOSPHERIC RADIATION

A Technical Report of Task 17:

Measuring and Modelling Spectral Radiation
Affecting Solar Systems and Buildings

December 1994

THE INTERNATIONAL ENERGY AGENCY
SOLAR HEATING AND COOLING PROGRAMME

International Energy Agency

The International Energy Agency, headquartered in Paris, was formed in November 1974 as an autonomous body within the framework of the Organization for Economic Cooperation and Development to establish cooperation in the area of energy policy. Twenty-one countries are presently members, with the Commission of the European Union participating under a special arrangement.

Collaboration in the research, development and demonstration of new energy technologies to help reduce dependence on oil and to increase long-term energy security has been an important part of the Agency's programme. The IEA R&D activities are headed by the Committee on Research and Development (CRD) which is supported by a small Secretariat staff. In addition, four Working Parties (in Conservation, Fossil Fuels, Renewable Energy and Fusion) are charged with monitoring the various collaborative energy Agreements, identifying new areas for cooperation and advising the CRD on policy matters.

Solar Heating and Cooling Programme

One of the first collaborative R&D agreements was the IEA Solar Heating and Cooling Programme which was initiated in 1977 to conduct joint projects in active and passive solar technologies, primarily for building applications. The twenty members of the Programme are:

Australia	France	Spain
Austria	Germany	Sweden
Belgium	Italy	Switzerland
Canada	Japan	Turkey
Denmark	Netherlands	United Kingdom
European Union	New Zealand	United States
Finland	Norway	

A total of twenty-one projects or "Tasks" have been undertaken since the beginning of the Programme. The overall programme is managed by an Executive Committee composed of one representative from each of the member countries, while the leadership and management of the individual Tasks is the responsibility of the Operating Agents. These Tasks and their respective Operating Agents are:

*Task 1:	Investigation of the Performance of Solar Heating and Cooling Systems - Denmark
*Task 2:	Coordination of Research and Development on Solar Heating and Cooling - Japan
*Task 3:	Performance Testing of Solar Collectors - United Kingdom
*Task 4:	Development of an Insolation Handbook and Instrument Package - United States
*Task 5:	Use of Existing Meteorological Information for Solar Energy Applications - Sweden
*Task 6:	Solar Heating, Cooling, and Hot Water Systems Using Evacuated Collectors - United States
*Task 7:	Central Solar Heating Plants with Seasonal Storage - Sweden
*Task 8:	Passive and Hybrid Solar Low Energy Buildings - United States
*Task 9:	Solar Radiation and Pyranometry Studies - Germany
*Task 10:	Material Research and Testing - Japan
*Task 11:	Passive and Hybrid Solar Commercial Buildings - Switzerland
Task 12:	Building Energy Analysis and Design Tools for Solar Applications - United States
Task 13:	Advanced Solar Low Energy Buildings - Norway
Task 14:	Advanced Active Solar Systems - Canada
Task 16:	Photovoltaics in Buildings - Germany
Task 17:	Measuring and Modelling Spectral Radiation - Germany
Task 18:	Advanced Glazing and Associated Materials - United Kingdom
Task 19:	Solar Air Systems - Switzerland
Task 20:	Solar Energy in Building Renovation - Sweden
Task 21:	Solar Daylighting in Buildings - Denmark

*Completed Task

Report No.IEA-SHCP-17F-2

REVIEW AND TEST OF PARAMETERIZATIONS OF ATMOSPHERIC RADIATION

Jan Asle Olseth[1]

Arvid Skartveit

Geophysical Institute, University of Bergen

Allégt. 70, N-5007 Bergen

Norway

Gerhard Czeplak

Deutscher Wetterdienst

Meteorologisches Observatorium Hamburg

Frahmredder 95, D-22393 Hamburg

Germany

Matthias Rommel

Fraunhofer-Institut für Solare Energiesysteme

Oltmannstrasse 5, D-79100 Freiburg

Germany

[1] Subtask leader. Also affiliated with The Norwegian Meteorological Institute.

This report documents work performed within the IEA Solar Heating and Cooling Programme
Task 17: Measuring and Modelling Spectral Radiation Affecting Solar Systems and Buildings
Subtask F: Broad-band Infrared Radiation Data Acquisition and Analysis

Additional Copies may be ordered from:

Det norske meteorologiske institutt
Pb. 43 Blindern
0313 Oslo
Norway Cost: 150 NKr

Distribution category: Unrestricted

ABSTRACT

The specific objectives of IEA-SHCP Subtask 17F were to measure, evaluate and analyze infrared (longwave atmospheric) radiation data in order to increase the available amount of such data required for design and analysis of solar systems and buildings.

The present technical report documents the data analysis performed in the Subtask. It gives a review of models for the estimation of longwave atmospheric radiation from available meteorological data, ranging from simple models using easily available surface data as input, to sophisticated models for the estimation of spectral longwave radiation from detailed temperature/humidity profiles. The simple models for broad-band and spectral longwave radiation on horizontal surfaces are tested against measured data and against a sophisticated spectral model. By both methods, the same models were identified as best performing. Recommendations on the applicability of the simple models are given.

CONTENTS

EXECUTIVE SUMMARY

The objective of IEA SHCP Task 17 was to improve the quantity and quality of spectral radiation data, both broad-band and narrow-band, needed for design and analysis of solar systems and buildings. While Subtasks 17A, C, and E were engaged in radiometry and solar radiation data acquisition, analysis and modelling, the specific objectives of Subtask F were to measure, evaluate and analyze infrared (longwave atmospheric) radiation data (3 - 100μm) in order to increase the available amount of such data. These data are important for, e.g., solar collector performances, freezing problems in liquid collectors, the heat transfer between buildings and the sky, and passive cooling systems. Experts from Canada, France, Germany, Norway, Sweden, and USA participated in Subtask 17F.

There were two primary components to Subtask 17F. The first involved the compilation of a data base of more than 90 site years of longwave atmospheric radiation and related meteorological data from 17 European and North-American stations (Technical Document No.IEA-SHCP-17F-1 "Description of the Atmospheric Radiation Data Base", G. Czeplak, DWD, Hamburg, Germany). The second involved the review and testing of models for estimating longwave atmospheric radiation data.

As measured data are scarce, longwave atmospheric radiation data often have to be estimated from available meteorological data, and a large number of such models are found in the literature. In order to guide the users of such models, Subtask F performed the model evaluation described in this report:

- A review of models for estimating longwave atmospheric radiation from easily available meteorological data,
- A test of simple models (both against measured data and against a more sophisticated spectral model) to find out which models perform best.

A review of more than 30 models for the estimation of longwave atmospheric radiation from available meteorological data, both under cloudless and cloudy skies, is given in this report. The models vary from simple models for the estimation of longwave atmospheric radiation from easily available surface data to sophisticated models for the estimation of spectral longwave radiation from detailed temperature/humidity profiles. Only simple models (using easily available surface data) for broad-band and spectral longwave radiation on horizontal surfaces were tested and reported here. These models express the atmospheric radiation as a function of easily obtainable meteorological parameters, and are therefore called parameterizations in the meteorological literature. Such parameterizations are most often derived from observations taken in climates covering a limited range of temperature, humidity, etc. A profile-based

model like MODTRAN may, however, be used to evaluate formulae, or as a guide for designing formulae which may be used outside the climatic range they were developed for, with minimum probability of significant error. The MODTRAN model is a moderate resolution (2 cm^{-1}) version of LOWTRAN7 (low resolution transmission model, version 7). It calculates spectral radiances from vertical profiles (up to 100 km) of temperature and atmospheric composition.

MODTRAN predictions nicely fit the average of 38 profile-based models, and the degree of consistency between such models is high. Indirect evidence, based on data from 15 European and North American stations, indicate that average observed irradiances and MODTRAN predictions agree within approximately 5 Wm^{-2} under cloudless sky, with a slight tendency of observations exceeding MODTRAN predictions.

Twenty-three simple formulae for estimating cloudless broad-band longwave atmospheric irradiance on horizontal surfaces were tested against data from the 15 stations, and against MODTRAN predictions. These tests strongly suggest that four of the 23 simple formulae are particularly suitable in the case of "normally" stratified boundary layers: Over a wide range of temperatures, the **Swinbank** (1963) and **Czeplak & Kasten** (1987) formulae, which express the emittance ϵ_0 as a quadratic function of dry bulb temperature, effectively reflect the radiation physics of cloudless and not too dry atmospheres. Over a wide range of both temperature and humidity, the **Berdahl & Fromberg** (1982) and **Frank & Püntener** (1986) formulae, which express the emittance ϵ_0 as a linear function of dew point temperature, are even more appropriate than the Swinbank and Czeplak & Kasten formulae. For "abnormally" stratified atmospheres, a correction to empirical surface-based formulae is proposed. This correction is derived from MODTRAN and requires summary information on the boundary layer temperature stratification. Alternatively, a table of empirical correction factors is given, based on hour, season, and geographical location.

Clouds increase the atmospheric emittance ϵ beyond its cloudless value ϵ_0, but at most, slightly beyond unity. Eight of the 23 cloudless models above were supplied with a cloud modification algorithm, and tests of these algorithms suggest that the emittance increase is most adequately phrased as $(\epsilon - \epsilon_0)/(1 - \epsilon_0)$, i.e., as the fractional reduction of the longwave radiation loss from a horizontal surface at ambient temperature (**Martin & Berdahl** 1984). This fraction is governed by fractional cloud cover, cloud emittance, and the surface minus cloud base temperature difference. Given these parameters, MODTRAN runs indicate that temperature, humidity and cloud base height are irrelevant.

In addition, two simple spectral models were tested against spectral irradiances derived from observed spectral zenith radiances in the Negev desert, Israel. It is shown that the observed data conform well with the model of **Berger** (1988) and with MODTRAN.

CHAPTER 1

DESCRIPTION AND PURPOSE OF THE REPORT

1.1 BRIEF DESCRIPTION OF IEA-SHCP TASK 17: MEASURING AND MODELLING SPECTRAL RADIATION AFFECTING SOLAR SYSTEMS AND BUILDINGS

The objective of IEA-SHCP Task 17 was to improve the quantity and quality of spectral radiation data, both broad-band and narrow-band, needed for design and analysis of solar systems and buildings. The objective was accomplished by co-ordinated international co-operation contributing the knowledge and experience of the national experts and making use of existing national facilities and information sources. The Task focused on three types of spectral radiation data:

- Narrow-band spectral radiation data for applications to solar and building materials
- Broad-band spectral radiation data in the visible range (that is, visible light) for applications to natural illumination in buildings, and
- Broad-band spectral radiation data in the infrared range (that is, longwave radiation) for applications to the energy balance of solar systems and buildings

Overall co-ordination of the Task was with the Operating Agent, dr Fritz Kasten (Germany). Research and development activities were carried out in the framework of the following 4 Subtasks, each coordinated by a lead country; in parenthesis:

- Subtask A: Narrow-band Spectral and Broad-band Infrared Radiometry (Germany)
- Subtask C: Narrow-band Spectral Radiation Data Acquisition, Analysis and Modelling (Germany)
- Subtask E: Broad-band Visible Radiation Data Acquisition and Analysis (USA)
- Subtask F: Broad-band Infrared Radiation Data Acquisition and Analysis (Norway)

Subtask A engaged in the comparison, characterization, and standardized calibration of narrow-band spectral and broad-band infrared radiometers in order to improve the quality of spectral radiation data measurements. The other three Subtasks focused on specific measurements, evaluations, and analyses of spectral radiation in different wavelength ranges in order to increase the available amount of such data.

1.2 OBJECTIVES OF IEA-SHCP SUBTASK 17F

Within the solar energy community, data of longwave atmospheric radiation are important for, e.g., solar collector performances, freezing problems in liquid collectors, the heat transfer between buildings and the sky, and passive cooling systems. As measured data are scarce, longwave atmospheric radiation data often

have to be estimated from available meteorological data, and a large number of such models are found in the literature. The specific objectives of Subtask F were to measure, evaluate and analyze broad-band infrared radiation data in order to increase the available amount of such data required for design and analysis of solar systems and buildings. Thus, the work in Subtask F can be outlined as:

- measurement, evaluation and compilation of longwave atmospheric radiation data and related data from various stations in the participating countries,
- undertaking a review of simple models for estimating longwave atmospheric radiation from easily available meteorological data,
- testing the simple models (both against measured data and against a more sophisticated spectral model),
- giving recommendations to the solar energy community on the suitability of the simple models.

1.3 THE STRUCTURE OF THE REPORT

In Chapter 2 of this report, a review of models for the estimation of longwave atmospheric radiation from available meteorological data, both under cloudless and cloudy skies, is given. The models vary from simple models for the estimation of longwave atmospheric radiation from easily available surface data (e.g. air temperature, water vapor pressure, dewpoint temperature, relative humidity) to sophisticated models for the estimation of spectral longwave radiation from detailed temperature/humidity profiles. Only simple models (using easily available surface data) for both broad-band and spectral longwave radiation on horizontal surfaces are tested in this report.

In Chapters 3 and 4, the models for longwave atmospheric radiation on horizontal surfaces are tested against a data base of measured data from 15 European and North-American stations, and against output from a sophisticated profile-based spectral model, MODTRAN, respectively. The data base of 15 stations, representing different climates, is described in the Technical Document No.IEA-SHCP-17F-1 "Description of the Atmospheric Radiation Data Base", by G. Czeplak. The input data for the spectral model, MODTRAN, are profiles from 6 standard atmospheres, ranging from the hot/humid Tropical atmosphere to the cold/dry Sub-Arctic Winter atmosphere, from several modifications of these atmospheres, and even from several observed profiles, thus representing a wide variety of climates. Some of the simple models consist of a clear sky model, in combination with modifications for cloudy conditions. These clear sky models may of course be used independently on their own, and are therefore also tested in Chapters 3 and 4. Besides, each cloud modification, in combination with its companion clear sky model, can be used to estimate the irradiance under cloud covers ranging from almost clear (1/8 cloud amount) to completely overcast (8/8 cloud amount). In Chapter 3 the cloud modifications are tested against data for this entire

range of cloud amounts. As MODTRAN only estimates irradiances under overcast sky, the cloud modifications are tested against MODTRAN only under such conditions (Chapter 4).

The review of models (Chapter 2) also contains simple models for the estimation of spectral longwave radiation. In Chapter 5 these models are tested against data from Israel, while these data in turn are compared to spectral output from MODTRAN.

In each of the Chapters 3, 4, and 5 conclusions are drawn. In the Executive Summary, the results are summarized, and recommendations are given on which simple models should be used to estimate longwave atmospheric radiation.

1.4 PARTICIPATING INSTITUTIONS/EXPERTS AND THEIR SPONSORS

Of the eight institutions participating in Subtask F, four were involved in both data acquisition and data analysis work, while the remaining four were only involved in the data acquisition part. The institutions, their supporting agencies and the participating experts are listed below:

AES : **Atmospheric Environment Service**, Downsview, Ontario, Canada, with **Bruce McArthur** as expert has provided the Subtask with data from Canada. The participation of AES was supported by Environment Canada.

DNMI : **Det norske meteorologiske institutt**, Bergen/Oslo, Norway, with **Jan Asle Olseth** and **Bjørn Aune** as experts has taken part in both data acquisition and analysis work. The participation of DNMI was supported under grant no. EK 28217 by the Norwegian Council of Scientific and Industrial Research.

DWD : **Deutscher Wetterdienst**, Meteorologisches Observatorium Hamburg, Germany, with **Gerhard Czeplak** as expert has taken part in both data acquisition and analysis work. DWD was responsible for the archiving of longwave radiation and related data. The participation of DWD was supported by the German Federal Ministry for Research and Technology (BMFT) through Forschungzentrum Jülich, Projektträger Biologie, Energie, Ökologie (FZ Jülich PBO) under grant no. 0328543C.

GIB : **Geofysisk institutt**, Universitetet i Bergen, Norway with **Arvid Skartveit** as expert has taken part in both data acquisition and analysis work. The participation of GIB was supported under grant no. EK 28217 by the Norwegian Council of Scientific and Industrial Research.

ISE : **Fraunhofer-Institut für Solare Energiesysteme**, Freiburg, Germany, with **Matthias Rommel** as expert has taken part in the data analysis work, and has besides provided the Subtask with spectral data from Israel. The participation of ISE was supported by the German Federal Ministry for Research and Technology (BMFT) under contract no. 0329294A.

METEO : **METEO France**, Centre radiométrique, Carpentras, France, with **Jean Oliviéri** as expert has provided the Subtask with data from Carpentras.

SMHI : **Sveriges meteorologiska og hydrologiska institut**, Norrköping, Sweden, with **Lars Dahlgren** as expert has provided the Subtask with data from Sweden. The participation of SMHI was supported by the Swedish Council for Building Research under contract no. 910661-8.

SUNYA : **State University of New York, Albany**, N.Y., USA, with **Richard Perez** as expert has provided the Subtask with data from Albany. The participation of SUNYA was supported by the US Department of Energy via the National Renewable Energy Laboratory (NREL) under contract no. AE-2-12202-1.

CHAPTER 2

REVIEW OF PARAMETERIZATIONS OF LONGWAVE ATMOSPHERIC RADIATION

Jan Asle Olseth[1] and Arvid Skartveit

Geophysical Institute, University of Bergen,
Allégt. 70, N-5007 Bergen, NORWAY

[1] Also at The Norwegian Meteorological Institute

2.1 INTRODUCTION

Within the solar energy community there is a need for data of longwave atmospheric radiation. As measured data are scarce, the data often have to be estimated from available meteorological data. A large number of models for the estimation of longwave atmospheric radiation are found in the literature, and in the present Chapter a list of such models is presented. The input data requirements range from surface temperature and some cloud cover information for the most "user-friendly" models to data derived from radiosondes or from satellites for other models. The output data range in complexity from irradiance on a horizontal surface over the entire longwave spectrum to output data with spectral and/or angular resolution. In the present report only simple models for broad-band and spectral longwave radiation on horizontal surfaces are tested.

2.2 MODELS FOR ATMOSPHERIC IRRADIANCE BASED ON GROUND DATA

2.2.1 Horizontal surfaces

On such models there exist useful review articles with comparisons of some of the models, for instance Idso (1974), Exell (1978), Arnfield (1979), Pissimanis and Notaridou (1981), Kasten et al (1983), Llebot and Jorge (1984), Schmetz (1984), and Mathis (1991).

To obtain a unified presentation, and to avoid confusion with respect to units and decadic prefixes, we express the parameterization formulae as relations between dimensionless numbers. Thus, rather than presenting downwelling irradiance ϕ at the horizontal surface, we rephrase the original formula to yield atmospheric emittance ϵ:

$$\epsilon = \epsilon\left(\frac{T_s}{T_*}, \frac{e_s}{e_*}, \ldots\right) = \frac{\phi}{\sigma\, T_s^4} \quad , \tag{2.1}$$

in terms of scaled surface air temperature (T_s/T_*), scaled surface water vapor pressure (e_s/e_*), etc. This dimensionless form is chosen even though some of the asterix-indexed constants get peculiar values (for example: in eqns. (2.19) we have the identity $0.179 e_s^{1/7} = (e_s/170\ 000)^{1/7}$). The nomenclature is given in Appendix A, while in Appendix B the formulae are listed in a mathematically equivalent format, namely that in which they were originally given.

The models can be divided in two groups, viz. models for cloudless skies only and models for both cloudless and cloudy skies.

2.2.1.1 Cloudless sky

The mixing ratios prevailing in the lower atmosphere are so large that the intensities of water vapor and carbon dioxide absorption bands effectively produce full black-body emission outside the atmospheric window. The air temperature near the ground is thus fairly representative for the shallow, a few hundred meters thick atmospheric layer which yields the major part of the downwelling longwave radiation at the surface. Moreover, there is a high correlation between surface air temperature and surface water vapor concentration. The following models take advantage of these facts, and express the cloudless atmospheric emittance ϵ_0 in terms of surface air temperature T_s only. This implies that even the irradiance ϕ_0 ($= \epsilon_0 \sigma T_s^4$) is a function of air temperature only, and these formulae are consequently named temperature-dependent formulae in the following chapters.

Swinbank (1963):

$$\epsilon_0 = \left(\frac{T_s}{T_*}\right)^2 \quad ; \quad T_* = 326.8K \quad . \tag{2.2}$$

Schieldrup Paulsen (1967):

$$\epsilon_0 = 0.895 - \frac{\phi_*}{\sigma T_s^4} \quad ; \quad \phi_* = 29.3 \ Wm^{-2} \quad . \tag{2.3}$$

Idso and Jackson (1969):

$$\epsilon_0 = 1 - 0.261 \exp\left[-\left(\frac{t_s}{t_*}\right)^2\right] \quad ; \quad t_* = 35.9°C \quad . \tag{2.4}$$

Unsworth and Monteith (1975):

$$\epsilon_0 = 1.06 - \frac{\phi_*}{\sigma T_s^4} \quad ; \quad \phi_* = 119 \ Wm^{-2} \quad . \tag{2.5}$$

Cole (1979):

$$\epsilon_0 = \frac{\phi_*}{\sigma T_s^4}\left(1+\frac{t_s}{t_*}\right) \quad ; \quad \phi_* = 222 \ Wm^{-2} \ , \ t_* = 44.9°C \quad . \tag{2.6}$$

Llebot and Jorge (1984):

$$\epsilon_0 = 1 - 0.25 \frac{\left(\frac{t_s}{t_{1*}}\right)^2 + 1}{\left(\frac{t_s}{t_{2*}}\right)^8 + 1} \quad ; \quad t_{1*} = 100°C \; , \; t_{2*} = 33.3°C \quad . \tag{2.7}$$

Czeplak and Kasten (1987):

$$\epsilon_0 = \left(\frac{T_s}{T_*}\right)^2 \quad ; \quad T_* = 317.8K \quad . \tag{2.8}$$

Since water vapor is the major emitter of longwave radiation in the cloudless atmosphere, several cloudless sky models include explicit information on humidity (water vapor pressure e_s, dewpoint temperature T_{ds}, or relative humidity RH_s) in the expression for the cloudless emittance ϵ_0. This makes the irradiance a function of both temperature and humidity, and these formulae are consequently named temperature/humidity-dependent formulae in the following chapters.

Ångström (1915):

$$\epsilon_0 = a - b \exp\left(-\frac{e_s}{e_*}\right) \quad , \tag{2.9}$$

where Ångström found the constants $a = 0.79$, $b = 0.174$, and $e_* = 10.53$ hPa. According to Houghton (1985) a, b, and e_* are later on found to be in the ranges 0.71 - 0.80, 0.24 - 0.325, and 6.20 - 10.86 hPa, respectively.

Brunt (1932):

$$\epsilon_0 = a + \left(\frac{e_s}{e_*}\right)^{0.5} \quad , \tag{2.10}$$

where Brunt proposed $a = 0.52$ and $e_* = 237$ hPa. According to Houghton (1985), a and e_* are later on found to be in the range 0.43 - 0.62 and 149 - 1189 hPa, respectively.

Efimova (1961, see Budyko 1974):

$$\epsilon_0 = 0.746 + \left(\frac{e_s}{e_*}\right) \quad ; \quad e_* = 202 \; hPa \quad . \tag{2.11}$$

Marshunova (1966, see Shine and Crane 1984):

$$\epsilon_0 = 0.67 + \left(\frac{e_s}{e_*}\right)^{0.5} \quad ; \quad e_* = 400\ hPa \quad . \tag{2.12}$$

Staley and Jurica (1972):

$$\epsilon_0 = \left(\frac{e_s}{e_*}\right)^{0.0875} \quad ; \quad e_* = 44\ hPa \quad . \tag{2.13}$$

Feussner (1973):

$$\epsilon_0 = 1 - 10^{-\left(\frac{e_s}{e_*}\right)^{0.2}} \quad ; \quad e_* = 32\ hPa \quad . \tag{2.14}$$

Brutsaert (1975):

$$\epsilon_0 = \left(\frac{e_s}{e_*}\right)^{\frac{1}{7}} \quad ; \quad e_* = 64\ hPa \quad . \tag{2.15}$$

Clark and Allen (1978):

$$\epsilon_0 = 0.787 + 0.764 \ln\left(\frac{T_{ds}}{T_*}\right) \quad ; \quad T_* = 273K \quad . \tag{2.16}$$

Sätterlund (1979):

$$\epsilon_0 = 1.08 \left[1 - \exp\left(-e_s^{\frac{T_s}{T_*}}\right)\right] \quad ; \quad T_* = 2016K \quad . \tag{2.17}$$

Idso (1981a):

$$\epsilon_0 = 0.7 + \frac{e_s}{e_*} \exp\left(\frac{T_*}{T_s}\right) \quad ; \; T_* = 1500K \; , \; e_* = 16800\ hPa \quad . \tag{2.18}$$

Idso (1981b):

$$\epsilon_0 = \left(\frac{e_s}{e_*}\right)^{\frac{1}{7}} \exp\left(\frac{T_*}{T_s}\right) \quad ; \quad T_* = 350K \quad , \quad e_* = 170000\ hPa \quad . \tag{2.19}$$

Berdahl and Fromberg (1982):

$$\epsilon_0 = 0.741 + \frac{t_{ds}}{t_{1*}} \quad ; \quad t_{1*} = 161.3°C \qquad (night) \quad ,$$

$$\epsilon_0 = 0.727 + \frac{t_{ds}}{t_{2*}} \quad ; \quad t_{2*} = 166.7°C \qquad (day) \quad . \tag{2.20}$$

Frank and Püntener (1986):

$$\epsilon_0 = 0.745 + \left(\frac{t_{ds}}{t_*}\right) \quad ; \quad t_* = 179°C \quad . \tag{2.21}$$

The models listed below use surface air temperature, humidity, and other information like time of day and the altitude above sea level as input:

Centeno (1982):

$$\epsilon_0 = \left[0.577 + 0.1\ (0.6)^z\right] \left(\frac{T_s}{T_*}\right)^{1.1893} \left(\frac{RH_s}{RH_*}\right)^{0.0665} \quad , \tag{2.22}$$

where z is the altitude of the station (km), RH_s is the surface relative humidity (%), T_* = 257.4K, and RH_* = 100%.

Berdahl and Martin (1984):

$$\epsilon_0 = 0.711 + 0.56\left(\frac{t_{ds}}{t_*}\right) + 0.73\left(\frac{t_{ds}}{t_*}\right)^2 + \Delta_h + \Delta_p \quad , \tag{2.23}$$

where t_* = 100°C, Δ_h = 0.013 cos(2π h/24) with solar time h in hours, Δ_p = 0.00012 (p_s - p_0) with the station surface pressure p_s (hPa) and p_0 = 1000 hPa.

2.2.1.2 Cloudy sky

Clouds account for a major part of the variation in downwelling longwave radiation at the surface, and some of the cloudless models presented above are therefore given with optional cloud modifications. Even though each cloud modification is an empirical adjustment of one or another cloudless

model, it can be used independently to estimate the irradiance changes caused by clouds. n is the fractional cloud cover (n = N/8, with N as cloud amount in octa).

Bolz (1949):

$$\epsilon = \epsilon_0 \left(1 + k\, n^2\right) \quad . \tag{2.24}$$

Here n is fractional cloud cover, while k is a cloud factor, with $k_{ci} = 0.04$, $k_{cs} = 0.08$, $k_{ac} = 0.17$, $k_{as} = 0.20$, $k_{cu} = 0.20$, and $k_{st} = 0.24$ for, respectively cirrus, cirrustratus, altocumulus, altostratus, cumulus, and stratus clouds.

Unsworth and Monteith (1975):

$$\epsilon = \epsilon_0 + 0.84 \left(1 - \epsilon_0\right) n \quad . \tag{2.25}$$

Cole (1979):

$$\epsilon = \epsilon_0 + \frac{\Phi_*}{\sigma T_s^4}\left(1+\frac{t_s}{t_*}\right) n \;\; ; \;\; \Phi_* = 65 \; Wm^{-2} \, , \, t_* = 46.8°C \quad . \tag{2.26}$$

Centeno (1982):

$$\epsilon = (1-n)\, \epsilon_0 + n \left\{1 - \left[1 + \left(\frac{z_s}{z_*}\right)^{0.652}\right]\left(\frac{T_*}{T_s}\right)\left(\frac{RH_*}{RH_s}\right)^{1.5}\right\}^4 \, , \tag{2.27}$$

where $z_* = 2.28$ km, $T_* = 3$K, and $RH_* = 100\%$.

Czeplak and Kasten (1987) and Czeplak (1993):

$$\begin{aligned} \epsilon = \epsilon_0 \, [1 &+ a_L \, n_L^{p_L} + a_M \, (1 - n_L) \, n_M^{p_M} \\ &+ a_H \, (1 - n_L)(1 - n_M) \, n_H^{p_H} \,] \quad , \end{aligned} \tag{2.28}$$

where n_L, n_M, and n_H are fractional cloud amounts of low, medium high, and high clouds respectively. For the original version, $a_L = 0.243$, $a_M = 0.196$, and $a_H = 0.091$, with $p_L=p_M=p_H=2.5$ (Czeplak and Kasten, 1987). For the latest version, $a_L = -0.007915\, T_s + 2.447$, $a_M = -0.009179\, T_s + 2.737$, and $a_H = -0.01089\, T_s + 3.165$, with $p_L=p_M=2$, and $p_H=3$ (Czeplak, 1993).

Martin and Berdahl (1984):

$$\epsilon = \epsilon_0 + (1 - \epsilon_0)\, \epsilon_c\, n \exp\left(-\frac{z_c}{z_*}\right) , \qquad (2.29)$$

where z_c is the cloud base height (km), and $z_* = 8.2$ km. The hemispherical cloud emittance ϵ_c is assumed to be ≈ 1 for low and medium high clouds. For cirrus clouds, $\epsilon_c = 0.74\text{-}0.084\ (z_c\text{-}4)$ for 11 km $> z_c >$ 4 km, and $\epsilon_c = 0.15$ for $z_c >$ 11 km.

All the above-mentioned models use cloud cover observations as input to their cloud algorithm. As cloud cover observations are sometimes not available, models using other parameters as input are valuable. The following model of Ineichen et al (1984) uses air temperature and global (G) and normal incidence beam (I_n) solar irradiance as input:

$$\epsilon = 1 - \frac{\phi_*}{\sigma T_s^4}\left(1 + 1.32\frac{I_n}{I_{n,\max}}\right) \; ; \; \phi_* = 44\ Wm^{-2} , \qquad (2.30a)$$

$$\epsilon = 1 - \frac{\phi_*}{\sigma T_s^4}\left(1 + 19.6\frac{I_n}{I_{n,\max}}\right) \; ; \; \phi_* = 24\ Wm^{-2} , \qquad (2.30b)$$

where $I_{n,max} = 1000$ Wm^{-2}. Eqns (2.30a) and (2.30b) are applicable for $I_n/I_{n,max} \geq 0.05$ and $I_n/I_{n,max} < 0.05$, respectively. These eqns are also phrased in terms of global irradiance G:

$$\epsilon = 1 - \frac{\phi_*}{\sigma T_s^4}\left(1 + 1.85\frac{\mu\, I_n}{G}\right) \; ; \; \phi_* = 34\ Wm^{-2} , \qquad (2.30c)$$

$$\epsilon = 1 - \frac{\phi_*}{\sigma T_s^4}\left(1 + 7.95\frac{\mu\, I_n}{G}\right) \; ; \; \phi_* = 22\ Wm^{-2} , \qquad (2.30d)$$

where $\mu = \sin\alpha$ (α = solar elevation angle). Eqns (2.30c) and (2.30d) are applicable for $I_n/G \geq 0.1$ and $I_n/G < 0.1$, respectively.

2.2.2 Inclined surfaces

If the atmospheric radiance and the radiance of the ground both have an isotropic angular distribution, the relation between ϕ_β and ϕ is particularly simple:

$$\phi_\beta = \epsilon_g \, \sigma T_g^4 \sin^2\left(\frac{\beta}{2}\right) + \phi \cos^2\left(\frac{\beta}{2}\right) , \tag{2.31}$$

where the first term is the irradiance of the ground impinging on the surface, and the second term is the atmospheric irradiance on the surface. ϵ_g and T_g are the emittance and the temperature of the ground, respectively.

The models listed below retain the isotropic assumption for the radiance of the ground, but they account for the fact that the sky radiance is anisotropic and yields an additional (positive) term in the atmospheric irradiance contribution.

Unsworth and Monteith (1975):

$$\phi_\beta = \epsilon_g \, \sigma T_g^4 \sin^2\left(\frac{\beta}{2}\right) + \phi \cos^2\left(\frac{\beta}{2}\right) + b \, I_7 \, \sigma T_s^4 , \tag{2.32}$$

where b ranges from 0.07 to 0.14, with a mean of 0.09. I_7 is given by the following figure:

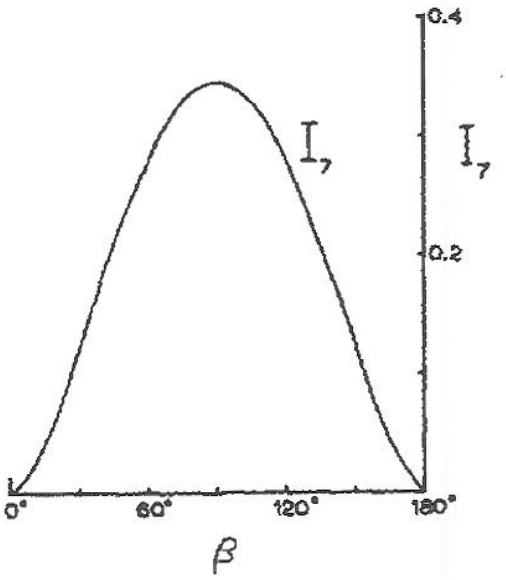

Fig. 2.1 Dependence of I_7 on slope inclination β (Unsworth and Monteith, 1975).

Cole (1979):

$$\phi_\beta = \epsilon_g \sigma T_g^4 \sin^2\left(\frac{\beta}{2}\right) + \phi \cos^2\left(\frac{\beta}{2}\right) + b_1 K_3 \sigma T_s^4 \quad , \tag{2.33}$$

where $b_1 = b[1 - n (0.7067 + 0.00822 t_s)]$, b is the same constant as for Unsworth and Monteith (mean 0.09, range 0.07 - 0.14), and K_3 is a function of β given by the following table:

β	0°	10°	20°	30°	40°	50°	60°	70°	80°	90°
K_3	0	.0221	.0613	.1225	.1798	.2339	.2803	.3159	.3381	.3457

2.3 MODELS FOR ATMOSPHERIC IRRADIANCE BASED ON SATELLITE DATA

Gupta (1989):

$$\phi = \phi_0 + (\phi_{ov} - \phi_0) n \quad . \tag{2.34a}$$

Here the cloudless sky irradiance is given by:

$$\phi_0 = [a_0 + a_1 \ln W_s + a_2 (\ln W_s)^2 + a_3 (\ln W_s)^3] T_e^{3.7} \quad , \tag{2.34b}$$

where $a_0 = 1.791 \cdot 10^{-7}$, $a_1 = 2.093 \cdot 10^{-8}$, $a_2 = -2.748 \cdot 10^{-9}$, and $a_3 = 1.184 \cdot 10^{-9}$. W_s is total precipitable water (mm) and T_e is a weighted temperature based on surface air temperature T_s and the temperatures in the two lowest layers T_1 (surface - 850 hPa) and T_2 (850 - 700 hPa) given by:

$$T_e = k_s T_s + k_1 T_1 + (1 - k_s - k_1) T_2 \quad . \tag{2.34c}$$

k_s and k_1 vary greatly with surface pressure and the temperature profile near the surface, and to a smaller extent with W_s. Reasonable average values are $k_s = 0.5$ and $k_1 = 0.4$. The difference between the overcast and the cloudless sky irradiance is given by:

$$(\phi_{ov} - \phi_0) = \frac{T_{cb}^4}{b_0 + b_1 W_c + b_2 W_c^2 + b_3 W_c^3} \quad , \tag{2.34d}$$

where $b_0 = 4.990 \cdot 10^7$, $b_1 = 2.688 \cdot 10^6$, $b_2 = -6.147 \cdot 10^3$, and $b_3 = 8.163 \cdot 10^2$. T_{cb} is the cloud base temperature, and W_c is the precipitable water below the cloud.

2.4 MODELS FOR ATMOSPHERIC IRRADIANCE BASED ON SOUNDINGS

Such models are given by Atwater and Ball (1978) and Kamada and Flocchini (1984), and use emittance approximations to integrate the radiative transfer equation with soundings data as input.

2.5 MODELS FOR NARROW BAND SPECTRAL LONGWAVE IRRADIANCE

There exist sophisticated models like LOWTRAN (Kneizys et al, 1988) and MODTRAN (Berk et al, 1989). MODTRAN is a moderate (2 cm^{-1}) resolution version of LOWTRAN7 (low resolution transmission model, version 7), and it calculates spectral radiances from vertical profiles (up to 100 km) of temperature, pressure, and atmospheric composition (of clouds, aerosols, and 13 gases).

Besides, there exist some simple narrow band models (Das and Iqbal, 1987 and Berger, 1988) using surface-based information as input. In the model of Das and Iqbal (1987), the spectral emittance $\epsilon(\lambda)$ is expressed as:

$$\epsilon(\lambda) = 1 - \exp(a_{0\lambda} + a_{1\lambda} w + a_{2\lambda} w^2 + a_{3\lambda} w^3) \quad , \tag{2.35}$$

where the spectral coefficients $a_{1\lambda}$, $a_{2\lambda}$, and $a_{3\lambda}$ are given for 105 wavelength intervals between 5.25 and 42.83 μm, and w is the precipitable water vapor in cm.

In the model of Berger (1988), the spectral emittance $\epsilon(\lambda)$ is based of the LOWTRAN6 (version 6 of LOWTRAN) code and it is expressed as:

$$\epsilon(\lambda) = 1 - \exp(- k_{\Delta\lambda}\, m_w) \quad , \tag{2.36a}$$

where $k_{\Delta\lambda}$ is estimated from surface dew point temperature t_{ds} by two alternative relations:

$$k_{\Delta\lambda} = C_1 + C_2\, t_{ds} \quad , \tag{2.36b}$$

$$k_{\Delta\lambda} = C_1 \exp(C_2\, t_{ds}) + C_3 \quad , \tag{2.36c}$$

The spectral coefficients C_1, C_2, and C_3 are given for 21 wavelength intervals between 7.5 and 22.5 μm. A blackbody emission is assumed below 7.5 μm, between 14 and 16.25 μm, and above 22.5 μm.

In Berger et al (1989), integrated values of this simple spectral model are compared with simple broad-band longwave parameterizations. Besides, in Berger et al (1992), the spectral model is presented as a function of altitude above m.s.l.

2.6 REFERENCES

Arnfield, A.J., Evaluation of empirical expressions for the estimation of hourly and daily totals of atmospheric longwave emission under all sky conditions. Quart. J.R. Met. Soc. **105**, 1041-1052 (1979).

Atwater, M.A. and J.T. Ball, Computation of IR sky temperature and comparison with surface temperature. Solar Energy **21**, 211-216 (1978).

Berdahl, P. and R. Fromberg, The thermal radiance of clear skies. Solar Energy **29**, 299-314 (1982).

Berdahl, P. and M. Martin, Emissivity of clear skies. Solar Energy **32**, 663-664 (1984).

Berger, X., A simple model for computing the spectral radiance of clear skies. Solar Energy **40**, 321-333 (1988).

Berger, X. and J. Bathiebo, From spectral sky emissivity to total clear sky emissivity. Solar and Wind Technology **6**, 551-556 (1989).

Berger, X., J. Bathiebo, F. Kieno and C.N. Awanou, Clear sky radiation as a function of altitude. Renewable Energy **2**, 139-157 (1992).

Berk, A., L.S. Bernstein and D.C. Robertson, MODTRAN: A moderate resolution model for LOWTRAN7. GL-TR-89-0122. Geophysics Laboratory, Air Force Systems Command, Hanscom AFB, MA 0173 (1989).

Bolz, H.M., Die Abhängigkeit der infraroten Gegenstrahlung von der Bewölkung. Z. Meteor. **3**, 201-203 (1949).

Brunt, D., Notes on radiation in the atmosphere. Quart. J.R. Met. Soc. **58**, 389-418 (1932).

Brutsaert, W., On a derivable formula for long-wave radiation from clear skies. Water. Resourc. Res. **11**, 742-744 (1975).

Budyko, M.I., Climate and life. International Geophysical Series 18, New York (1974).

Centeno, M., New formulae for the equivalent night sky emissivity. Solar Energy **28**, 489-498 (1982).

Clark, G. and C.P. Allen, The estimation of atmospheric radiation for clear and cloudy skies. Proc. Second Nat. Passive Solar Conf., Vol. 2, 676, Philadelphia (1978).

Cole, R.J., The longwave radiation incident upon inclined surfaces. Solar Energy **22**, 459-462 (1979).

Czeplak, G., Personal communication (1993).

Czeplak, G. and F. Kasten, Parametrisierung der atmosphärischen Wärmestrahlung bei bewölktem Himmel. Met. Rundschau **6**, 184-187 (1987).

Das, A.K. and M. Iqbal, A simplified technique to compute spectral atmospheric radiation. Solar Energy **39**, 143-155 (1987).

Efimova, N.A., On methods of calculating monthly values of net-long-wave radiation. Meteorol. Gidrol. No. 10, 28-33 (1961).

Exell, R.H.B., The atmospheric radiation climate of Thailand. Solar Energy **21**, 73-79 (1978).

Feussner, as cited by F. Möller, Einführung in die Meteorologie II, 53, Mannheim (1973).

Frank, Th. and T.W. Püntener, Oberflächentemperaturen von besonnten Fensterglasscheiben und ihre Auswirkungen auf Raumklima und Komfort, NEFF-Projekt Nr. 266, (1986).

Gupta, S.K., A parameterization for longwave surface radiation from sun-synchronous satellite data. J. of Climate **2**, 305-320 (1989).

Gupta, S.K., W.L. Darnell and A.C. Wilber, A parameterization for longwave surface radiation from satellite data : Recent improvements. J. Appl. Met. **31**, 1361-1367 (1992).

Houghton, H.G., Physical Meteorology. The MIT Press. Cambridge, London, 186 (1985).

Idso, S.B., On the use of equations to estimate atmospheric thermal radiation. Arch. Met. Geoph. Biokl., B, **22**, 287-299 (1974).

Idso, S.B., On the systematic nature of diurnal patterns of differences between calculations and measurements of clear sky atmospheric thermal radiation. Quart. J.R. Met. Soc. **107**, 737-741 (1981a).

Idso, S.B., A set of equations for full spectrum and 8 to 14 μm and 10.5 to 12.5 μm thermal radiation from cloudless skies. Water Resour. Res. **17**, 295-304 (1981b).

Idso, S.B. and R.D. Jackson, Thermal radiation from the atmosphere. J. Geophys. Res. **74**, 5397-5403 (1969).

Ineichen, P., J.M. Gremaud, O. Guisan and A. Mermoud, Infrared sky radiation in Geneva. Solar Energy **32**, 537-545 (1984).

Kamada, R.F. and R.G. Flocchini, Gaussian thermal flux model - I. Theory. Solar Energy **32**, 505-514 - II. Validation. Solar Energy **32**, 505-514 (1984).

Kasten, F., H.J. Golchert and M. Stolley, Parameterization of radiation fluxes as function of solar elevation, cloudiness, and turbidity. In Solar Energy R&D in the European Community, Series F, Vol. 2, 108-114 (1983).

Kneizys, F.X., E.P. Shettle, L.W. Abreu, J.H. Chetwynd, G.P Anderson, W.O. Gallery, J.E.A. Selby and S.A. Clough, Users Guide to LOWTRAN7, AFGL-TR-88-0177, Air Force Geophysics Laboratory, Hanscom AFB, MA 01731 (1988).

Llebot, J.E. and J. Jorge, Some results of thermal atmospheric radiation measurements in Manresa (Spain). Solar Energy **32**, 473-477 (1984).

Marshunova, M.S., Principal characteristics of the radiation balance of the underlying surface, Soviet data on the Arctic heat budget and its climatic influence. Rand Corp. Memo. RM-5003-PR, Santa Monica, Calif. (1966).

Martin, M. and P. Berdahl, Characteristics of infrared sky radiation in the United States. Solar Energy **33**, 321-336 (1984).

Mathis, K., Validation of models for estimating sky temperature radiation. Report IEA-SHCP Task 9 - Solar Radiation and Pyranometry Studies, Subtask E - Representative Design Years (1991).

Pissimanis, D.K. and V.A. Notaridou, The atmospheric radiation in Athens during the summer. Solar Energy **26**, 525-528 (1981).

Sätterlund, D.R., An improved equation for estimating longwave radiation from the atmosphere. Water Resour. Res. **15**, 1649-1650 (1979).

Schieldrup Paulsen, H., Some experiences with the calibration of radiation balance meters. Arch. Met. Geoph. Biokl., B, **15**, 156-174 (1967).

Schmetz, P., Groβräumige Bestimmung der Gegenstrahlung aus Satelliten- und Analysendaten (Large scale determination of atmospheric radiation from satellite and synoptic analysis data). Diplomarbeit (master thesis), University of Köln (1984).

Shine, K.P. and R.G. Crane, The sensitivity of a one-dimensional thermodynamic sea ice model to changes in cloudiness. J. Geophys. Res. **89**, No. C6, 10615-10622 (1984).

Staley, D.O. and G.M. Jurica, Effective atmospheric emissivity under clear skies. J. Appl. Met. **11**, 349-356 (1972).

Swinbank, W.C., Long-wave radiation from clear skies. Quart. J.R. Met. Soc. **89**, 339-348 (1963).

Unsworth, M.H. and J.L. Monteith, Long-wave radiation at the ground - I. Angular distribution of incoming radiation. Quart. J.R. Met. Soc. **101**, 13-24 - II. Geometry of interception by slopes, solids, and obstructed planes. Quart. J.R. Met. Soc. **101**, 25-34 (1975).

Ångström, A., A study of the radiation of the atmosphere. Smithson. Inst. Misc. Coll., **65**(3), 1-159 (1915).

APPENDIX A

Nomenclature:

ϕ_0	longwave atmospheric irradiance (horiz.), clear sky	[W m^{-2}]
ϕ_{ov}	longwave atmospheric irradiance (horiz.), overcast sky	[W m^{-2}]
ϕ	longwave atmospheric irradiance (horiz.), arbitr. sky	[W m^{-2}]
ϕ_β	longwave atmospheric irradiance (slope)	[W m^{-2}]
e_s	water vapor pressure at the surface (2m)	[hPa]
N	total cloud amount	(0-8)
n	fractional cloud amount (= N/8)	
t_s	air temperature at the surface (2m)	[°C]
t_{ds}	dew point temperature at the surface (2m)	[°C]
T_s	air temperature at the surface (2m)	[K]
T_{ds}	dew point temperature at the surface (2m)	[K]
T_g	temperature of the horizontal ground surface	[K]
β	slope angle	
ϵ_0	emittance of clear sky	
ϵ	emittance of arbitrary (cloudy) sky	
ϵ_c	hemispherical cloud emittance	
ϵ_g	emittance of the horizontal ground surface	
σ	Stefan-Boltzmann constant	$5.67\ 10^{-8}$ W m^{-2} K^{-4}

APPENDIX B

Swinbank (1963):

$$\phi_0 = 5.31\ 10^{-13}\ T_s^6 \tag{2.2}$$

Schieldrup Paulsen (1967):

$$\phi_0 = -\ 29.3 + 0.895\ \sigma T_s^4 \tag{2.3}$$

Idso and Jackson (1969):

$$\phi_0 = \left[1 - 0.261\ \exp\left(-7.77\ 10^{-4}\ t_s^2\right)\right]\ \sigma T_s^4 \tag{2.4}$$

Unsworth and Monteith (1975):

$$\phi_0 = \left(1.06 - \frac{119}{\sigma T_s^4}\right)\ \sigma T_s^4 \tag{2.5}$$

Cole (1979):

$$\phi_0 = 222 + 4.94\ t_s \tag{2.6}$$

Llebot and Jorge (1984):

$$\phi_0 = \left[1 - \frac{7.5\ 10^6\ t_s^2 + 7.5\ 10^{10}}{0.2\ t_s^8 + 3.0\ 10^{11}}\right]\ \sigma T_s^4 \tag{2.7}$$

Czeplak and Kasten (1987):

$$\phi_0 = \left(9.9\ 10^{-6}\ T_s^2\right)\ \sigma T_s^4 \tag{2.8}$$

Ångström (1915):

$$\phi_0 = \left[0.79 - 0.174\ 10^{-0.04125 e_s}\right]\ \sigma T_s^4 \tag{2.9}$$

Brunt (1932):

$$\phi_0 = \left[0.52 + 0.065\ e_s^{0.5}\right]\ \sigma T_s^4 \tag{2.10}$$

Efimova (1961):

$$\phi_0 = \left[0.746 + 0.00495\ e_s\right]\ \sigma T_s^4 \tag{2.11}$$

Marshunova (1966):

$$\phi_0 = \left[0.67 + 0.05\, e_s^{0.5}\right] \sigma T_s^4 \tag{2.12}$$

Staley and Jurica (1972):

$$\phi_0 = 0.718\, e_s^{0.0875}\, \sigma T_s^4 \tag{2.13}$$

Feussner (1973):

$$\phi_0 = \left[1 - 10^{\left(-0.5 e_s^{0.2}\right)}\right] \sigma T_s^4 \tag{2.14}$$

Brutsaert (1975):

$$\phi_0 = 0.552\, e_s^{\frac{1}{7}}\, \sigma T_s^4 \tag{2.15}$$

Clark and Allen (1978):

$$\phi_0 = \left[0.787 + 0.764 \ln\left(\frac{t_{ds} + 273}{273}\right)\right] \sigma T_s^4 \tag{2.16}$$

Sätterlund (1979):

$$\phi_0 = 1.08 \left[1 - \exp\left(-e_s^{\frac{T_s}{2016}}\right)\right] \sigma T_s^4 \tag{2.17}$$

Idso (1981a):

$$\phi_0 = \left[0.7 + 5.95\ 10^{-5}\, e_s \exp\left(\frac{1500}{T_s}\right)\right] \sigma T_s^4 \tag{2.18}$$

Idso (1981b):

$$\phi_0 = \left[0.179\, e_s^{\frac{1}{7}} \exp\left(\frac{350}{T_s}\right)\right] \sigma T_s^4 \tag{2.19}$$

Berdahl and Fromberg (1982):

$$\phi_0 = \left(0.741 + 0.0062\, t_{ds}\right) \sigma T_s^4 \qquad \textit{(night)}$$

$$\phi_0 = \left(0.727 + 0.0060\, t_{ds}\right) \sigma T_s^4 \qquad \textit{(day)} \tag{2.20}$$

Frank and Püntener (1986):

$$\phi_0 = \left(0.745 + 0.0056\, t_{ds}\right) \sigma T_s^4 \tag{2.21}$$

Centeno (1982):

$$\phi_0 = \left\{ \left[5.7723 + 0.9955 \cdot (0.6017)^z\right] T_s^{1.1893}\, RH_s^{0.0665}\, 10^{-4} \right\} \sigma T_s^4 \qquad (2.22)$$

Berdahl and Martin (1984):

$$\phi_0 = \left[0.711 + 0.56\left(\frac{t_{ds}}{100}\right) + 0.73\left(\frac{t_{ds}}{100}\right)^2 + \Delta_h + \Delta_p\right] \sigma T_s^4 \qquad (2.23)$$

Bolz (1949):

$$\phi = \epsilon_0 \left(1 + k\, n^2\right) \sigma T_s^4 \qquad (2.24)$$

Unsworth and Monteith (1975):

$$\phi = \left[\epsilon_0 + 0.84 \left(1 - \epsilon_0\right) n\ \right] \sigma T_s^4 \qquad (2.25)$$

Cole (1979):

$$\phi = \phi_0 + \left(65 + 1.39\ t_s\right) n \qquad (2.26)$$

Centeno (1982):

$$\phi = \left\{(1 - n)\epsilon_0 + n[1 - (3000 + 1751\ z^{0.652})\ RH_s^{-\frac{3}{2}}\ T_s^{-1}]\right\}^4 \sigma T_s^4 \qquad (2.27)$$

Czeplak and Kasten (1987) and Czeplak (1993):

$$\phi = \epsilon_0 \left[1 + a_L\, n_L^{p_L} + a_M\, (1 - n_L)\, n_M^{p_M} + a_H\, (1 - n_L)(1 - n_M)\, n_H^{p_H}\ \right] \sigma T_s^4 \qquad (2.28)$$

Martin and Berdahl (1984):

$$\phi = \left[\epsilon_0 + (1 - \epsilon_0)\, \epsilon_c\, n \exp\left(-\frac{z_c}{8.2}\right)\right] \sigma T_s^4 \qquad (2.29)$$

Ineichen et al (1984):

$$\phi = \sigma T_s^4 - 44 - 58 \frac{I_n}{I_{n,\max}}, \qquad for \quad \frac{I_n}{I_{n,\max}} \geq 0.05 \qquad (2.30a)$$

$$\phi = \sigma T_s^4 - 24 - 471 \frac{I_n}{I_{n,\max}}, \qquad for \quad \frac{I_n}{I_{n,\max}} < 0.05 \qquad (2.30b)$$

or

$$\phi = \sigma T_s^4 - 34 - 63 \frac{\mu\, I_n}{G}, \qquad for \quad \frac{\mu\, I_n}{G} \geq 0.1 \qquad (2.30c)$$

$$\phi = \sigma T_s^4 - 22 - 175 \frac{\mu\, I_n}{G}, \qquad for \quad \frac{\mu\, I_n}{G} < 0.1 \qquad (2.30d)$$

IEA-SHCP-17F-2

REVIEW AND TEST OF PARAMETERIZATIONS OF ATMOSPHERIC RADIATION

CHAPTER 3

COMPARISON OF PARAMETERIZATION FORMULAE FOR ATMOSPHERIC RADIATION

Gerhard Czeplak

Deutscher Wetterdienst
Meteorologisches Observatorium Hamburg
Frahmredder 95, D-22393 Hamburg, GERMANY

3.1 INTRODUCTION

A review of simple models for the estimation of longwave atmospheric irradiance from meteorological data was made by Olseth and Skartveit in Chapter 2 of this report. By testing the models against data from several stations, the aim of this investigation is to find the formulae which are best suited to estimate incoming atmospheric radiation at the surface. Tables 3.1a and 3.1b list the authors of the models tested in this Chapter.

3.2 GENERAL ASPECTS

The models can be put in two groups: models for cloudless skies and models for both cloudless and cloudy skies. Data sets from a total of 15 stations in Norway, Sweden, Germany, France, USA and Canada (see Table 3.2) served for testing and comparing the models.

3.2.1 Cloudless sky

The intensity of water vapor and carbon dioxide absorption bands is large enough to produce complete black-body emission outside the atmospheric window.

All levels of the troposphere take part in the emission and absorption of atmospheric radiation. However, the various levels make different contributions to the irradiance at ground level. In case of cloudless sky, the lowest 100 meters of the atmosphere already make up for a major part of the atmospheric radiation (Schmetz et al., 1986). Therefore, many empirical formulae published in the literature are based on data of air temperature and water vapor pressure measured at 2 m height above ground. Moreover, there is a high correlation between surface air temperature and surface water vapor pressure, and many empirical formulae are thus based on data of air temperature alone. However, in case of a temperature inversion, these parameterizations may produce severe errors.

In a previous comparison with measurements of the station Schleswig (Germany) the parameterization formulae from Brunt (1932) and Swinbank (1963) came off well (Czeplak and Kasten, 1987). The Swinbank formula is very simple, it only includes a T^6-dependency and reads in a slightly modified form (Czeplak and Kasten, 1987) as follows:

$$\phi_0 = \epsilon_0 \, \sigma T_s^4 \quad , \tag{3.1}$$

where

ϕ_0 = atmospheric radiation in case of cloudless sky,

σ = $5.67 \cdot 10^{-8}$ $Wm^{-2}K^{-4}$ (= Stefan-Boltzmann constant),

T_s = air temperature measured at a 2 m height above ground,

ϵ_0 = $0.99 \cdot 10^{-5}$ $(T_s/K)^2$ = effective emittance of the atmosphere,

K = Kelvin .

For comparison, the original Swinbank formula (Swinbank, 1963) has $\epsilon_0 = 0.936 \cdot 10^{-5}$ $(T_s/K)^2$. In our investigation we assume that ϵ_0 also depends on the location. Therefore, our aim is to find a dependency of ϵ_0 on climate zones. On account of the simplicity, the Swinbank formula seems to be the best suited formula for this investigation. Details will follow later.

3.2.2 Cloudy sky

In case of cloudy sky, the emittance from the clouds must be taken into account. This contribution to atmospheric radiation is dependent on temperature, humidity, height of cloud base, cloud amount and type of clouds and their liquid water content. The models usually consist of a cloudless sky model with modifications for cloudiness. Each cloud modification, however, is an empirical adjustment to the cloudless model used.

At the beginning of our analysis, we investigated the ratio of the atmospheric radiation ϕ (measured in the presence of clouds) and ϕ_0 (calculated for the cloudless case) as function of the amount of low, medium high and high clouds. Low clouds (C_L) include cumulus (Cu), cumulonimbus (Cb), stratocumulus (Sc) and stratus (St). C_L is formed in lowest atmospheric layer ($<$ 2000 m). The cloud tops of Cu and Cb can reach 5000 m and the tropopause, respectively. Medium high clouds (C_M) include altocumulus (Ac), altostratus (As) and nimbostratus (Ns). In the temperate zones C_M are formed in an atmospheric layer between 2000 m and about 5000 m (about 7000 m in summertime) above ground. Concerning Ns the cloud base can often be observed between 600 m and 800 m above ground. High clouds (C_H) include cirrus (Ci), cirrostratus (Cs) and cirrocumulus (Cc). In the temperate zones C_H generally occur higher than 5000 m above ground.

First we used the above modified Swinbank formula to calculate clear sky emittance. Then we did a curve fit of ϕ/ϕ_0 with respect to cloud amount of a particular type (C_L, C_M and C_H). We used an power function as follows:

$$\frac{\phi}{\phi_0} = 1 + a\, n^x \quad , \tag{3.2}$$

where n is the fractional cloud amount of the cloud type C_L, C_M or C_H. In this respect, the first investigations were made by Bolz (1949) and Exell (1978). An improved version was given by Czeplak (1993) and the coefficient a is given in Chapter 2, formula 2.28. We evaluated the RMSEs for the unknown exponent x in steps of 0.2, and found that a square function (x=2) yields best fit for low and medium high clouds, while a cubic function (x=3) yields best fit for high clouds. The results for Luleå, Bergen and Schleswig are shown in Figures 3.1, 3.2 and 3.3, respectively. In conclusion, we recommend the use of a cloudless sky model with modifications for cloudy conditions.

3.3 RESULTS OF THE COMPARISON

3.3.1 Cloudless sky

The comparison of the calculated and observed hourly sums of atmospheric radiation for cloudless hours in summer (May-August) and in winter (November to December) at various sites is given in Tables 3.3a-b), 3.4a-d) and 3.5a-d). Tables 3.3a) and 3.3b) give an overview of the averages and the standard deviations of the measured data for the two seasons. In the following Tables 3.4a-d) and 3.5a-d) one finds statistical information on the comparison of the observed and modelled hourly irradiance for clear skies. This might be a good means of quantitatively assessing the best models.

For instance, looking at the temperature-dependent models, we see that model 3 (Idso & Jackson) has the smallest MBE and RMSE in summer (Tables 3.4a-b) while model 7 (Czeplak & Kasten) has the smallest MBE and RMSE in winter (Tables 3.5a-b). Among the models using air temperature and humidity as input without reference to time of day, we see that model 23 (Frank & Püntener) has the lowest MBE and RMSE both in summer and in winter (Tables 3.4a-b and 3.5a-b). Moreover, the time-of-day-dependent models 19 and 20 (Berdahl & Fromberg) and 22 (Berdahl & Martin) perform similarly well as does model 23. The average correlation coefficients between calculated and observed hourly values (Tables 3.4c and 3.5c) are slightly higher for the temperature/humidity-

dependent models than for the temperature-dependent models, and they are slightly higher in summer than in winter. Moreover, most models yield hourly values with slightly lower standard deviations than the standard deviations of the observed values (the ratios in Tables 3.4d and 3.5d tend to be less than unity).

A graphic comparison of the output from the original Swinbank model and measured data of 6 selected stations is given in Figure 3.4. It becomes obvious that this model underestimates the irradiation above 300 Whm^{-2} at three stations. This is particularly visible in the diagram for the station Bergen.

Figures 3.5a and 3.5b demonstrate the results of the modified formula of Swinbank using the effective emittance of the atmosphere for cloudless sky $\varepsilon_0 = \alpha_0 (T_s/K)^2$, where $\alpha_0 = 0.997 \cdot 10^{-5}$ derived from Schleswig data for the whole year. A good correspondence was found for Schleswig (RMSE = 6.7 %), but also good results were found for Bergen, Stockholm and Hamburg data (RMSE = 6.9 %). Out of the 12 graphs depicting the results of this model, 7 show a model overestimation of irradiance by 2% or more. In a further investigation we tried to derive the effective emittance ϵ_0 for each station for summer, winter and the whole year. As our aim was to find a model as simple but efficient as possible, we chose again the Swinbank formula, because the corresponding ϵ_0 includes only one parameter (α_0), which can be assumed as variable. We defined the seasons as before. Daytime and nighttime are indicated if the sun elevation angle is greater than 5° or less than -6°, respectively. Using the least square method we found diurnal, seasonal and local differences (Table 3.6), where the values are often higher in winter than in summer, higher in the nighttime than in the daytime and lower in the inland than at the coast. The diagrams given in Fig. 3.6 were prepared using the coefficient α_0 for annual averages at each station (Table 3.6). Due to the adjustment to the observed data at each station the agreement is of course excellent. Also the other models would have improved by a similar site specific modification. For some models the efforts would, however, be greater because there are more than one unknown coefficient α_0 of the emittance ϵ_0.

Most of the stations are very similar in latitude and macro-climate zones, except Bergen (maritime influenced) and Hohenpeißenberg (mountain station). Nevertheless, we have tried to classify the coefficient α_0 with the help of the climate classification according to Köppen and Trewartha (1954, see Table 3.7). The atmospheric radiation stations are grouped according to the corresponding climate zones. For instance, the zone Dfc is representative for Luleå and Dfb for Edmonton, while Cfb maritime is representative for Bergen and Schleswig. If there is more than one station in one class, the average of α_0 was taken. Calculating the atmospheric radiation separately for the nighttime or the daytime, the used coefficient α_0 would be 2 - 3 % higher or lower, respectively, than the

corresponding value in Table 3.7.

3.3.2 Cloudy sky

The comparison of the calculated and observed hourly sums of atmospheric radiation for cloudy sky at various sites is given in Tables 3.8 and 3.9a-d). Table 3.8 gives an overview of the averages and the standard deviations of the measured data, while the following Tables 3.9a-d) give statistical information on the comparison of the observed and modelled hourly irradiance.

For instance, models 4 (Centeno) and 7 (Czeplak) performs well having the lowest MBEs and RMSEs (Tables 3.9a and 3.9b). Compared to these results, the outputs from the other models are worse. In case of high clouds, the model of Czeplak is superior because the amount of low, medium high and high clouds are taken into account. A comparison of the results from the models of Czeplak and of Centeno for the station Schleswig is given in Figure 3.7. It turns out that the model of Czeplak performs better particularly at higher irradiances.

3.4 CONCLUSIONS

Atmospheric radiation can be sufficiently well parameterized with the help of surface air temperature and the amount of low, medium high and high clouds. Since diurnal, seasonal and local influences exist, the coefficient α_0 of the atmospheric emittance $\epsilon_0 = \alpha_0(T_s/K)^2$ used in the Swinbank formula should be adjusted as given in Table 3.7. The present determination of α_0 is to be regarded as a first step. Besides, the models should be tested for a number of other climate regions if data are available.

3.5 REFERENCES

Berdahl, P. and R. Fromberg, The thermal radiance of clear skies. Solar Energy **32**, 663-664 (1984).

Bolz, H.M., Die Abhängigkeit der infraroten Gegenstrahlung von der Bewölkung. Z. Meteor. **3**, 201-203 (1949).

Centeno, M., New formulae for the equivalent night sky emissivity. Solar Energy **28**, 489-498 (1982).

Czeplak, G. and F. Kasten, Parametrisierung der atmosphärischen Wärmestrahlung bei bewölktem Himmel. Met. Rundschau **6**, 184-187 (1987).

Czeplak, G., Personal communication (1993).

Excell, R.H.B., The atmospheric radiation climate of Thailand. Solar Energy **21**, 73-79 (1978).

Frank, Th. and T.W. Püntener, Oberflächentemperaturen von besonnten Fensterglasscheiben und ihre Auswirkungen auf Raumklima und Komfort, NEFF-Projekt Nr. 266 (1986).

Schmetz, P., J. Schmetz and R. Raschke, Estimation of daytime downward longwave radiation at the surface from satellite and grid point data. Theor. Appl. Climatol. **37**, 136-149 (1986).

Swinbank, W.C., Long-wave radiation from clear skies. Quart. J. R. Met. Soc. **89**, 339-348 (1963).

Trewartha, G.T., An introduction to climate, 3rd ed., McGraw-Hill Book Co. (1954).

Table 3.1a Models of atmospheric radiation in case of cloudless sky

Model No.	Authors
	Models with only surface air temperature as input
1	Swinbank (1963)
2	Schieldrup Paulsen (1967)
3	Idso and Jackson (1969)
4	Unsworth and Monteith (1975)
5	Cole (1979)
6	Llebot and Jorge (1984)
7	Czeplak and Kasten (1987)
	Models with both surface air temperature and humidity as input
8	Ångström (1915)
9	Brunt (1932)
10	Efimowa (1961)
11	Marshunowa (1966)
12	Staley and Jurica (1972)
13	Feussner (1975)
14	Brutsaert (1975)
15	Clark and Allen (1978)
16	Satterlund (1979)
17	Idso (1981a)
18	Idso (1981b)
19	Berdahl and Fromberg (1982), night
20	Berdahl and Fromberg (1982), day
21	Centeno (1982)
22	Berdahl and Martin (1984)
23	Frank and Püntener (1986)

Table 3.1b Models of atmospheric radiation in case of cloudy sky

Model No.	Authors
1	Bolz (1949)
2	Unsworth and Monteith (1975)
3	Cole (1979)
4	Centeno (1982)
5	Frank and Püntener (1986)
6	Martin and Berdahl (1984)
7	Czeplak (1993)

Table 3.2 List of atmospheric radiation stations. The altitude is given in m above m.s.l. Radiation instrument: S = Schulze Pyrradiometer, E = Eppley Pyrgeometer (PIR)

WMO Number	Name	Latitude	Longitude	Altitude	Instrument
	Norway				
01317	Bergen	60°24'N	05°19'E	45	S
	Sweden				
02183	Luleå	65°33'N	22°08'E	17	E
02749	Borlänge	60°29'N	15°26'E	140	E
02483	Stockholm	59°21'N	18°04'E	30	E
02071	Norrköping	58°35'N	16°09'E	43	E
02627	Lund	55°43'N	13°13'E	73	E
	Germany				
10035	Schleswig	54°32'N	09°33'E	59	S
10141	Hamburg	53°39'N	10°07'E	49	S
10348	Braunschweig	52°18'N	10°27'E	83	S
10628	Geisenheim	49°59'N	07°57'E	131	S
10738	Stuttgart	48°50'N	09°12'E	318	S
10962	Hohenpeißenberg	47°48'N	11°01'E	990	S
	France				
07586	Carpentras	44°05'N	05°03'E	109	E
	Canada				
71121	Edmonton/Namao	53°40'N	113°28'W	688	E
	USA				
72518	Albany	42°42'N	73°51'W	79	E

Table 3.3a Atmospheric radiation in summer (May-August) for cloudless sky at various sites. Number of observation hours (N). Means of observed hourly sums (ϕ_0) and standard deviation (S) in Whm^{-2}.

	Berg	Luleå	Borl	Stock	Norrk	Lund	Schle	Hamb	Braun
N	731	433	230	385	655	791	1205	2221	1218
ϕ_0(obs)	318.7	289.5	288.2	312.1	296.4	294.4	313.7	316.9	326.7
S(obs)	42.4	41.3	33.3	40.0	30.8	36.5	34.0	35.4	38.4

	Geis	Stutt	Hohen	Carp	Alba	Edmon	Mean
N	1151	643	783	60	0	342	723
ϕ_0(obs)	331.8	314.2	292.6	360.0	0.0	306.6	312.6
S(obs)	39.9	33.8	27.5	31.5	0.0	28.9	35.8

Table 3.3b Same as Table 3.3a, but for the winter (November-February).

	Berg	Luleå	Borl	Stock	Norrk	Lund	Schle	Hamb	Braun
N	1385	1694	348	644	1421	1051	1399	2437	1409
ϕ_0(obs)	220.3	187.5	211.0	208.6	206.3	196.5	236.0	225.0	244.5
S(obs)	22.0	23.9	24.5	26.1	27.2	28.5	27.3	26.5	27.1

	Geis	Stutt	Hohen	Carp	Alba	Edmon	Mean
N	1174	620	1276	24	353	786	1068
ϕ_0(obs)	237.0	235.4	222.1	306.5	182.4	186.7	217.2
S(obs)	23.5	26.4	24.9	34.5	19.7	34.4	26.0

Table 3.4a Comparison between calculated and observed atmospheric radiation for cloudless sky at various sites in summer (May-August): Mean bias error (MBE = calculated$_{Mod\ i}$ - observed) of hourly sums in Whm^{-2}. The model numbers refer to Table 3.1a.

	Berg	Luleå	Borl	Stock	Norrk	Lund	Schle	Hamb	Braun
Mod 1	-28.0	5.2	6.3	-5.4	.4	5.0	-13.8	-9.5	-9.6
Mod 2	-8.9	23.1	24.5	9.8	18.1	22.1	3.2	5.7	3.2
Mod 3	-24.9	8.6	9.3	-2.5	3.0	7.6	-11.3	-7.1	-7.2
Mod 4	-36.1	-3.6	-2.2	-15.1	-8.2	-3.9	-22.7	-19.1	-20.3
Mod 5	-34.5	-2.8	-1.1	-15.8	-7.2	-3.3	-22.1	-19.6	-22.2
Mod 6	-35.7	-3.4	-2.5	-18.2	-9.2	-5.5	-24.6	-22.5	-25.0
Mod 7	-9.1	24.2	25.4	7.9	19.6	24.4	5.6	10.4	10.9
Mod 8	-47.0	-13.9	-12.4	-28.4	-18.9	-13.5	-29.8	-28.5	-32.6
Mod 9	-46.5	-11.7	-10.7	-26.0	-17.1	-10.1	-24.9	-23.5	-28.0
Mod 10	-18.1	15.4	16.3	1.4	9.9	15.5	-1.5	.4	-3.4
Mod 11	-7.0	27.3	28.4	13.9	22.2	28.6	12.9	14.9	11.4
Mod 12	11.4	45.5	47.0	32.7	40.8	47.0	31.5	33.8	30.8
Mod 13	-3.2	30.1	31.7	16.7	25.4	30.9	14.6	16.7	13.6
Mod 14	-31.7	3.0	4.4	-10.8	-1.9	5.1	-9.1	-7.5	-11.6
Mod 15	-14.6	18.2	19.7	4.3	13.2	18.2	1.0	2.9	-.5
Mod 16	-13.7	19.6	21.1	6.2	14.8	20.2	3.6	5.7	2.6
Mod 17	-13.3	21.4	22.6	7.0	16.2	23.4	8.8	9.7	4.5
Mod 18	-2.5	31.7	33.4	16.3	26.8	33.6	19.8	20.2	14.6
Mod 19	-10.8	11.7	8.7	-2.7	5.3	14.8	-4.0	-1.4	-16.1
Mod 20	-42.6	4.7	7.4	-11.4	-2.2	1.1	-11.0	-10.8	1.9
Mod 21	-38.2	-4.7	-5.8	-19.5	-10.4	-6.0	-22.5	-20.8	-25.5
Mod 22	-30.3	4.3	5.4	-9.6	-.9	5.9	-9.1	-7.5	-11.6
Mod 23	-24.4	9.6	11.0	-4.3	4.7	10.8	-4.6	-2.9	-6.7

Table 3.4a (continued)

	Geis	Stutt	Hohen	Carp	Alba	Edmon	Mean
Mod 1	-14.0	3.9	13.8	-8.1		9.0	-5.9
Mod 2	-1.3	16.6	29.5	-4.4		22.1	9.4
Mod 3	-11.8	6.0	15.9	-5.2		11.7	-3.4
Mod 4	-24.6	-6.7	4.6	-23.1		-1.6	-15.5
Mod 5	-26.5	-8.5	4.5	-30.7		-3.5	-15.9
Mod 6	-29.8	-12.3	.5	-29.2		-5.9	-18.5
Mod 7	6.6	24.5	33.7	14.7		29.5	13.7
Mod 8	-37.0	-18.2	-7.3	-36.7		-16.5	-26.2
Mod 9	-32.2	-12.3	-4.4	-22.9		-13.7	-22.3
Mod 10	-7.7	11.4	21.7	-3.6		13.4	2.9
Mod 11	7.2	26.6	35.1	15.4		26.7	16.7
Mod 12	26.6	45.8	54.2	34.2		45.9	35.6
Mod 13	9.2	28.0	38.0	12.3		29.5	19.0
Mod 14	-15.8	4.0	11.5	-6.3		2.1	-6.5
Mod 15	-4.9	13.6	24.9	-4.8		16.5	5.6
Mod 16	-1.8	17.0	27.2	1.3		18.8	8.1
Mod 17	.4	20.5	28.3	9.0		18.8	10.8
Mod 18	10.3	30.2	38.9	15.1		27.9	21.1
Mod 19	-12.1	-0.3	12.7			-3.2	-2.1
Mod 20	-13.8	16.0	25.0	-5.3		2.4	-5.6
Mod 21	-31.0	-16.1	-15.2	-31.0		-21.3	-20.5
Mod 22	-15.8	4.0	12.0	-6.8		3.0	-6.1
Mod 23	-10.9	8.4	17.3	-5.2		8.3	-1.1

Table 3.4b Comparison between calculated and observed atmospheric radiation for cloudless sky at various sites in summer (May-August): Root mean square error (RMSE) of hourly sums in Whm^{-2}. The model numbers refer to Table 3.1a.

	Berg	Luleå	Borl	Stock	Norrk	Lund	Schle	Hamb	Braun
Mod 1	34.4	21.2	19.3	14.1	15.5	17.1	22.5	20.0	33.7
Mod 2	24.1	30.5	29.3	16.7	22.7	27.8	17.3	17.5	29.1
Mod 3	32.3	21.6	20.6	13.6	15.7	18.2	21.0	18.8	33.1
Mod 4	41.5	20.2	16.9	19.4	16.3	16.5	28.3	25.3	36.6
Mod 5	40.8	20.4	15.7	20.5	15.3	17.0	27.8	25.7	36.5
Mod 6	43.7	21.1	17.4	24.2	17.5	19.4	30.5	28.3	37.6
Mod 7	21.8	32.5	31.9	15.9	25.7	29.7	19.4	21.3	35.4
Mod 8	51.9	21.9	17.6	30.5	21.6	20.0	33.9	32.1	42.3
Mod 9	51.1	19.5	15.4	27.8	19.5	17.3	29.5	27.4	38.8
Mod 10	28.2	22.8	20.8	10.4	14.5	21.2	16.0	14.5	27.6
Mod 11	21.5	31.8	30.7	16.2	24.2	31.6	20.4	20.5	29.8
Mod 12	22.8	48.5	48.5	33.7	42.1	49.0	35.3	36.7	41.6
Mod 13	20.8	34.5	34.1	18.9	27.4	33.9	21.5	22.0	30.8
Mod 14	37.8	16.2	11.9	14.5	9.8	15.0	18.4	15.8	29.5
Mod 15	26.2	25.3	23.8	11.6	17.3	23.5	16.2	15.4	27.6
Mod 16	24.8	25.9	24.6	11.0	18.1	24.6	16.3	15.6	27.8
Mod 17	25.4	26.4	25.1	12.8	18.8	27.6	18.3	17.4	27.0
Mod 18	22.9	35.3	35.3	20.9	28.7	37.0	25.7	25.0	30.2
Mod 19	16.5	26.3	16.0	9.6	11.3	21.4	14.8	11.3	22.4
Mod 20	46.1	14.7	13.0	14.6	9.4	10.9	20.9	20.8	34.3
Mod 21	44.3	18.0	14.5	22.7	15.1	16.3	27.8	25.8	37.3
Mod 22	36.7	16.3	12.4	13.2	9.5	15.0	18.3	15.8	29.5
Mod 23	32.0	18.6	15.9	9.9	10.6	17.5	16.4	14.3	28.0

Table 3.4b (continued)

	Geis	Stutt	Hohen	Carp	Alba	Edmon	Mean
Mod 1	29.6	25.1	23.3	27.1		28.3	24.0
Mod 2	25.1	27.8	33.9	17.4		29.5	24.0
Mod 3	28.6	25.7	24.5	27.5		29.0	23.5
Mod 4	35.3	24.1	18.1	31.1		23.5	26.7
Mod 5	36.7	23.7	17.3	34.5		20.0	26.6
Mod 6	38.5	26.6	17.4	37.6		20.2	28.6
Mod 7	27.7	35.7	39.0	32.1		41.5	27.6
Mod 8	44.6	27.2	16.8	39.3		21.7	32.1
Mod 9	40.7	23.4	16.0	28.9		20.4	28.9
Mod 10	25.7	23.3	26.7	16.8		21.1	20.7
Mod 11	25.5	33.5	38.4	24.1		31.7	26.1
Mod 12	36.1	50.3	56.5	39.0		49.4	40.6
Mod 13	26.1	34.7	41.1	20.7		33.9	27.6
Mod 14	29.4	20.5	19.6	19.0		16.4	20.6
Mod 15	25.2	24.8	29.5	16.2		23.2	21.6
Mod 16	24.5	26.7	31.4	16.9		25.3	22.0
Mod 17	25.4	28.5	32.1	18.5		23.2	23.1
Mod 18	28.0	36.1	41.7	20.2		30.4	29.4
Mod 19	25.2	12.3	17.7			12.7	16.5
Mod 20	31.6	25.6	29.8	16.6		15.6	23.2
Mod 21	39.8	26.1	21.7	34.1		25.5	27.8
Mod 22	29.3	20.4	19.6	19.2		16.1	20.4
Mod 23	26.9	21.7	23.2	17.3		17.7	19.9

Table 3.4c Comparison between calculated and observed atmospheric radiation for cloudless sky at various sites in summer (May-August): Correlation coefficient (R) between modelled and observed hourly sums. The model numbers refer to Table 3.1a.

	Berg	Luleå	Borl	Stock	Norrk	Lund	Schle	Hamb	Braun
Mod 1	.884	.881	.870	.951	.895	.898	.869	.888	.675
Mod 2	.885	.879	.875	.953	.897	.899	.870	.887	.673
Mod 3	.880	.884	.859	.947	.890	.894	.865	.887	.675
Mod 4	.885	.879	.875	.953	.897	.899	.870	.887	.673
Mod 5	.886	.873	.881	.954	.899	.899	.871	.886	.669
Mod 6	.881	.880	.863	.945	.886	.892	.866	.884	.693
Mod 7	.884	.881	.870	.951	.895	.898	.869	.888	.675
Mod 8	.895	.918	.933	.980	.948	.929	.886	.917	.712
Mod 9	.886	.928	.944	.972	.952	.923	.884	.919	.722
Mod 10	.896	.915	.925	.979	.940	.926	.885	.914	.706
Mod 11	.894	.922	.937	.980	.949	.928	.886	.918	.715
Mod 12	.895	.919	.934	.979	.948	.928	.886	.917	.712
Mod 13	.896	.914	.928	.979	.944	.928	.885	.914	.707
Mod 14	.884	.927	.944	.970	.952	.923	.885	.920	.723
Mod 15	.896	.907	.917	.977	.935	.924	.883	.910	.700
Mod 16	.896	.913	.924	.979	.941	.927	.884	.913	.705
Mod 17	.882	.928	.946	.968	.951	.918	.881	.914	.723
Mod 18	.867	.928	.943	.951	.944	.909	.880	.914	.725
Mod 19	.886	.780	.908	.969	.925	.848	.859	.906	.842
Mod 20	.849	.938	.946	.976	.958	.951	.824	.888	.721
Mod 21	.896	.914	.926	.979	.942	.927	.885	.914	.707
Mod 22	.889	.926	.942	.976	.952	.926	.886	.919	.720
Mod 23	.892	.922	.939	.978	.951	.928	.887	.919	.716

Table 3.4c (continued)

	Geis	Stutt	Hohen	Carp	Alba	Edmon	Mean
Mod 1	.781	.751	.789	.878		.814	.835
Mod 2	.778	.753	.791	.883		.813	.835
Mod 3	.782	.747	.784	.874		.814	.833
Mod 4	.778	.753	.791	.883		.813	.835
Mod 5	.772	.756	.794	.888		.811	.835
Mod 6	.793	.721	.778	.838		.807	.833
Mod 7	.781	.751	.789	.878		.814	.835
Mod 8	.790	.802	.833	.909		.898	.868
Mod 9	.780	.811	.840	.918		.919	.869
Mod 10	.790	.799	.827	.913		.878	.864
Mod 11	.789	.806	.835	.915		.901	.869
Mod 12	.790	.803	.834	.912		.899	.868
Mod 13	.790	.796	.829	.906		.890	.865
Mod 14	.782	.811	.840	.918		.922	.869
Mod 15	.789	.788	.822	.903		.872	.860
Mod 16	.791	.794	.827	.905		.884	.864
Mod 17	.772	.811	.842	.919		.921	.866
Mod 18	.764	.809	.841	.921		.932	.863
Mod 19	.758	.895	.884			.893	.868
Mod 20	.787	.865	.856	.885		.912	.870
Mod 21	.791	.796	.828	.907		.886	.865
Mod 22	.784	.810	.839	.917		.914	.870
Mod 23	.788	.806	.837	.914		.908	.869

Table 3.4d Comparison between calculated and observed atmospheric radiation for cloudless sky at various sites in summer (May-August): Ratio between standard deviations of modelled and observed hourly sums. The model numbers refer to Table 3.1a.

	Berg	Luleå	Borl	Stock	Norrk	Lund	Schle	Hamb	Braun
Mod 1	.816	1.038	1.111	1.058	1.125	.984	1.030	1.073	1.082
Mod 2	.634	.800	.856	.808	.860	.754	.788	.814	.814
Mod 3	.774	.997	1.070	1.032	1.102	.959	1.007	1.060	1.079
Mod 4	.751	.947	1.014	.958	1.018	.893	.934	.965	.963
Mod 5	.660	.823	.880	.821	.872	.768	.801	.818	.806
Mod 6	.524	.712	.739	.718	.749	.657	.684	.749	.811
Mod 7	.868	1.105	1.183	1.104	1.198	1.048	1.097	1.142	1.152
Mod 8	.624	.824	.814	.788	.841	.769	.779	.787	.742
Mod 9	.704	.976	.915	.901	.959	.901	.909	.910	.827
Mod 10	.645	.874	.855	.824	.878	.803	.838	.849	.803
Mod 11	.726	.986	.951	.925	.985	.910	.931	.938	.874
Mod 12	.762	1.012	.995	.968	1.026	.941	.953	.963	.906
Mod 13	.702	.917	.919	.890	.942	.856	.869	.881	.839
Mod 14	.754	1.021	.973	.961	1.018	.952	.944	.946	.864
Mod 15	.640	.834	.845	.812	.862	.777	.800	.814	.785
Mod 16	.689	.905	.906	.877	.930	.844	.863	.877	.838
Mod 17	.688	.957	.896	.869	.930	.878	.884	.880	.785
Mod 18	.665	.897	.847	.843	.890	.844	.811	.807	.717
Mod 19	.826	.721	.849	.895	.903	.877	.852	.986	.884
Mod 20	.813	.988	.955	.912	1.012	.938	.871	.796	.628
Mod 21	.608	.803	.794	.774	.821	.744	.761	.774	.736
Mod 22	.720	.987	.936	.918	.978	.913	.923	.926	.850
Mod 23	.706	.944	.918	.897	.951	.878	.884	.891	.830

Table 3.4d (continued)

	Geis	Stutt	Hohen	Carp	Alba	Edmon	Mean
Mod 1	.975	1.070	1.084	1.555		1.539	1.055
Mod 2	.730	.800	.826	1.142		1.164	.802
Mod 3	.977	1.076	1.068	1.587		1.524	1.039
Mod 4	.865	.948	.978	1.352		1.379	.949
Mod 5	.720	.786	.834	1.091		1.163	.807
Mod 6	.749	.817	.717	1.361		1.120	.741
Mod 7	1.038	1.139	1.154	1.655		1.639	1.122
Mod 8	.673	.762	.848	1.089		1.109	.777
Mod 9	.761	.886	.985	1.320		1.256	.893
Mod 10	.729	.826	.879	1.244		1.174	.828
Mod 11	.797	.911	.998	1.350		1.302	.920
Mod 12	.823	.933	1.035	1.354		1.354	.950
Mod 13	.759	.854	.943	1.227		1.246	.871
Mod 14	.792	.918	1.042	1.332		1.327	.936
Mod 15	.709	.792	.855	1.145		1.150	.802
Mod 16	.758	.852	.930	1.236		1.237	.864
Mod 17	.728	.856	.955	1.253		1.192	.862
Mod 18	.664	.781	.917	1.100		1.136	.804
Mod 19	.762	.937	.967			1.064	.906
Mod 20	.664	.798	.893	1.208		1.251	.864
Mod 21	.664	.738	.776	1.088		1.042	.756
Mod 22	.779	.900	.999	1.332		1.283	.909
Mod 23	.756	.863	.965	1.254		1.251	.879

Table 3.5a Comparison between calculated and observed atmospheric radiation for cloudless sky at various sites in winter (November-February): Mean bias error (MBE = calculated$_{Mod\ i}$ - observed) of hourly sums in Whm^{-2}. The model numbers refer to Table 3.1a.

	Berg	Luleå	Borl	Stock	Norrk	Lund	Schle	Hamb	Braun
Mod 1	-17.6	-13.8	-1.0	-3.2	-5.8	2.6	-20.0	-13.8	-18.9
Mod 2	17.1	23.2	32.7	30.9	28.8	37.4	13.0	19.8	12.6
Mod 3	1.8	18.8	16.1	15.8	15.5	24.2	-4.9	3.1	-6.5
Mod 4	-23.4	-22.3	-6.6	-9.2	-12.1	-3.7	-25.4	-19.4	-24.3
Mod 5	-18.0	-21.3	-1.1	-4.3	-7.8	.7	-19.5	-13.9	-18.5
Mod 6	3.0	13.1	17.6	16.5	14.8	23.7	-2.9	4.4	-4.7
Mod 7	-4.5	-2.6	12.6	5.7	7.2	15.4	-6.0	-.1	-4.3
Mod 8	-22.8	-12.5	-6.5	-7.2	-9.2	.0	-24.3	-17.8	-25.0
Mod 9	-30.5	-21.1	-13.2	-13.8	-16.2	-6.9	-29.6	-23.6	-29.8
Mod 10	7.0	16.0	22.6	21.5	19.7	28.6	3.8	10.5	3.0
Mod 11	6.2	12.9	23.5	22.3	19.7	28.8	6.7	12.6	7.1
Mod 12	16.3	19.1	35.3	33.5	29.8	39.0	19.9	25.0	21.2
Mod 13	7.4	10.8	26.1	24.4	20.8	30.0	10.1	15.6	11.0
Mod 14	-26.4	-21.2	-7.0	-8.2	-11.8	-2.3	-21.5	-16.3	-20.4
Mod 15	6.8	13.4	23.6	22.2	19.6	28.7	5.7	12.0	5.5
Mod 16	1.2	6.7	18.9	17.5	14.4	23.6	2.0	7.9	2.4
Mod 17	3.6	11.8	20.6	19.8	17.4	26.7	4.3	10.2	4.0
Mod 18	10.1	16.4	29.5	28.7	25.0	34.9	15.4	20.7	15.7
Mod 19	-15.4	-10.4	1.8	1.8	-1.6	7.7	-11.9	-8.1	-17.2
Mod 20	-24.0	-13.3	6.9	-1.9	-6.9	3.6	-17.3	-3.8	6.8
Mod 21	-13.5	-4.4	1.8	2.5	-.1	8.7	-14.8	-8.1	-15.9
Mod 22	-16.5	-8.2	.9	.1	-2.4	6.8	-15.4	-9.5	-15.3
Mod 23	-12.9	-7.3	5.5	4.3	1.0	10.3	-10.3	-4.7	-9.7

Table 3.5a (continued)

	Geis	Stutt	Hohen	Carp	Alba	Edmon	Mean
Mod 1	-20.6	-10.6	5.2	-35.7	7.2	-22.7	-11.5
Mod 2	12.3	21.0	36.3	-12.1	43.3	14.6	22.4
Mod 3	-5.6	2.2	17.8	-31.8	31.9	14.2	8.0
Mod 4	-26.0	-16.0	-.4	-42.2	.7	-32.6	-17.7
Mod 5	-20.2	-10.3	5.1	-38.3	4.9	-34.3	-13.2
Mod 6	-3.7	3.8	18.7	-36.2	30.9	8.2	8.0
Mod 7	-6.6	3.9	19.9	-18.2	19.4	-12.1	1.6
Mod 8	-25.9	-16.9	-5.6	-47.0	3.6	-20.4	-15.6
Mod 9	-31.6	-21.8	-12.1	-46.7	-5.2	-30.2	-22.2
Mod 10	2.6	11.2	24.6	-19.8	33.8	8.1	13.2
Mod 11	5.1	15.1	26.2	-9.0	30.8	3.2	13.9
Mod 12	18.0	29.2	39.1	8.8	38.2	5.9	24.9
Mod 13	8.4	19.1	29.4	-5.1	29.8	-2.9	15.6
Mod 14	-23.8	-12.5	-4.8	-32.3	-4.4	-34.4	-16.8
Mod 15	4.4	13.8	26.0	-16.1	31.8	3.1	13.6
Mod 16	.5	10.6	21.8	-15.7	25.0	-4.8	8.8
Mod 17	2.3	11.9	22.1	-12.7	28.8	2.6	11.5
Mod 18	12.9	23.7	29.9	.1	32.2	2.0	19.8
Mod 19	-18.4	-7.1	3.5	-29.5	6.7	-26.2	-8.1
Mod 20	-3.2	4.2	11.6	-23.5	3.9	-19.8	-3.1
Mod 21	-17.4	-11.2	-8.0	-39.7	11.4	-22.4	-8.1
Mod 22	-17.4	-7.3	2.7	-31.2	8.4	-17.2	-8.2
Mod 23	-12.2	-1.6	7.9	-25.4	10.2	-19.6	-4.4

Table 3.5b Comparison between calculated and observed atmospheric radiation for cloudless sky at various sites in winter (November-February): Root mean square error (RMSE) of hourly sums in Whm^{-2}. The model numbers refer to Table 3.1a.

	Berg	Luleå	Borl	Stock	Norrk	Lund	Schle	Hamb	Braun
Mod 1	22.1	23.3	16.5	12.8	14.1	17.8	25.5	19.8	29.0
Mod 2	21.7	28.9	36.5	33.1	31.1	41.1	20.9	24.4	24.6
Mod 3	14.6	23.4	23.0	20.9	20.1	29.8	18.5	15.5	22.4
Mod 4	27.0	30.5	18.0	16.0	18.4	18.7	29.9	24.2	32.7
Mod 5	22.5	32.6	17.2	15.4	17.4	19.7	25.1	20.4	28.5
Mod 6	14.0	19.8	23.8	20.5	18.9	29.2	17.5	15.5	21.4
Mod 7	14.3	20.5	21.1	13.9	15.6	23.9	16.9	14.6	23.0
Mod 8	26.1	19.3	16.2	12.8	13.7	15.9	28.7	22.0	31.9
Mod 9	32.8	26.1	19.6	17.2	19.1	17.4	33.1	26.7	35.7
Mod 10	14.8	22.2	27.4	24.3	22.5	33.0	16.4	17.2	20.6
Mod 11	13.8	21.4	27.9	24.8	22.6	33.2	16.4	18.1	21.5
Mod 12	20.5	28.2	38.5	35.7	32.8	43.2	24.8	28.4	29.7
Mod 13	14.4	23.0	30.2	27.1	24.5	35.0	17.9	20.4	23.1
Mod 14	29.2	28.7	16.4	14.1	17.4	18.0	26.0	20.9	28.6
Mod 15	14.1	21.8	28.1	24.8	22.5	33.2	16.3	17.8	21.0
Mod 16	12.3	19.4	24.2	20.7	18.5	29.1	15.0	15.2	20.4
Mod 17	12.8	19.9	25.3	22.4	20.3	31.2	15.5	16.2	20.1
Mod 18	16.1	24.9	32.8	30.8	27.9	39.0	21.1	24.1	24.8
Mod 19	19.5	21.7	15.6	11.6	12.5	19.7	18.9	14.8	23.4
Mod 20	27.9	21.3	10.1	11.7	13.6	14.7	22.9	13.7	21.8
Mod 21	18.3	16.5	15.0	10.9	10.4	18.4	21.3	15.3	25.4
Mod 22	20.6	18.0	14.6	10.4	10.9	17.6	21.4	15.8	25.1
Mod 23	17.8	19.9	15.8	11.9	11.9	20.1	17.9	13.6	22.2

Table 3.5b (continued)

	Geis	Stutt	Hohen	Carp	Alba	Edmon	Mean
Mod 1	27.5	22.2	18.9	45.8	15.4	27.3	21.6
Mod 2	21.3	28.0	39.8	30.6	45.2	20.3	28.0
Mod 3	18.2	18.8	23.8	42.8	34.4	23.8	20.7
Mod 4	31.7	25.1	18.2	50.8	14.2	36.6	25.6
Mod 5	27.2	21.7	18.9	47.4	16.1	40.5	23.8
Mod 6	17.6	18.7	24.3	46.0	33.3	18.8	19.7
Mod 7	19.8	20.5	27.7	34.2	24.1	20.2	19.1
Mod 8	30.2	24.2	15.3	53.9	11.4	24.8	22.0
Mod 9	35.0	27.7	18.6	53.5	11.4	33.2	26.7
Mod 10	16.5	21.0	28.8	33.6	35.8	16.1	21.2
Mod 11	16.6	23.2	30.1	28.1	32.8	14.3	21.3
Mod 12	24.2	34.3	42.1	28.0	39.9	17.5	30.1
Mod 13	17.8	26.0	33.0	27.0	31.8	16.7	23.1
Mod 14	28.3	21.4	15.6	41.4	11.1	37.5	23.5
Mod 15	16.5	22.4	30.0	31.5	33.7	14.1	21.2
Mod 16	15.8	20.6	26.4	31.0	27.3	15.1	18.9
Mod 17	15.5	20.9	26.4	28.9	30.7	13.9	19.6
Mod 18	19.4	29.0	33.2	25.4	33.6	15.0	25.4
Mod 19	21.5	16.5	13.8	36.0	11.9	29.3	18.1
Mod 20	19.6	18.3	19.1	40.7	10.5	24.9	18.6
Mod 21	23.3	20.6	16.3	47.9	15.4	25.9	18.1
Mod 22	23.2	18.8	14.6	40.8	13.4	22.1	18.1
Mod 23	19.6	17.4	16.6	36.5	14.6	24.3	17.4

Table 3.5c Comparison between calculated and observed atmospheric radiation for cloudless sky at various sites in winter (November-February): Correlation coefficient (R) between modelled and observed hourly sums. The model numbers refer to Table 3.1a.

	Berg	Luleå	Borl	Stock	Norrk	Lund	Schle	Hamb	Braun
Mod 1	.796	.819	.757	.893	.908	.808	.814	.847	.632
Mod 2	.797	.819	.756	.890	.905	.805	.814	.845	.636
Mod 3	.788	.819	.757	.891	.911	.816	.808	.848	.615
Mod 4	.797	.819	.756	.890	.905	.805	.814	.845	.636
Mod 5	.798	.816	.753	.884	.901	.799	.814	.840	.640
Mod 6	.797	.817	.755	.892	.905	.804	.814	.843	.638
Mod 7	.796	.819	.757	.893	.908	.808	.814	.847	.632
Mod 8	.825	.832	.796	.915	.928	.829	.838	.876	.686
Mod 9	.831	.837	.806	.920	.933	.835	.842	.882	.699
Mod 10	.812	.825	.776	.903	.918	.818	.827	.862	.662
Mod 11	.827	.832	.794	.914	.927	.828	.837	.875	.685
Mod 12	.833	.835	.800	.916	.929	.829	.841	.878	.693
Mod 13	.833	.835	.798	.914	.928	.827	.841	.876	.691
Mod 14	.833	.841	.811	.922	.935	.837	.846	.886	.710
Mod 15	.826	.830	.786	.909	.922	.822	.834	.868	.674
Mod 16	.830	.833	.794	.913	.927	.826	.838	.874	.683
Mod 17	.829	.834	.802	.917	.931	.833	.838	.879	.698
Mod 18	.831	.843	.817	.922	.936	.839	.848	.889	.724
Mod 19	.831	.839	.796	.919	.931	.836	.848	.879	.793
Mod 20	.763	.676	.945	.903	.944	.820	.816	.916	.723
Mod 21	.831	.833	.794	.913	.927	.826	.839	.874	.684
Mod 22	.830	.836	.803	.919	.932	.833	.841	.880	.695
Mod 23	.834	.837	.804	.918	.931	.832	.843	.881	.699

Table 3.5c (continued)

	Geis	Stutt	Hohen	Carp	Alba	Edmon	Mean
Mod 1	.683	.717	.784	.551	.774	.908	.799
Mod 2	.683	.719	.785	.556	.773	.915	.799
Mod 3	.678	.706	.777	.539	.775	.893	.795
Mod 4	.683	.719	.785	.556	.773	.915	.799
Mod 5	.682	.721	.785	.563	.771	.924	.798
Mod 6	.683	.720	.785	.556	.772	.882	.798
Mod 7	.683	.717	.784	.551	.774	.908	.799
Mod 8	.754	.755	.820	.622	.836	.914	.831
Mod 9	.772	.764	.826	.633	.860	.918	.838
Mod 10	.720	.739	.805	.595	.799	.915	.816
Mod 11	.753	.755	.820	.618	.838	.918	.831
Mod 12	.765	.760	.825	.623	.862	.927	.836
Mod 13	.764	.759	.824	.618	.865	.930	.835
Mod 14	.787	.772	.826	.642	.885	.928	.844
Mod 15	.739	.747	.815	.601	.834	.924	.825
Mod 16	.754	.754	.821	.610	.852	.925	.831
Mod 17	.765	.764	.824	.640	.844	.918	.836
Mod 18	.802	.780	.820	.660	.900	.935	.848
Mod 19	.861	.806	.848	.816	.887	.942	.858
Mod 20	.748	.800	.852	.424	.877	.923	.834
Mod 21	.754	.754	.821	.612	.851	.925	.832
Mod 22	.767	.762	.825	.630	.853	.914	.836
Mod 23	.773	.764	.826	.630	.870	.927	.839

Table 3.5d Comparison between calculated and observed atmospheric radiation for cloudless sky at various sites in winter (November-February): Ratio between standard deviations of modelled and observed hourly sums. The model numbers refer to Table 3.1a.

	Berg	Luleå	Borl	Stock	Norrk	Lund	Schle	Hamb	Braun
Mod 1	.862	1.358	.928	1.037	1.121	.997	.767	.930	.876
Mod 2	.756	1.248	.809	.930	.998	.889	.663	.806	.739
Mod 3	.553	.763	.611	.635	.691	.611	.521	.631	.656
Mod 4	.895	1.478	.958	1.102	1.182	1.053	.785	.955	.875
Mod 5	.943	1.675	1.001	1.207	1.273	1.139	.809	.989	.869
Mod 6	.643	1.051	.686	.780	.852	.758	.559	.681	.614
Mod 7	.918	1.446	.988	1.081	1.194	1.062	.816	.990	.933
Mod 8	.717	1.104	.764	.870	.952	.864	.699	.812	.747
Mod 9	.784	1.182	.823	.942	1.035	.947	.778	.892	.820
Mod 10	.708	1.134	.760	.869	.941	.847	.664	.790	.729
Mod 11	.826	1.285	.874	1.003	1.095	.995	.796	.927	.850
Mod 12	.968	1.510	.995	1.163	1.270	1.160	.906	1.045	.945
Mod 13	.940	1.484	.955	1.129	1.228	1.123	.859	.993	.891
Mod 14	.960	1.438	.969	1.133	1.245	1.145	.920	1.041	.941
Mod 15	.797	1.278	.833	.971	1.052	.954	.730	.858	.779
Mod 16	.862	1.356	.892	1.039	1.131	1.030	.797	.927	.842
Mod 17	.786	1.219	.831	.961	1.051	.960	.785	.903	.820
Mod 18	.946	1.415	.926	1.107	1.214	1.125	.897	.999	.886
Mod 19	.943	1.416	.922	1.112	1.192	1.095	.875	1.004	.891
Mod 20	.798	1.189	1.107	1.028	1.336	1.183	.877	.933	.959
Mod 21	.759	1.199	.780	.917	.998	.906	.703	.818	.740
Mod 22	.809	1.225	.853	.974	1.070	.975	.799	.919	.844
Mod 23	.898	1.384	.918	1.073	1.174	1.075	.847	.971	.878

Table 3.5d (continued)

	Geis	Stutt	Hohen	Carp	Alba	Edmon	Mean
Mod 1	.930	.967	1.171	.699	1.048	1.049	1.005
Mod 2	.788	.808	.990	.554	.941	.998	.883
Mod 3	.686	.747	.869	.637	.614	.570	.659
Mod 4	.933	.957	1.173	.656	1.115	1.182	1.046
Mod 5	.932	.939	1.170	.593	1.215	1.418	1.109
Mod 6	.656	.669	.825	.444	.809	.740	.739
Mod 7	.991	1.029	1.247	.744	1.116	1.117	1.069
Mod 8	.789	.779	.862	.571	.839	.840	.839
Mod 9	.865	.840	.903	.651	.904	.902	.911
Mod 10	.772	.779	.900	.581	.855	.887	.835
Mod 11	.898	.887	.985	.663	.974	.995	.964
Mod 12	.998	.976	1.083	.695	1.149	1.223	1.105
Mod 13	.942	.922	1.035	.636	1.128	1.235	1.065
Mod 14	.995	.949	1.019	.698	1.112	1.154	1.082
Mod 15	.823	.822	.945	.574	.965	1.035	.920
Mod 16	.889	.879	.991	.622	1.031	1.099	.987
Mod 17	.867	.839	.915	.640	.919	.937	.924
Mod 18	.943	.873	.929	.624	1.096	1.181	1.046
Mod 19	.966	.860	1.030	.501	1.029	1.097	1.054
Mod 20	.853	.883	.895	.609	1.227	1.179	.990
Mod 21	.779	.760	.825	.546	.905	.927	.863
Mod 22	.891	.869	.944	.663	.936	.920	.941
Mod 23	.927	.899	.988	.647	1.058	1.119	1.021

Table 3.6 Coefficient $\alpha_0 \cdot 10^5$ of the cloudless atmospheric emittance ε_0 (= α_0 $(T_s/K)^2$) for various sites. Daytime, nighttime, and diurnal averages are given for the whole year and for summer and winter.

Station	Year		Summer		Winter	
	Day	Night	Day	Night	Day	Night
Bergen	1.014		1.026		1.017	
	1.032	1.007	1.043	1.001	1.006	1.018
Luleå	0.956		0.917		0.980	
	0.922	0.971	0.907	0.912	0.997	0.980
Borlänge	0.925		0.914		0.939	
	0.884	0.944	0.882	0.942	0.899	0.946
Stockholm	0.952		0.951		0.949	
	0.939	0.959	0.938	0.983	0.928	0.952
Norrköping	0.950		0.933		0.959	
	0.923	0.959	0.913	0.952	0.948	0.962
Lund	0.929		0.920		0.921	
	0.918	0.937	0.913	0.930	0.906	0.925
Schleswig	0.997		0.977		1.023	
	0.960	1.013	0.955	0.997	1.010	1.025
Hamburg	0.973		0.962		0.996	
	0.941	0.989	0.945	0.978	0.950	1.005
Braunschweig	0.986		1.035		1.011	
	0.890	1.035	0.897	1.016	0.906	1.042
Geisenheim	0.995		0.974		1.023	
	0.936	1.029	0.943	0.999	0.940	1.050
Stuttgart	0.937		0.915		0.981	
	0.882	0.977	0.874	0.961	0.914	1.003
Hohenpeißenberg	0.900		0.892		0.911	
	0.849	0.915	0.849	0.910	0.865	0.921
Edmonton	0.965		0.927		1.054	
	0.918	1.013	0.902	0.978	1.008	1.080

Table 3.7 Coefficient $\alpha_0 \cdot 10^5$ of the cloudless atmospheric emittance ϵ_0 (= α_0 $(T_s/K)^2$) for various climates. The given coefficients are averages for the stations listed under the respective climate.

Climate* / Stations	Summer	Winter
Dfb Borlänge Stockholm Norrköping Edmonton	0.931	0.975
Dfb (mountainous) Hohenpeißenberg	0.892	0.911
Dfc Luleå	0.917	0.980
Cfb Lund Hamburg Braunschweig Geisenheim Stuttgart	0.946	0.986
Cfb (maritime) Bergen Schleswig	1.002	1.020
Csa Carpentras	0.950	1.058

* In explanation of the climate classification:

Df - Cold snow-forest climate. Constantly moist.
Cf - Mild temperate rainy climate. Constantly moist.
Cs - Mild temperate rainy climate. Dry season in summer.
a - Average temperature > 22°C in warmest month.
b - Average temperature < 22°C in warmest month.
c - Average temperature > 10°C in less than 4 months.

Table 3.8 Atmospheric radiation (whole year) for cloudy sky (cloud amount = 1-8 octas) at various sites. Number of observation hours (N). Means of observed hourly sums (ϕ) and standard deviation (S) in Whm^2.

	Luleå	Borl	Schl	Hamb	Brau	Stut	Mean
N	70959	5516	49680	77316	26351	12281	40350
ϕ(obs)	281.5	300.8	319.3	321.7	321.4	321.6	308.9
S(obs)	52.4	43.7	38.9	41.5	37.5	39.9	43.7

Table 3.9a Comparison between calculated and observed atmospheric radiation (whole year) for cloudy sky at various sites: Mean bias error (MBE = calculated$_{Mod\ i}$ - observed) of hourly sums in Whm^2. The model numbers refer to Table 3.1b.

	Luleå	Borl	Schl	Hamb	Brau	Stut	Mean
Mod 1	-21.1	-14.8	-27.3	-30.5	-22.1	-16.0	-25.1
Mod 2	10.3	19.4	3.3	1.5	10.6	17.1	6.6
Mod 3	5.2	17.3	3.0	1.4	10.7	17.9	5.1
Mod 4	7.6	7.1	-1.1	-3.8	1.8	1.3	1.2
Mod 5	16.5	23.4	9.8	8.1	16.1	22.5	12.9
Mod 6	18.8	29.3	17.3	13.6	20.7	25.4	17.6
Mod 7	3.9	14.9	-4.5	-5.6	5.9	8.9	-.1

Table 3.9b Comparison between calculated and observed atmospheric radiation (whole year) for cloudy sky at various sites: Root mean square error (RMSE) of hourly sums in Whm^2. The model numbers refer to Table 3.1b.

	Luleå	Borl	Schl	Hamb	Brau	Stut	Mean
Mod 1	28.6	24.5	31.7	35.4	31.5	26.0	31.5
Mod 2	24.0	29.4	17.9	19.3	26.3	28.9	21.9
Mod 3	27.4	30.0	19.3	21.1	28.1	31.1	24.0
Mod 4	19.9	20.2	16.1	17.7	21.5	19.6	18.6
Mod 5	26.4	31.4	19.5	20.4	28.1	31.8	23.6
Mod 6	27.0	35.4	24.4	21.4	31.4	33.1	25.7
Mod 7	22.5	24.5	17.7	19.9	23.1	24.9	20.9

Table 3.9c Comparison between calculated and observed atmospheric radiation (whole year) for cloudy sky at various sites: Correlation coefficient (R) between modelled and observed hourly sums. The model numbers refer to Table 3.1b.

	Luleå	Borl	Schl	Hamb	Brau	Stut	Mean
Mod 1	.931	.896	.915	.902	.828	.870	.903
Mod 2	.922	.871	.897	.890	.804	.836	.888
Mod 3	.905	.860	.890	.878	.798	.823	.876
Mod 4	.937	.904	.911	.913	.821	.872	.907
Mod 5	.926	.882	.902	.893	.814	.843	.893
Mod 6	.939	.904	.907	.920	.814	.864	.908
Mod 7	.915	.898	.900	.890	.829	.834	.890

Table 3.9d Comparison between calculated and observed atmospheric radiation (whole year) for cloudy sky at various sites: Ratio between standard deviations of modelled and observed hourly sums. The model numbers refer to Table 3.1b.

	Luleå	Borl	Schl	Hamb	Brau	Stut	Mean
Mod 1	.964	.961	.988	.943	1.038	1.016	.973
Mod 2	1.062	.996	.993	.967	1.052	1.036	1.014
Mod 3	1.191	1.097	1.069	1.043	1.143	1.116	1.108
Mod 4	.922	.834	.880	.836	.870	.847	.874
Mod 5	1.029	.965	.955	.935	1.014	1.005	.979
Mod 6	1.078	1.058	1.042	.997	1.052	1.040	1.040
Mod 7	1.039	.977	.964	.945	1.038	1.026	.992

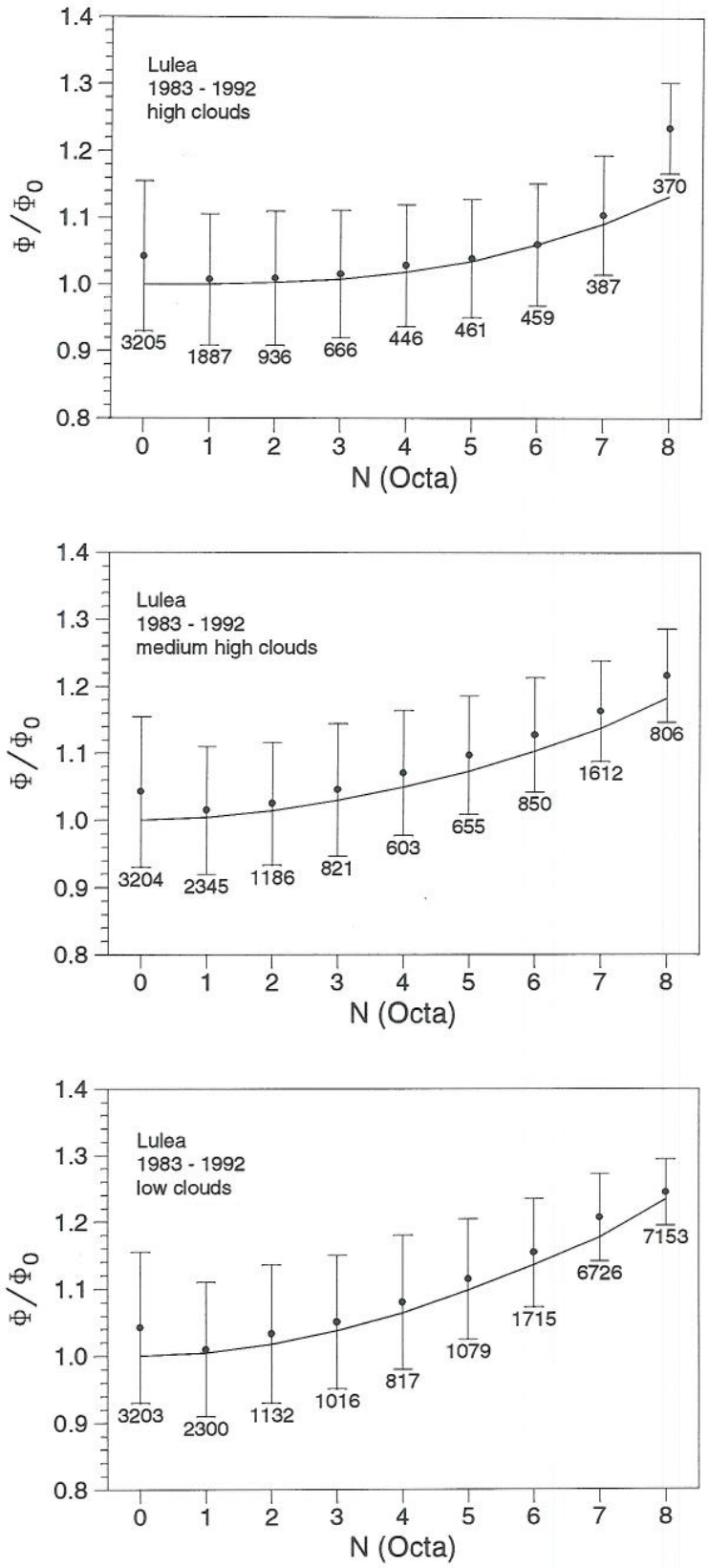

Fig. 3.1 For Luleå, Sweden: Average ratios ϕ/ϕ_0 (with standard deviations given as bars) between hourly irradiation measured (ϕ) for cloud amount N and calculated (ϕ_0) for clear sky by eqn (3.1). Average ratios obtained from eqn (3.2) are given as continous curves, and the number of hours is printed for each cloud amount.

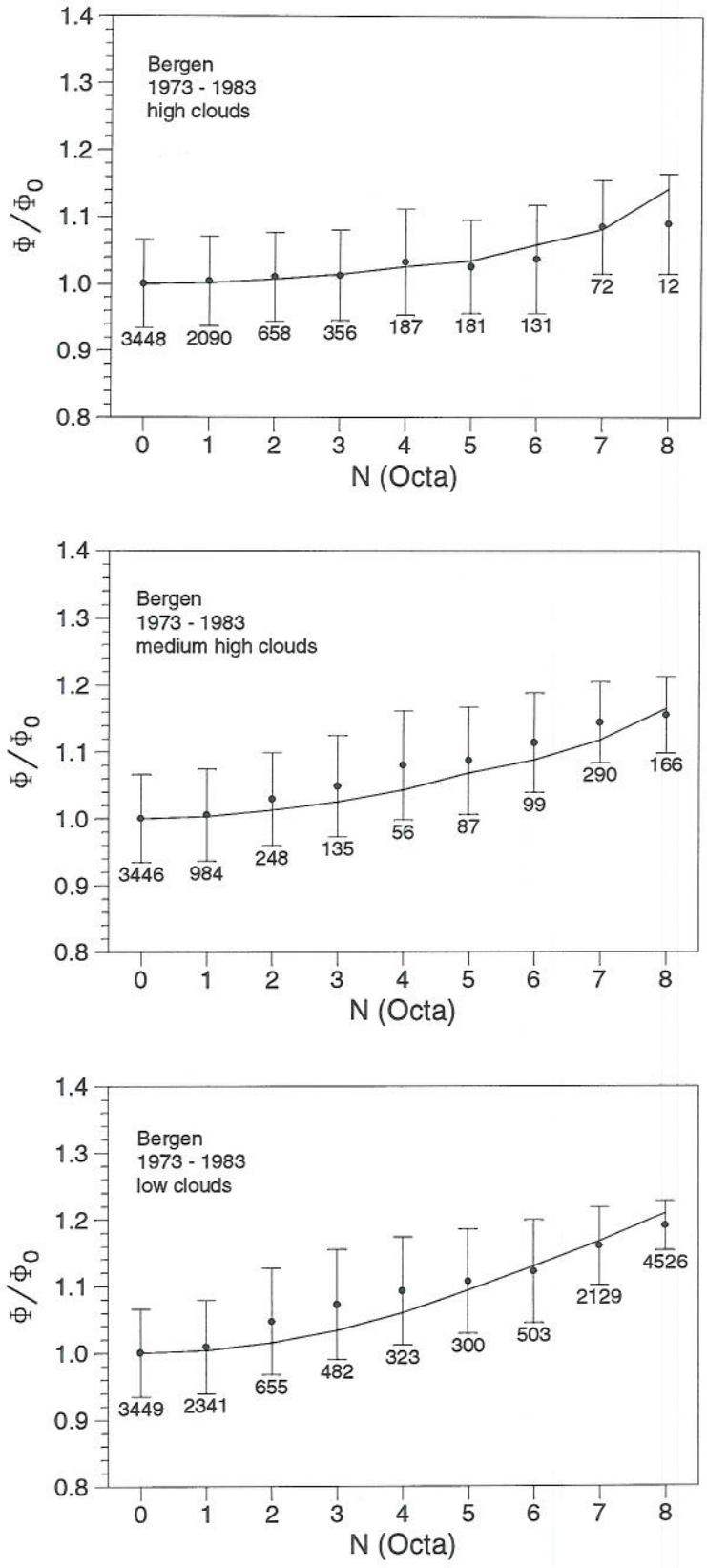

Fig. 3.2 Same as Fig. 3.1 but for Bergen, Norway.

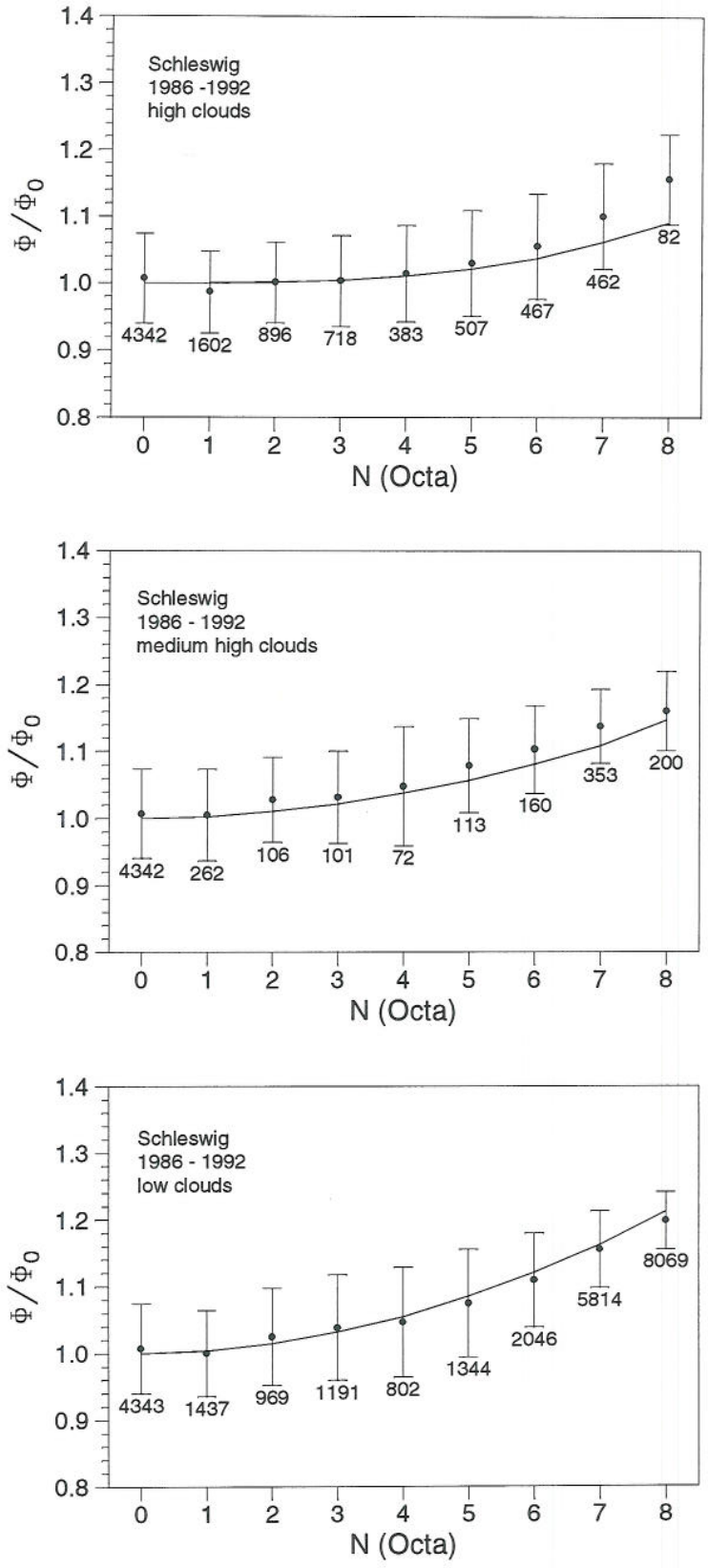

Fig. 3.3 Same as Fig. 3.1, but for Schleswig, Germany.

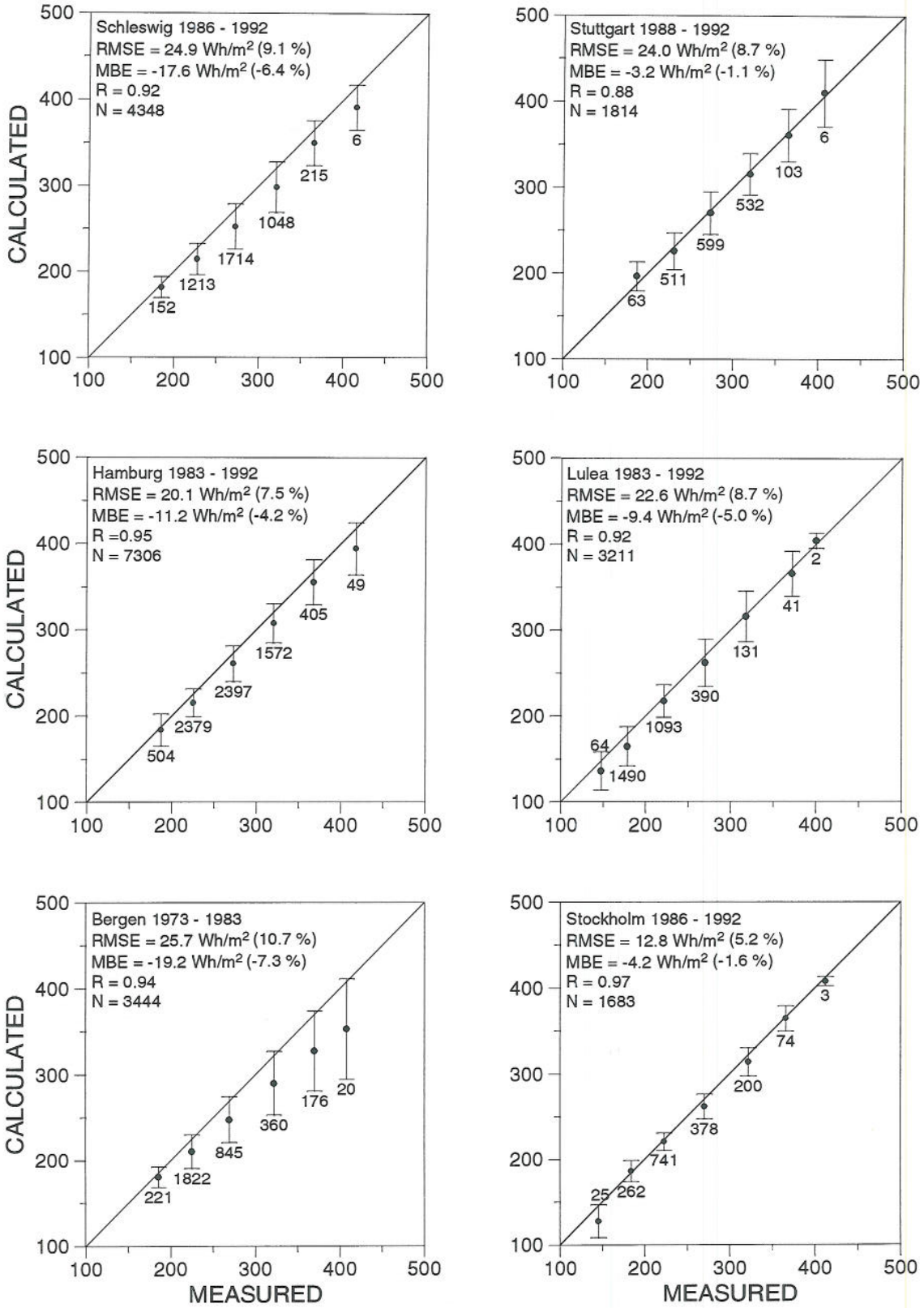

Fig. 3.4 Calculated (Swinbank (1963): effective emittance $\epsilon_0 = 0.936 \times 10^{-5}$ $(T/K)^2$) vs measured group mean values of hourly atmospheric radiation for clear sky (Whm^{-2}) at six stations. Data are grouped into 50 Whm^{-2} intervals of measured radiation, with root-mean-square errors (RMSE) indicated by error bars and number of hours printed for each group. The total number of hours N, overall correlation coefficients R, mean bias errors MBE, and root-mean-square errors RMSE are also printed.

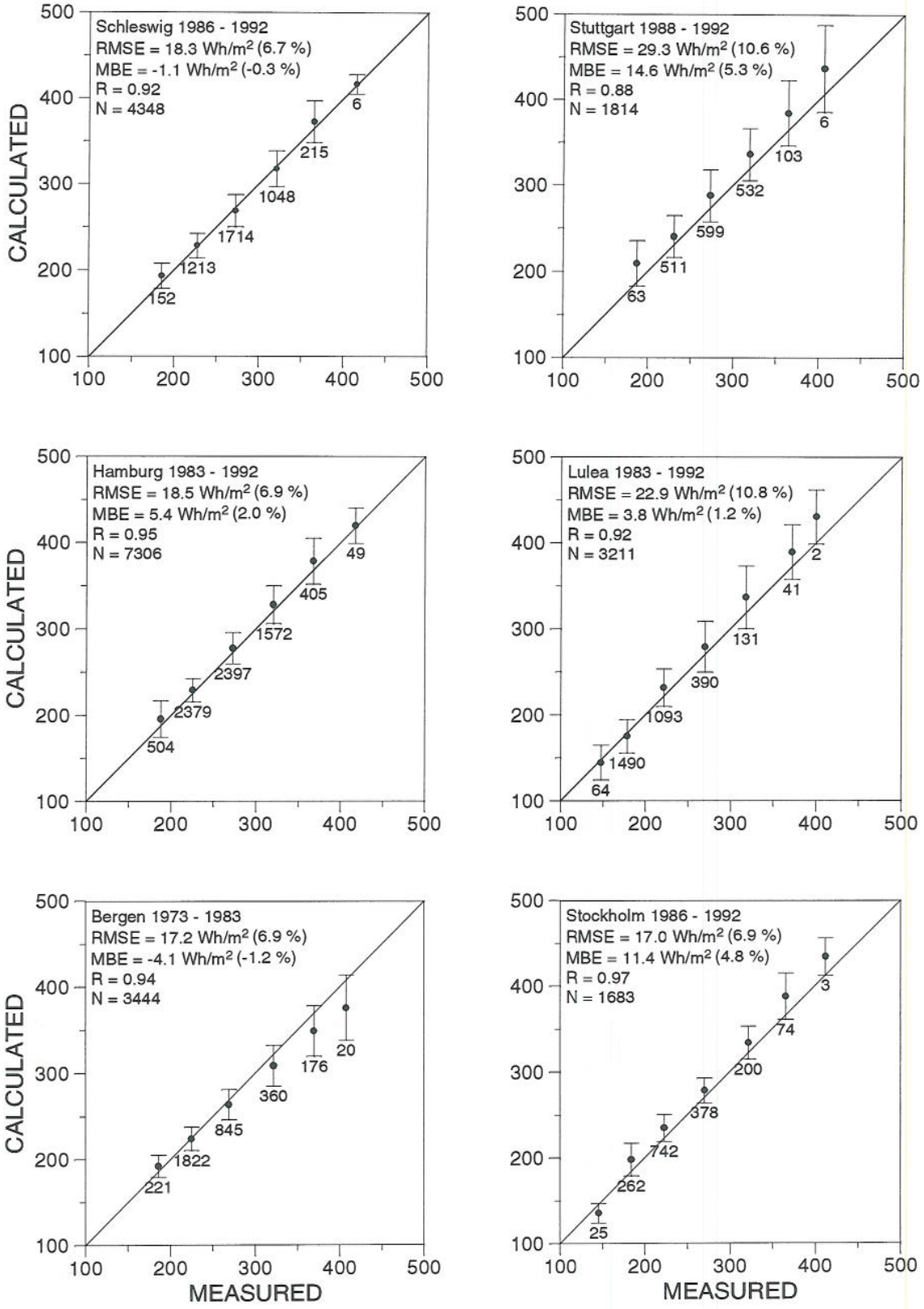

Fig. 3.5a Same as Fig. 3.4, but for calculations by the model of Czeplak and Kasten (1987) (effective emittance $\epsilon_0 = 0.997 \times 10^{-5}\ (T/K)^2$).

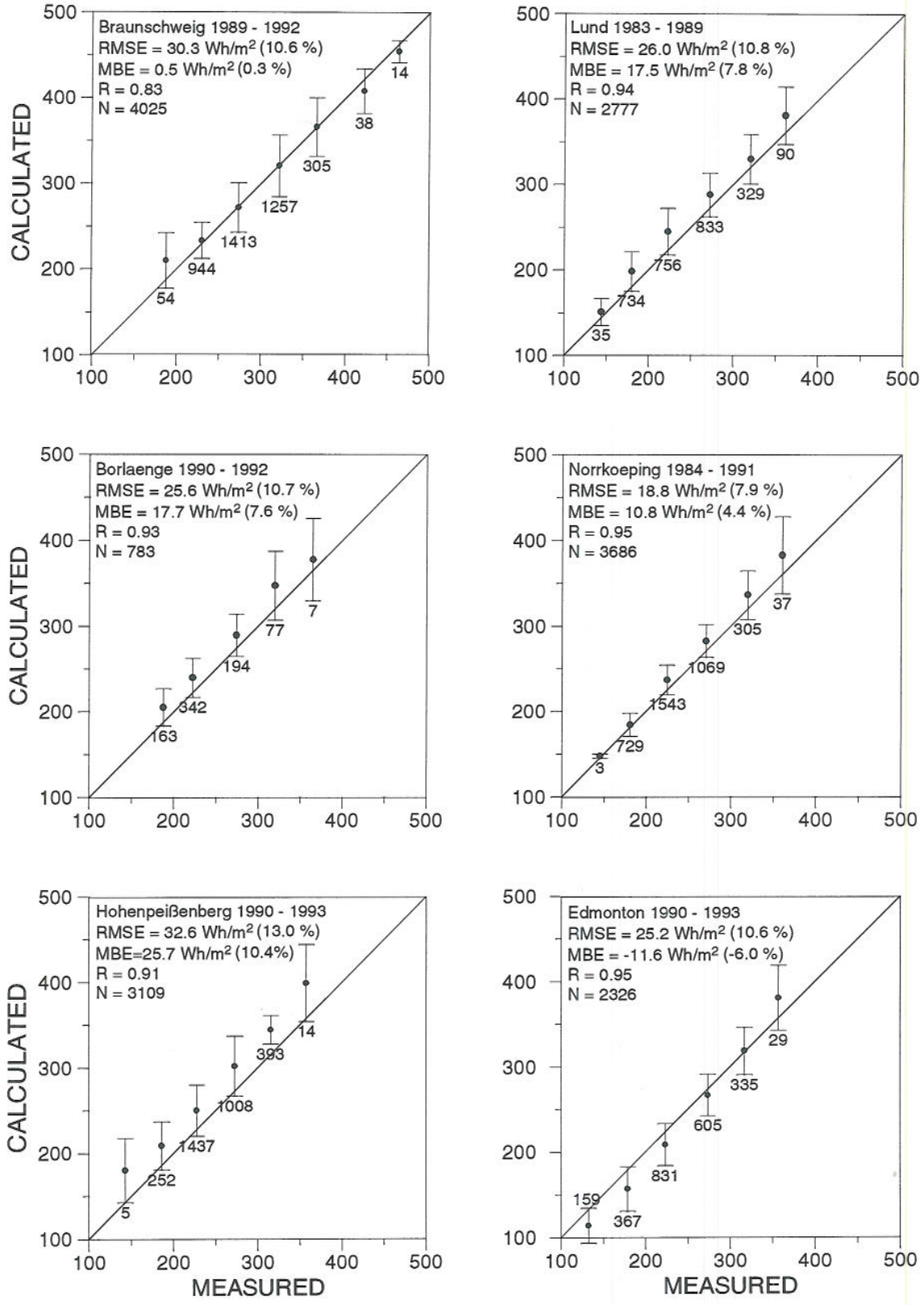

Fig. 3.5b Same as Fig. 3.4, but for calculations by the model of Czeplak and Kasten (1987) (effective emittance $\epsilon_0 = 0.997 \times 10^{-5}\ (T/K)^2$*) for six other stations.*

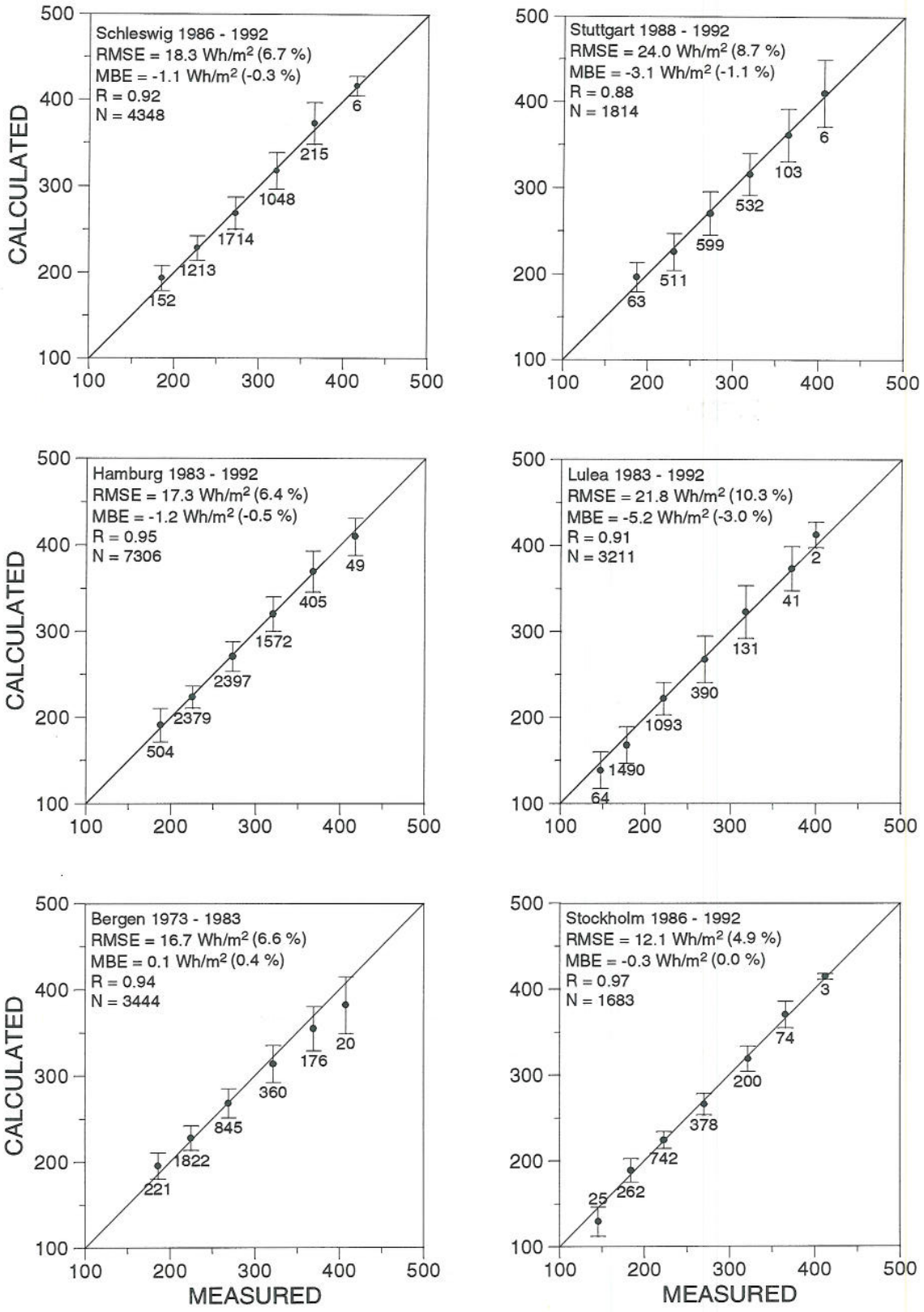

Fig. 3.6 Same as Fig. 3.4, but for calculations with effective emittance $\epsilon_0 = \alpha_0 (T/K)^2$, where α_0 is the annual average diurnal value calculated from the measured data at each station by least square analysis (Table 3.6).

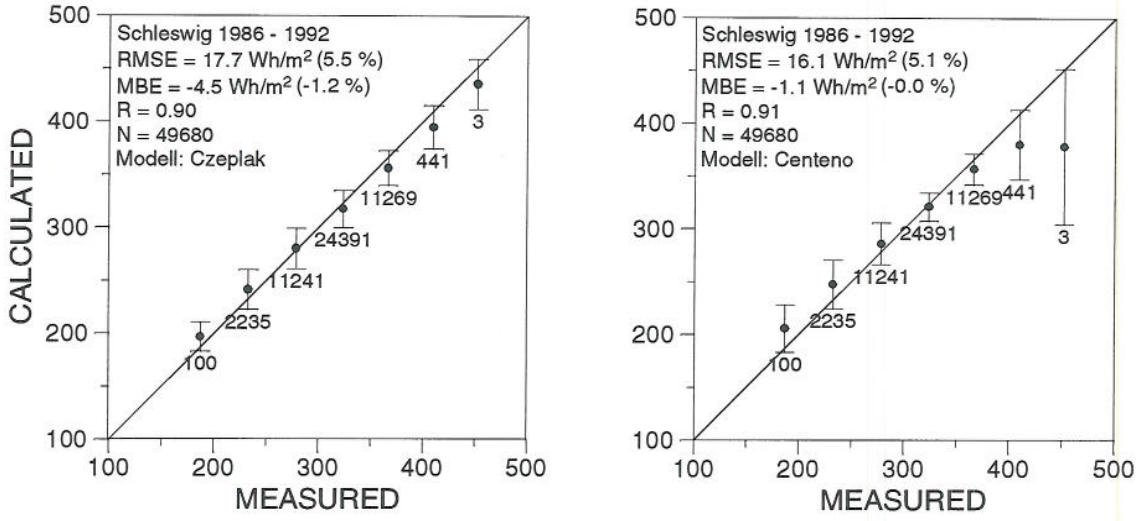

Fig. 3.7 Calculated (left: Czeplak, 1993, right: Centeno, 1982) vs measured group mean values of hourly atmospheric radiation (Whm^{-2}) for cloudy sky (cloud amount = 1-8 octas). The data grouping and the statistical information are similar to that in Fig. 3.4.

CHAPTER 4

A COMPARISON BETWEEN LONGWAVE ATMOSPHERIC IRRADIANCE FORMULAE AND MODTRAN OVER A WIDE RANGE OF CLIMATES

Jan Asle Olseth[1] and Arvid Skartveit

Geophysical Institute, University of Bergen,
Allégt. 70, N-5007 Bergen, NORWAY

[1] Also at The Norwegian Meteorological Institute

4.1 INTRODUCTION

A number of simple formulae for the estimation of longwave atmospheric irradiance from meteorological data, both under cloudless and cloudy skies, are listed in Chapter 2. In Chapter 3, these formulae are tested against measured data from 15 stations representing different climates. In the present Chapter, the same formulae are compared to the output from the spectral model MODTRAN (Kneizys et al 1988) for 6 standard atmospheres ranging from a Tropical to a Sub-Arctic Winter atmosphere, for several modifications of these atmospheres, and for 24 radiosoundings from Schleswig, Germany.

All the simple "cloudless" formulae require surface air temperature as input, while some formulae, in addition, require information about surface air humidity. Some of the simple "cloudy" formulae consist of a "cloudless" formula which is complemented with a cloud formula to account for the irradiance change caused by clouds. In the present paper, all cloudless formulae are compared to MODTRAN without reference to their companion cloud formula and, vice versa, all cloud formulae, for the overcast case only, are compared to MODTRAN without reference to their companion cloudless formula.

4.2 DATA AND RADIATION MODELS

4.2.1 Data

The MODTRAN package is supplied with 6 standard atmospheres: Tropical (Tr), Mid Latitude Summer (MLS), Mid Latitude Winter (MLW), Sub-Arctic Summer (SAS), Sub-Arctic Winter (SAW), and 1976 US Standard (US), each containing 34 layers with specified properties between the earth surface and 100 km altitude. These atmospheres are put together from a variety of sources, and they are intended to represent average seasonal and latitudinal variations of atmospheric properties. The temperature and humidity profiles of these model atmospheres are shown in Figs. 4.1 and 4.3. Table 4.1 gives the air temperatures at the surface, at 1 km, and at 2 km altitudes together with humidity at the surface. To extend the climatic range, the temperature profiles were also modified as shown in Fig. 4.2, and several humidity profiles were combined with these temperature profiles as discussed later.

Table 4.1 Air temperature at the surface (T_s), at 1 km (T_1), and at 2 km (T_2) altitude; dew point temperature (T_{ds}), relative humidity (RH_s), actual water vapor pressure (e_s), and black-body radiation (ϕ_b) at the surface for the 6 standard atmospheres (see text). The last two lines give cloudless irradiance (ϕ_{MODT}) and emittance ($\epsilon_0 = \phi_{MODT}/\phi_b$) calculated by MODTRAN.

	Tr	MLS	MLW	SAS	SAW	US
T_s (K)	299.7	294.2	272.2	287.2	257.2	288.2
T_1 (K)	293.7	289.7	268.7	281.7	259.1	281.7
T_2 (K)	287.7	285.2	265.2	276.3	255.9	275.2
T_{ds} (K)	295.0	289.9	268.6	282.8	254.6	276.6
RH_s (%)	76	76	77	75	80	46
e_s (hPa)	26.2	19.0	4.4	12.0	1.4	7.8
ϕ_b (Wm^{-2})	457	425	311	386	248	391
ϕ_{MODT}(Wm^{-2})	392	348	223	299	174	286
ϵ_0	0.857	0.818	0.718	0.776	0.701	0.732

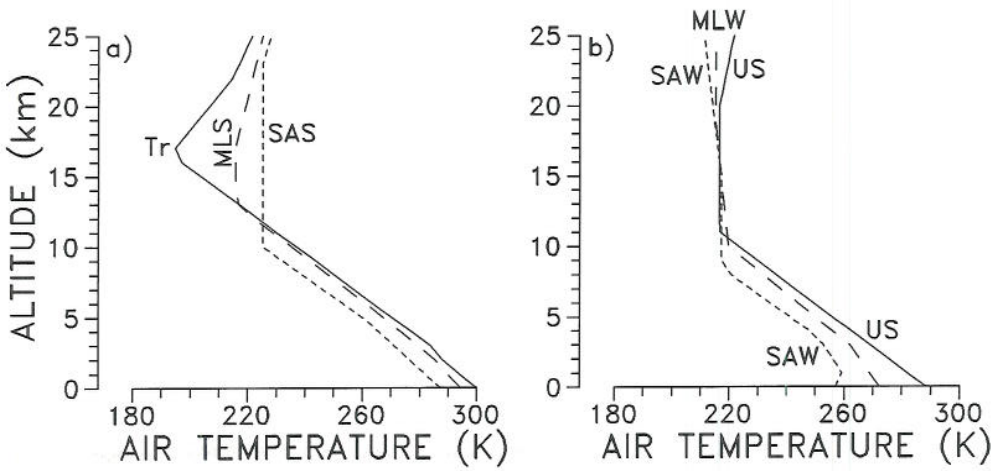

Fig. 4.1 Temperature profiles of the 6 standard atmospheres in the MODTRAN package.

G. Czeplak, DWD Hamburg, kindly supplied longwave atmospheric irradiance data recorded with a Schulze radiation balance meter and simultaneous radiosoundings for 24 cloudless cases at Schleswig (54°30' N, 9°50' E). These 24 cases comprise 10 winter nights, 4 winter days, 6 summer nights, and 4 summer days. The winter cases are characterized by a 1 km thick temperature inversion of 5K/km (Fig. 4.3a) with high relative humidity (70-80%) at the surface, decreasing rapidly with altitude to

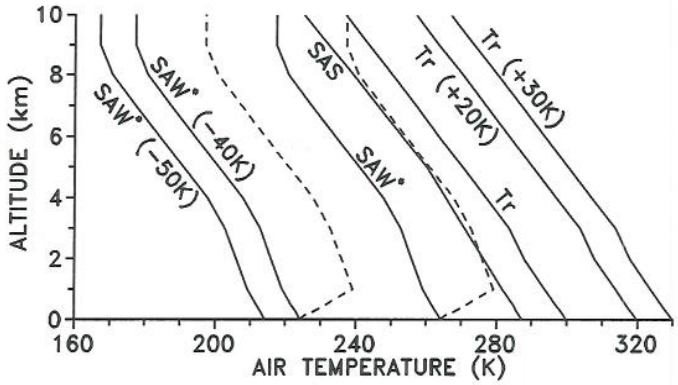

Fig. 4.2 Temperature profiles of the Tropical, the SAS and the modified SAW (-5K/km from 0 to 1 km altitude) atmospheres and of two hot atmospheres (Tropical +20K/+30K), two cold atmospheres (modified SAW -40K/ -50K), and two atmospheres (modified SAW ± 20K, dashed curves) with a 1km deep 15K/km inversion.

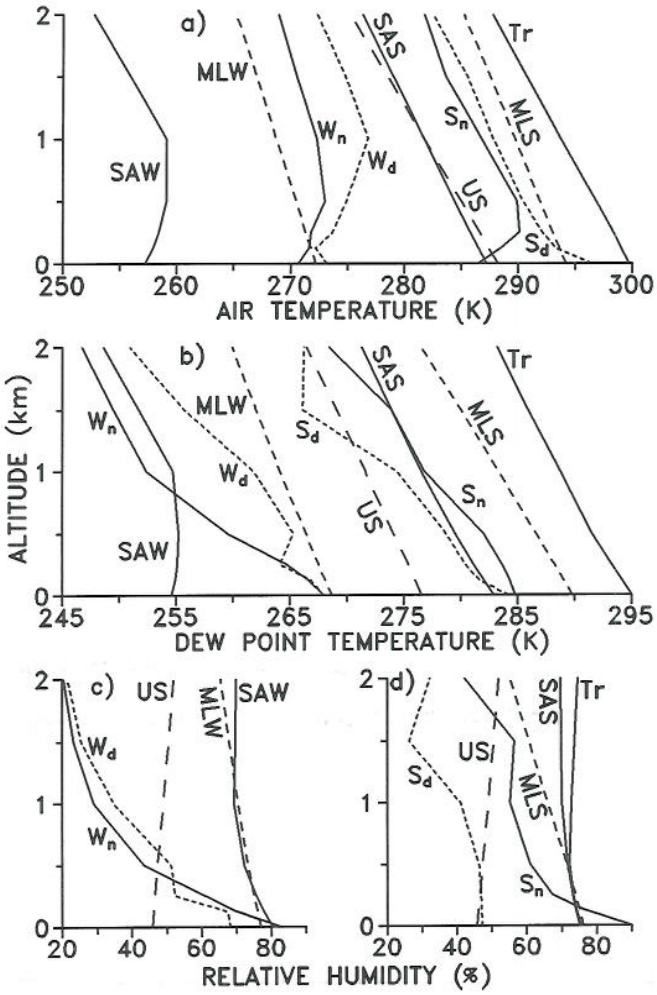

Fig. 4.3 Profiles of temperature (a), dew point (b), and relative humidity (c and d) within the lowest 2 km of the 6 standard atmospheres (Tr, MLS, MLW, SAS, SAW, and US) and of the average of, respectively, 10 winter nights (W_n), 4 winter days (W_d), 6 summer nights (S_n), and 4 summer days (S_d) under cloudless sky at Schleswig, Germany.

20% at 1.5-2 km (Fig. 4.3c). At the summer nights more shallow (200-300 m) and stronger (15K/km) inversions prevail, with a similar, but not that strong humidity decrease with altitude (from 90% at the surface to about 50% at 1.5-2 km). The summer days are characterized by a shallow ($\approx$ 100 m) surface layer with a temperature gradient of -25K/km, and the relative humidity varies from 50% at surface to 30% at 2 km. Except right at the surface and during the summer nights, Fig. 4.3 shows that the atmosphere at Schleswig may have even lower relative humidity than the dry US atmosphere. At altitudes above some 15-20 km, where sounding data are missing, the air temperatures and dew points of the US Standard Atmosphere are used. Data other than temperature and dew point are also taken from the US Standard Atmosphere.

4.2.2 The profile-based model (MODTRAN).

The MODTRAN model (Berk et al 1989) of the Phillips Laboratory/Geophysics Directorate, formerly the Air Force Geophysics Laboratory, is a 2 cm^{-1} resolution version of LOWTRAN 7 (Kneizys et al 1988). The absorption by atmospheric molecules are treated as a function of temperature and pressure for the following species: water vapor, carbon dioxide, ozone, nitrous oxide, carbon monoxide, methane, diatomic oxygen, nitric oxide, sulphur dioxide, nitrogen dioxide, ammonia, nitric acid, and diatomic nitrogen. Atmospheric aerosol and clouds are also accounted for in a detailed manner. In this report, MODTRAN was run without multiple scattering.

MODTRAN calculates spectral radiances. Irradiances (3-100 μm) may be obtained by weighting radiances from selected zenith angles θ_z as outlined by Stamnes et al (1988). For all 6 standard atmospheres it turned out that irradiances based on 20 different θ_z differed by less than 1% from those based on one single θ_z (53°), and by less than 0.4% from those based on three θ_z. In this paper, we take the radiances at θ_z = 27.5°, 60°, and 83.5°, multiply them by $2\pi \cos\theta_z$, and subsequently add them with the weights 0.2778, 0.4444, and 0.2778, respectively.

The irradiance at the surface strongly depends on the boundary layer temperature and humidity profiles. MODTRAN was therefore run both with the original vertical resolution (0 km, 1 km, 2 km, ...), and with three additional levels (0.125, 0.25, and 0.5 km) within the lowest km. For all 6 atmospheres, except the SAW atmosphere, the irradiance increased when using these additional levels (Tr: +2.4%, MLS: +1.7%, MLW: +1.3%, SAS: +2.1%, SAW: -0.1%, US +2.5%). Negligible changes were obtained by using additional levels. The lowest km was therefore resolved by a (0.0, 0.125, 0.25, 0.5, 1.0 km) grid in our MODTRAN runs.

MODTRAN offers different aerosol models for different atmospheric layers. The introduction of "background" tropospheric and stratospheric aerosol above 2 km altitude, and rural aerosol with 23 km surface visibility below 2 km, yielded a moderate irradiance increase compared to the aerosol-free case (Tr: +0.5%, MLS: +0.6%, MLW: +1.3%, SAS: +0.9%, SAW: +1.5%, US +1.1%). Rural aerosol with 5 km surface visibility below 2 km altitude, yielded a threefold larger irradiance increase. Unless otherwise noted, in this work MODTRAN is run with rural aerosol and 23 km surface visibility below 2 km and "background" aerosol above. For the lowest 2 km, this yields spectral aerosol optical depths of 0.235 and 0.016 at 0.5 μm and 11 μm, respectively. 5 km surface visibility yields spectral optical depths 1.20 and 0.080, i. e. a very heavy aerosol loading.

4.2.3 Surface-based formulae

The simple formulae (Table 4.2) are chosen from those listed in Chapter 2. These formulae require surface air temperature and humidity, and cloud cover as input, and they implicitly rely on some average empirical relation between the surface air temperature and the temperature of the air layers contributing the major part of the irradiance at the surface.

The Swinbank (1963) formula was chosen to exemplify differences between surface-based formulae and MODTRAN, caused by temperature gradients deviating from the average. For this purpose, the dry bulb temperature of each of the six standard atmospheres was modified by an amount decreasing linearly from 7K at the surface to 0K at altitudes Δh equal to 0.125, 0.25, 0.5, and 1 km (Fig. 4.4). The relative humidity was not changed. The difference Δ of the irradiance under the original and under the modified atmosphere was then calculated by MODTRAN and by the Swinbank formula for each of the 6 atmospheres. Fig. 4.5 shows the resulting ratios $\Delta_{MODTR}/\Delta_{Sw}$, and the following equation may be taken as an average for the 6 atmospheres:

$$r_\Delta = \frac{\Delta_{MODTR}}{\Delta_{Sw}} = 1 - \exp[-(\frac{\Delta h}{h_*})^{0.5}] \quad , \tag{4.1}$$

where $h_* = 1.56$ km. Assuming that the Swinbank formula most adequately applies to a slightly stable boundary layer (-5K/km), we propose an interpolation formula to correct for boundary layers deviating significantly from this "normal" boundary layer gradient:

$$\phi_{Sw}(T_s,\Delta T_s,r_\Delta) = r_\Delta\ \phi_{Sw}(T_s) + (1-r_\Delta)\ \phi_{Sw}(T_s+\Delta T_s) \ . \tag{4.2}$$

T_s is the observed surface air temperature, and the boundary layer temperature gradient deviation is

Table 4.2 Simple cloudless sky and cloudy sky formulae and the corresponding equation number in Chapter 2.

Model	Abbrev.	Cloudless (Eqn)	Cloudy (Eqn)
Temperature-dependent formulae			
Swinbank (1963)	Sw	(2.2)	-
Schieldrup-Paulsen (1967)	S-P	(2.3)	-
Idso & Jackson (1969)	I&J	(2.4)	-
Unsworth & Monteith (1975)	U&M	(2.5)	(2.25)
Cole (1979)	COLE	(2.6)	(2.26)
Llebot & Jorge (1984)	LL&J	(2.7)	-
Ineichen et al (1984)	IN	(2.30a)	(2.30b)
Czeplak & Kasten (1986)	C&K	(2.8)	(2.28)
Temperature/humidity-dependent formulae			
Ångström (1915)	A	(2.9)	-
Brunt (1932)	BRUNT	(2.10)	-
Bolz (1949)	BOLZ	-	(2.24)
Efimova (1961, see Budyko, 1974)	E	(2.11)	-
Marshunova (1966, see Shine and Crane, 1984)	M	(2.12)	-
Staley & Jurica (1972)	S&J	(2.13)	-
Feussner (1973)	F	(2.14)	-
Brutsaert (1975)	Bruts	(2.15)	-
Clark & Allen (1978)	C&A	(2.16)	-
Sätterlund (1979)	S	(2.17)	-
$Idso_1$ (1981a)	I_1	(2.18)	-
$Idso_2$ (1981b)	I_2	(2.19)	-
Centeno (1982)	C	(2.22)	(2.27)
Berdahl & Fromberg (1982, night & day)	B&Fr	(2.20)	-
Frank & Püntener (1986)	F&P	(2.21)	(2.28)
Berdahl & Martin (1984) + Martin & Berdahl (1984)	B&M	(2.23)	(2.29)

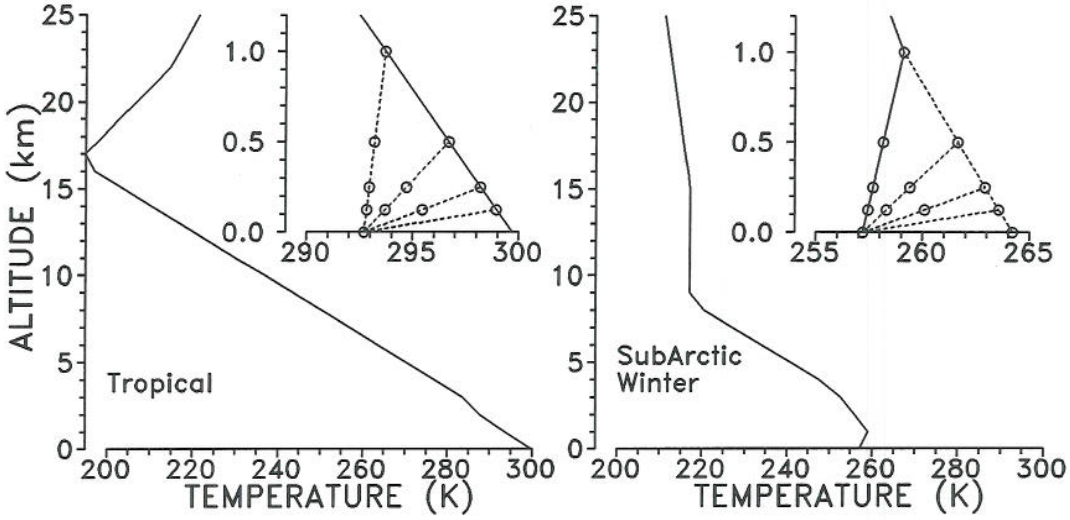

Fig. 4.4 Unmodified temperature profiles of the Tropical and the Subarctic Winter atmospheres. Inserted: four different modified profiles in the boundary layer, where the modifications decrease from 7 K at the surface to 0 K at 0.125, 0.25, 0.5, and 1 km altitude, respectively.

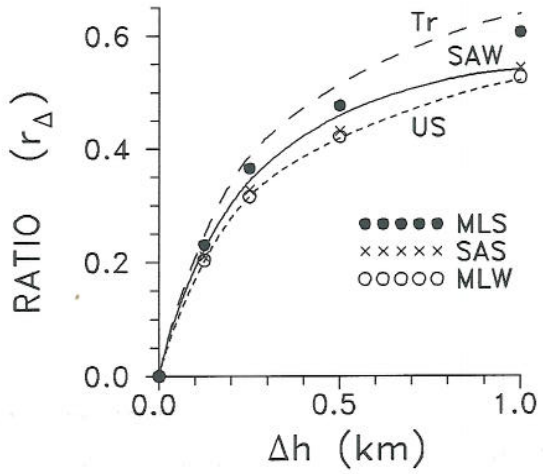

Fig. 4.5 Ratios r_Δ for each of the 6 standard atmospheres, plotted against the thickness Δh of the temperature-adjusted layer. See eqn (4.1) and text for further details.

specified in terms of ΔT_s and Δh, where ΔT_s is the surface air temperature adjustment resulting if a bottom inversion or a superadiabatic layer below an altitude Δh is replaced by a "normally" stratified layer (-5K/km). The Swinbank irradiances (ϕ_{Sw}) on the right hand side of eqn (4.2) are obtained by using Swinbanks formula for the respective temperatures, and r_Δ is obtained from eqn (4.1).

Note that r_Δ and eqn (4.2) are neither sensitive to the choice of -5K/km as the "normal" boundary layer gradient nor to the choice of the Swinbank formula as example. Thus, for the SAW atmosphere, the above Swinbank ratio r_Δ is the median among the corresponding ratios for the 23 simple formulae in Table 4.3, and the individual ratios are all (except for the Idso & Jackson formula) in the range $(1 \pm 0.22)\ r_\Delta$. Thus, eqns (4.1-4.2) can also be used with reasonable accuracy for simple formulae other than the Swinbank formula. They should, however, not be used to correct formulae that implicitly account for variations of the boundary layer temperature gradient. For example, the Idso & Jackson (1969) and Llebot & Jorge (1984) formulae apparently imply a correlation between temperature and temperature gradient, while the Berdahl & Fromberg (1982) and Berdahl & Martin (1984) formulae express the effect of varying temperature gradient in terms of time of day.

4.3 RESULTS

4.3.1 Cloudless sky

MODTRAN was run for the 6 standard cloudless atmospheres. Irradiance and emittance ranged from 392 Wm^{-2} and 0.857 under the Tropical atmosphere to 174 Wm^{-2} and 0.701 under the SAW atmosphere (Table 4.1). MODTRAN was also run in the aerosol-free mode. These results nicely fit the average of 38 profile-based models (Ellingson et al 1991), and the standard deviations for these models reveal a high degree of consistency between such models (Fig. 4.6a).

Irradiances under the 6 standard atmospheres were also calculated with the help of the 23 surface-based formulae in Table 4.2. Note that in the formulae with diurnal variation (Berdahl & Fromberg and Berdahl & Martin), the average for noon and midnight was used. Bias errors of irradiance and emittance are given in Table 4.3a-b. For each of the 6 standard atmospheres, the Mean Bias Errors (MBE) and standard deviations of the temperature-dependent and of the temperature/humidity-dependent formulae are plotted separately (Fig. 4.6b-c). These MBEs cover a wider range than the differences between profile-based models (Fig. 4.6a). Moreover, the MBEs of the temperature-dependent formulae cover a somewhat wider range than the MBEs of the temperature/humidity-dependent formulae.

To elucidate the relationship between emittance and temperature/humidity, MODTRAN and the simple formulae were applied to the temperature profiles in Fig. 4.2. These 9 atmospheres were run with the following humidity modifications: 20, 60 or 100% relative humidity between the surface and 10

Table 4.3a Differences $\Delta\phi=\phi_{formula}-\phi_{MODTRAN}$ (Wm^{-2}) of the irradiance estimated by the cloudless formulae in Table 4.2 ($\phi_{formula}$) and by MODTRAN ($\phi_{MODTRAN}$), for the 6 standard atmospheres. Mean bias (MBE) and root-mean-square (RMSE) errors (or differences) for each formula are given. MBE is also given for each atmosphere.

	Tr	MLS	MLW	SAS	SAW	US	MBE	RMSE
Temperature-dependent formulae								
Sw	-7	-3	-7	-1	-20	18	-4	12
I&J	-4	-1	7	0	21	19	7	12
C&K	15	16	5	16	-11	35	13	19
U&M	-26	-16	-12	-10	-30	9	-14	19
LL&J	-40	-31	10	-12	11	5	-9	22
S-P	-12	3	26	17	19	35	15	21
COLE	-39	-22	-6	-8	-31	10	-16	23
IN	-37	-25	-14	-16	-28	3	-20	23
MBE	-19	-10	1	-2	-9	17	-4	
Temperature/humidity-dependent formulae								
B&M	5	3	-10	-2	-17	0	-3	8
B&Fr	5	8	-4	7	-20	9	1	10
F&P	5	9	1	9	-15	13	4	10
Bruts	8	9	-9	5	-28	3	-2	13
C	-28	-17	-2	-8	-9	1	-10	14
E	9	9	16	11	13	21	13	14
C&A	-5	6	18	15	8	26	11	15
S	5	13	14	17	0	26	12	15
BRUNT	-2	-6	-19	-12	-26	-12	-13	15
A	-37	-24	-13	-16	-16	-10	-19	21
I_1	35	28	15	22	7	21	21	23
F	15	24	22	28	2	36	21	24
M	32	30	18	26	7	30	24	25
I_2	28	33	26	34	8	30	26	28
S&J	45	47	31	45	10	50	38	40
MBE	8	11	7	12	-5	16	8	

Table 4.3b Same as Table 4.3a, but for differences $\Delta\epsilon = \epsilon_{formula} - \epsilon_{MODTRAN}$ (10^{-3}).

	Tr	MLS	MLW	SAS	SAW	US	MBE	RMSE
Temperature-dependent formulae								
Sw	-16	-7	-24	-4	-81	46	-14	40
I&J	-8	-3	21	0	85	49	24	41
C&K	32	39	16	41	-46	90	29	49
U&M	-57	-38	-40	-24	-121	24	-43	61
LL&J	-87	-73	32	-31	43	13	-17	53
S-P	-27	8	83	43	76	88	45	62
COLE	-85	-51	-20	-21	-124	26	-46	67
IN	-80	-58	-46	-40	-112	3	-47	66
MBE	-41	-23	3	-5	-35	42	-9	
Temperature/humidity-dependent formulae								
B&M	12	7	-31	-4	-69	-1	-14	31
B&Fr	11	18	-12	17	-80	23	-4	36
F&P	11	21	2	23	-60	32	5	31
Bruts	18	20	-30	12	-112	8	-14	49
C	-61	-39	-7	-20	-35	3	-27	34
E	19	22	50	29	52	53	38	40
C&A	-11	15	57	38	33	65	33	42
S	10	30	44	44	-1	66	32	39
BRUNT	-4	-15	-62	-31	-104	-30	-41	53
A	-81	-57	-43	-42	-63	-25	-52	55
I_1	76	67	47	56	27	53	54	56
F	34	56	69	73	7	92	55	62
M	69	70	57	67	28	78	62	64
I_2	61	78	82	88	31	77	70	72
S&J	98	111	99	116	38	127	98	102
MBE	17	27	21	31	-21	41	20	

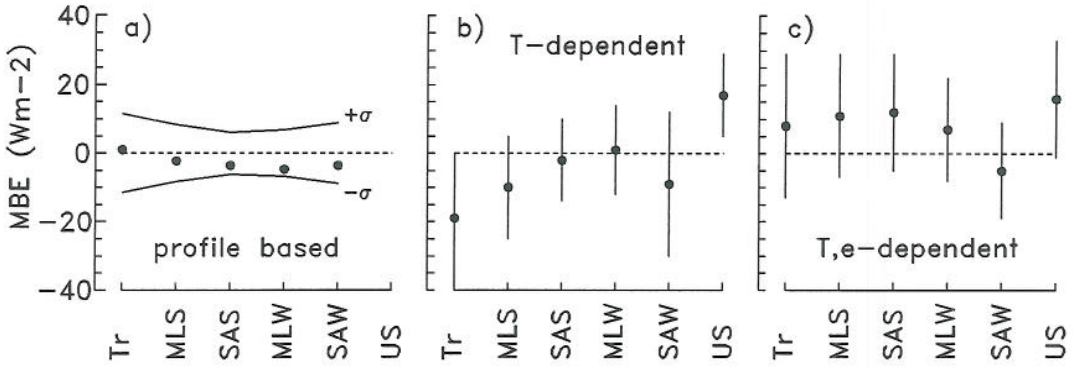

Fig. 4.6 a) Differences (average irradiance from 38 profile-based models minus MODTRAN irradiance). Curves: ± one standard deviation of the individual predictions from the 38 models.
b-c) Mean values and standard deviations of the bias errors (Simple formula minus MODTRAN) of temperature-dependent and temperature/humidity-dependent formulae.

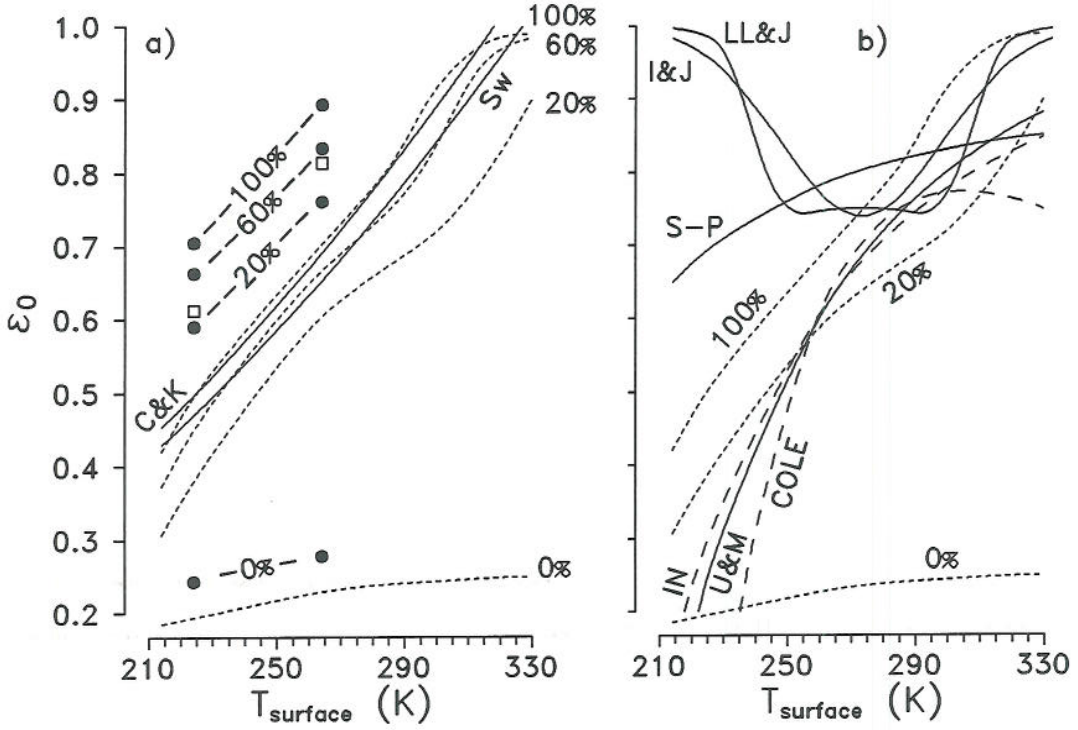

Fig. 4.7 a) Cloudless emittances ϵ_0 predicted by MODTRAN for 100, 60, 20% relative humidity below 10 km, and for a waterfree atmosphere (short dashes: inversion-free cases; long dashes: inversion cases). Predictions by the Swinbank and Czeplak & Kasten formulae (unbroken curves), and by the adjusted Swinbank formula (open squares). See text and Fig. 4.2 for further details.
b) Predictions by 6 different temperature-dependent formulae and the 0, 20, and 100% MODTRAN curves from Fig. 4.7a).

km altitude (and original relative humidities above), or even with zero humidity throughout. Note that all the 7 inversion-free atmospheres have -5 to -6K/km temperature gradient in the lowest km which is regarded as a fairly "normal" stratification.

The substantial greenhouse effect of water vapor is obvious in Fig. 4.7a where the MODTRAN curves for inversion-free cases are drawn by cubic spline interpolation. Over the surface air temperature range 214 to 330K, the vapor-free emittances (MODTRAN) under the inversion-free atmospheres are only 0.19-0.25, while the saturated atmospheres have emittances 0.42-0.99. Over the same temperature range, and humidities ranging from 20 to 100%, the temperature/humidity-dependent formulae yield emittances 0.25-1.65, while MODTRAN predicts 0.31-0.99 (Figs. 4.8-4.9). Among the three temperature/humidity-dependent formulae with the lowest MBEs and RMSEs (Table 4.3), those which express ϵ_0 as a linear function of dew point temperature fit the inversion-free MODTRAN predictions nicely for both 20% and 100% relative humidity (Figs. 4.8a-4.9a). These linear emittance formulae adequately reflect the physics of cloudfree atmospheres with "normal" boundary layer stratification. The remaining formulae (Figs. 4.8-4.9) deviate from MODTRAN predictions more than the above-mentioned formulae, but their response to humidity variations is similar to that of MODTRAN.

The humidity-dependency of ϵ_0, revealed by the inversion-free atmospheres in Fig. 4.2, is corroborated even by the unmodified standard atmospheres, and the two linear ϵ_0 vs. dew point formulae fit the overall inversion-free picture very well (Fig. 4.10). Fig. 4.6b-c shows that for the SAS and the US atmospheres which have approximately equal surface air temperatures, the MBE of the temperature-dependent formulae increases from the SAS to the dry US atmosphere, while the MBE of the temperature/humidity-dependent formulae remains unchanged. This adequate response of the latter formulae to humidity variations is also exemplified in Fig. 4.11 which shows that only the temperature/humidity-dependent Berdahl & Martin formula predicts the same low ϵ_0 for the dry US atmosphere as MODTRAN does, while the temperature-dependent formulae (Swinbank, Idso & Jackson) predict markedly higher ϵ_0. Similarly, Culf & Gash (1993) report that, relative to observations in the Sahel desert region, the MBEs change significantly from the dry to the wet season for temperature-dependent formulae (Swinbank, Idso & Jackson), but remain comparatively unchanged for temperature/humidity-dependent formulae (Sätterlund, Brunt, Brutsaert). In particular, the temperature-dependent formulae (Swinbank, Idso & Jackson) significantly exceed observations during the Sahel dry season (relative humidity $\approx$ 20%) while they reasonably well fit observations during the wet season (relative humidity $\approx$ 90%), thus corroborating the particularly strong dependency on humidity of ϵ_0 at high temperatures (Fig. 4.7a).

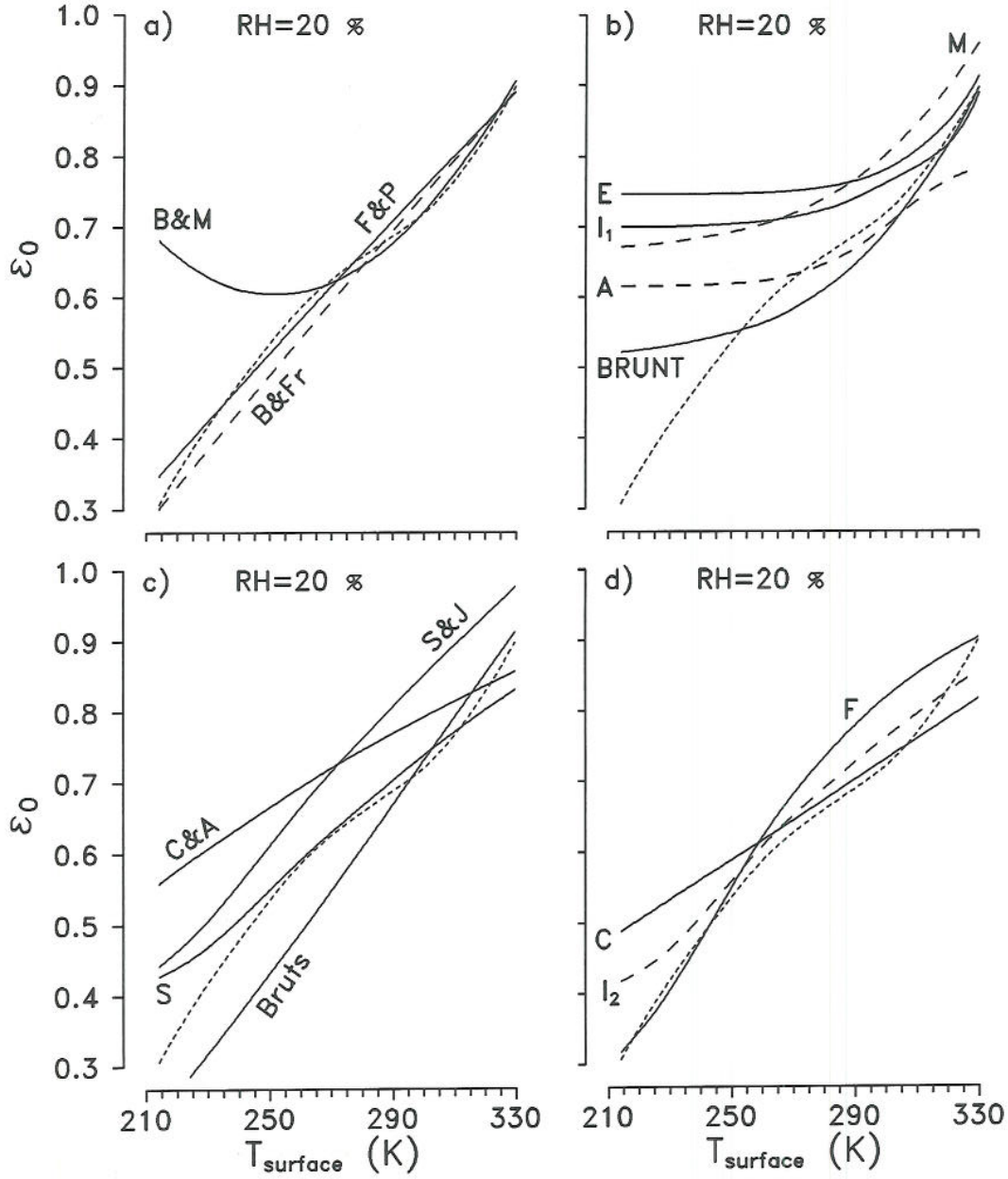

Fig. 4.8 MODTRAN predictions for 20% relative humidity (Fig. 4.7, short dashes), and predictions from 15 temperature/humidity-dependent formulae (Table 4.2, long dashes or unbroken curves), plotted against surface air temperature.

The scatter between temperature-dependent formulae (Fig. 4.7) is least at intermediate temperatures; probably most of the data which the formulae are derived from, have been taken at these temperatures. The Swinbank and the Czeplak & Kasten formulae reasonably well fit the inversion-free MODTRAN predictions for some 60 and 90-100% relative humidity, respectively, over the entire temperature range (Fig. 4.7a). It thus appears that these formulae adequately reflect the radiation

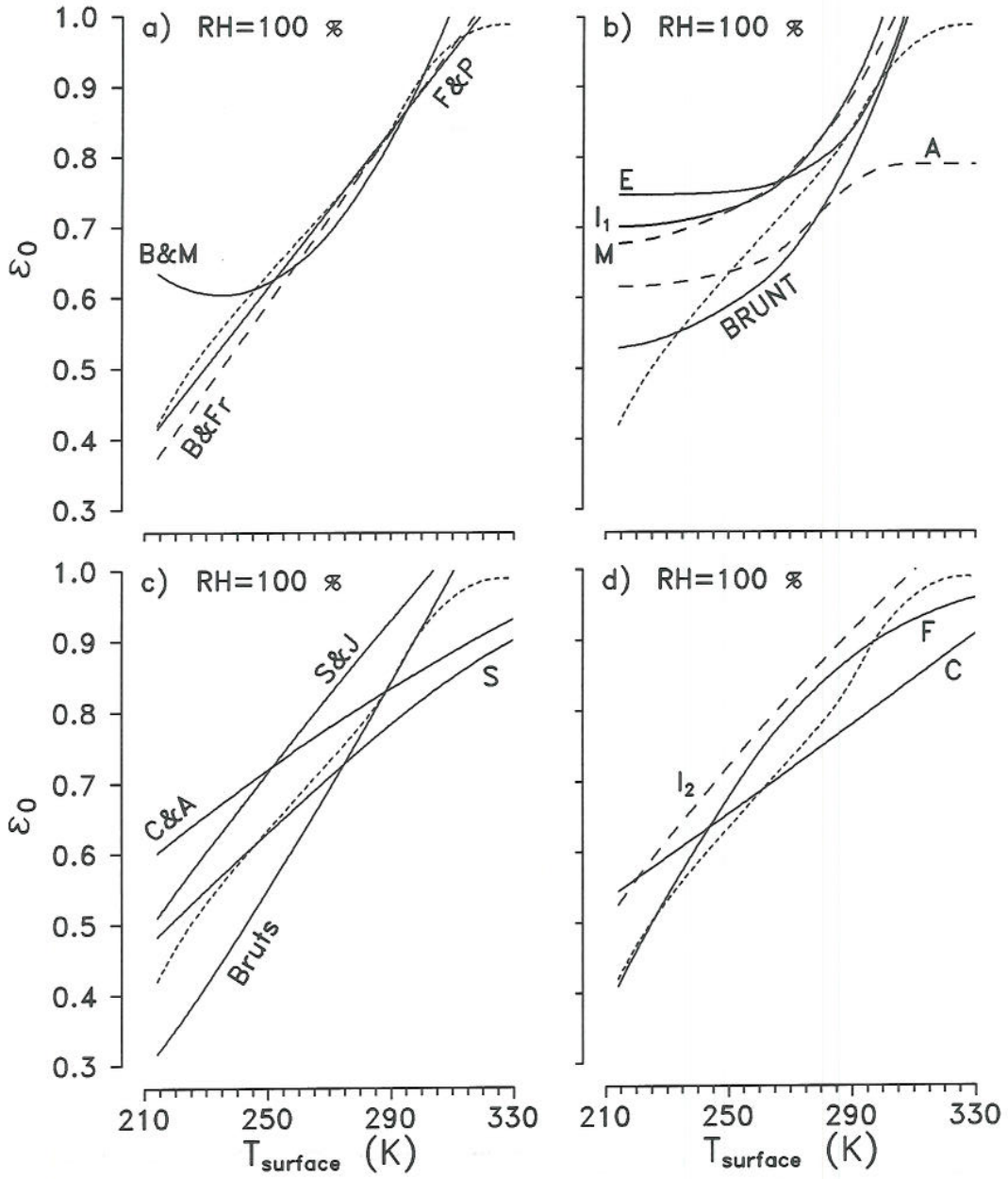

Fig. 4.9 Same as Fig. 4.8, but for 100% relative humidity (temperature = dew point temperature).

physics of cloudless, "normally" stratified, and not too dry atmospheres. Note, however, that these formulae significantly overestimate ϵ_0 under dry and extremely hot atmospheres (desert conditions). The remaining temperature-dependent formulae deviate from MODTRAN predictions more than these two formulae (Fig. 4.7).

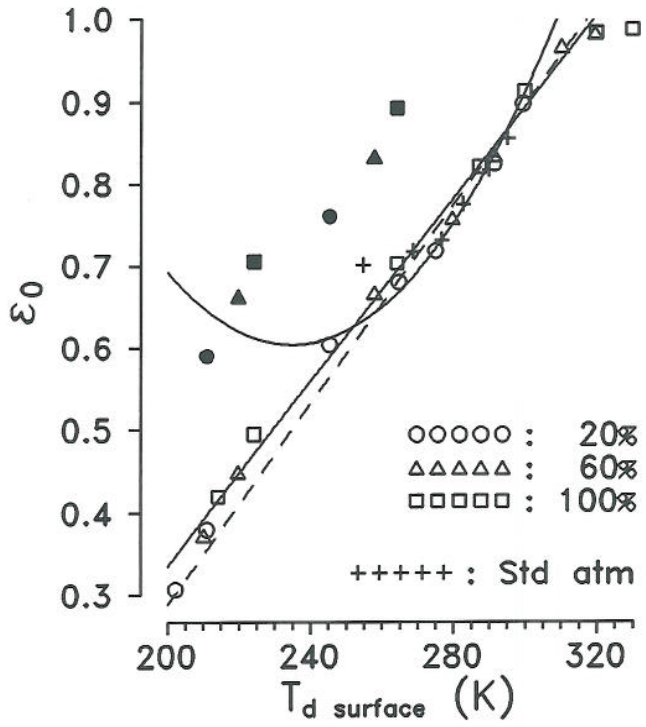

Fig. 4.10 Cloudless emittances ϵ_0 under the 6 standard atmospheres and under the 27 atmospheres from Fig. 4.2 (9 atmospheres and three humidities), plotted against dewpoint temperature. Inversion cases (Fig. 4.2) are plotted as filled symbols, the three formulae from Fig. 4.9a are plotted as curves.

Some of the simple surface-based formulae exceed the inversion-free saturated MODTRAN prediction at low temperatures (Figs. 4.7, 4.9, 4.10), and this fact deserves some comments. The simple formulae are biased towards some average temperature and humidity decrease with increasing altitude in the boundary layer, while MODTRAN explicitly accounts for deviations from such average boundary layer gradients. The modified SAW , the MLW and the SAW atmospheres have 70 - 80% relative humidity and -5.0, -3.5, and 2.0 (inversion) K/km temperature gradient in the lowest km, and are thus examples of such deviations in boundary layer gradients. The MODTRAN emittance exceeds those from the Swinbank and Berdahl & Martin formulae (Fig. 4.11), most in the inversion case (SAW) and least (negligibly) in the "normally" stratified case (modified SAW). The Idso & Jackson (1969) formula, for example, predicts increasing ϵ_0 with temperatures decreasing below 0°C. These authors ascribe this finding to the conversion of water vapor into ice crystals, and they found empirical support for their assumption by observations at Point Barrow, Alaska. An equally probable explanation may be a positive correlation between low temperature and temperature inversion in continental high latitude regions. The MODTRAN predictions (Fig. 4.7a) for the two inversion profiles in Fig. 4.2 demonstrate that inversions can explain a quite considerable increase of the emittance. Note also that our modified Swinbank formula (eqns 4.1 and 4.2), developed from the

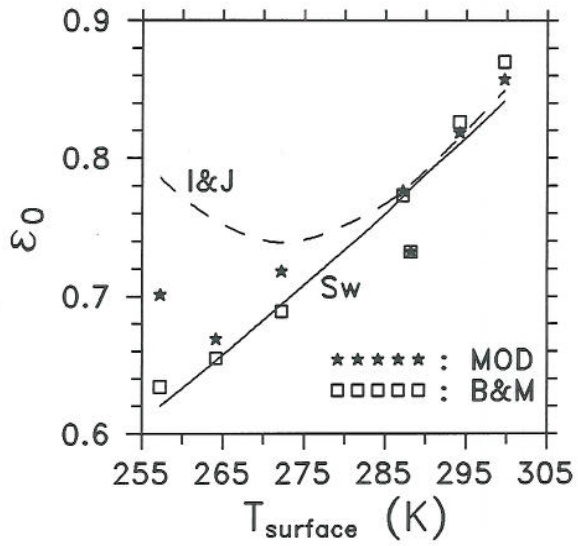

Fig. 4.11 Emittances ϵ_0 predicted by MODTRAN and the Berdahl & Martin formula (symbols) and by the Swinbank and the Idso & Jackson formulae (curves) for 7 atmospheres (from left to right): SAW, adjusted SAW (see text), MLW, SAS, US, MLS, and Tr.

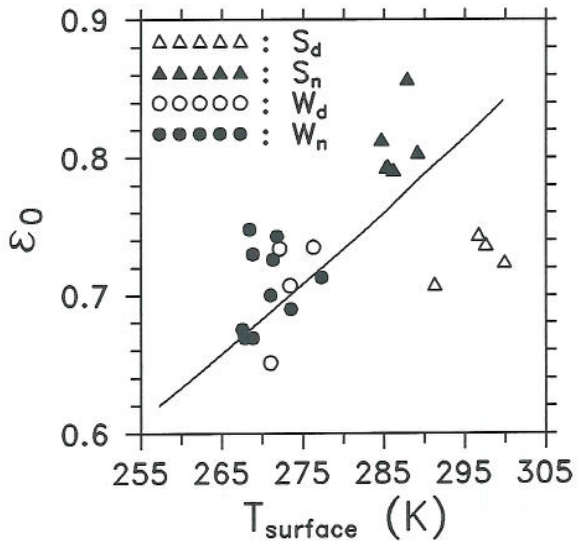

Fig. 4.12 Emittances ϵ_0 predicted by the Swinbank formula (curve) and by MODTRAN (symbols) for summer days (S_d), summer nights (S_n), winter days (W_d), and winter nights (W_n) at Schleswig, Germany.

standard atmospheres, reasonably well fit the MODTRAN predictions for the cold atmospheres with inversion (Fig. 4.7a). Emittances modelled from the Schleswig soundings (Fig. 4.12), however, show that the diurnal variation of the boundary layer temperature gradient explains a wide range of differences of a profile-based model (MODTRAN) and a surface-based formula (Swinbank) even during warm summer months.

Emittances were estimated from the Schleswig soundings by MODTRAN, the Berdahl & Martin formula, the Swinbank formula and the Swinbank formula adjusted for boundary layer gradient according to eqns (4.1) and (4.2). The observed ϵ_0 and those predicted by the three simple formulae are plotted against MODTRAN predictions in Fig. 4.13, while ϵ_0 predicted by MODTRAN and the three simple formulae are plotted against observations in Fig. 4.14. The emittance pairs in Fig. 4.14 are finally plotted as irradiance pairs in Fig. 4.15.

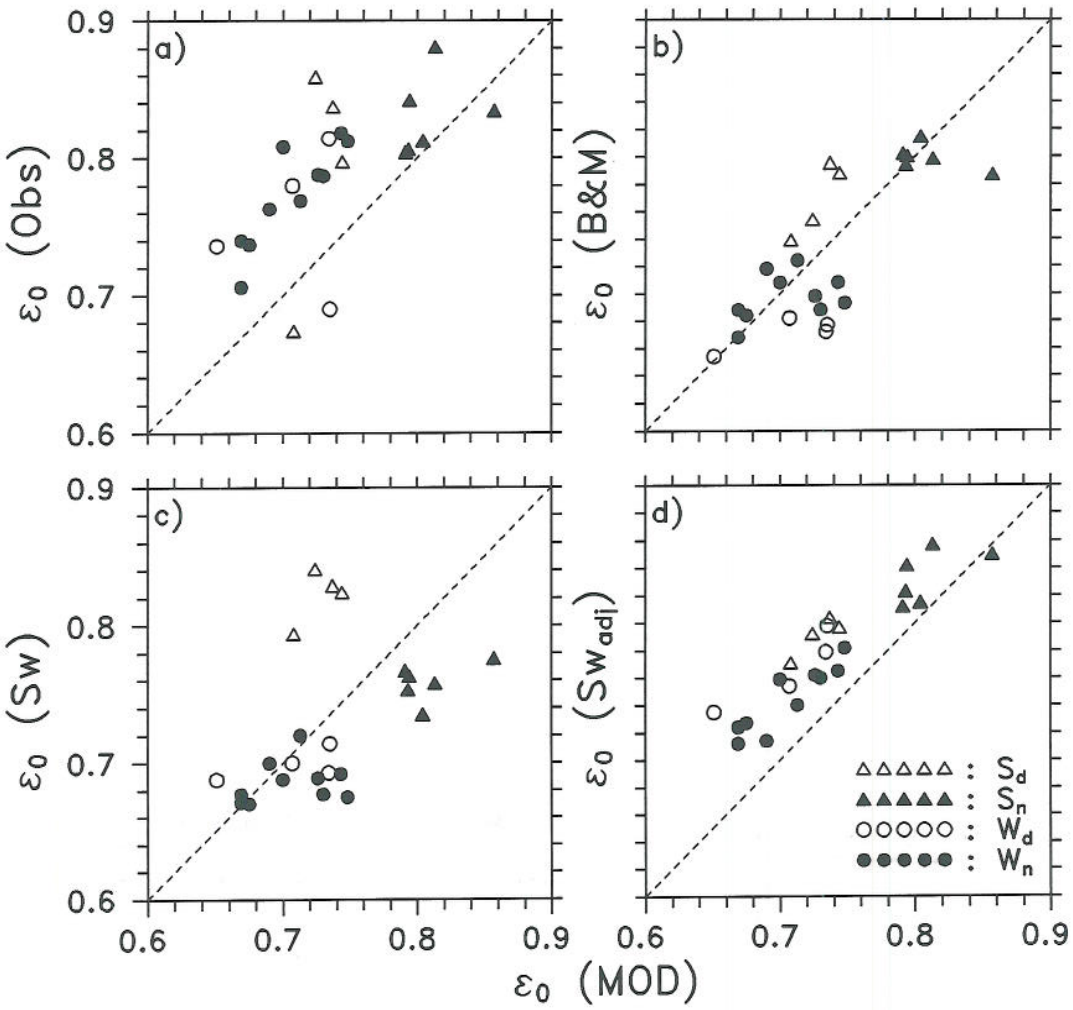

Fig. 4.13 Observed emittances ϵ_0 and predictions from the Berdahl & Martin, the Swinbank, and the adjusted (see text) Swinbank formulae, plotted against MODTRAN predictions (same data and symbols as in Fig. 4.12). The 1:1 line is given as a dotted line.

Plots against both MODTRAN predictions (Fig. 4.13b-d) and observations (Fig. 4.14b-d) show most scatter for the Swinbank formula and least scatter for the adjusted Swinbank formula. This again demonstrates the effect of variations of the boundary layer temperature gradient. To exemplify the effect of humidity profile variations, MODTRAN was run for the two standard winter atmospheres with relative humidity profiles similar to the winter cases at Schleswig (Figs. 4.3c-d). This humidity decrease aloft reduced ϵ_0 by 0.035 (MLW) and 0.044 (SAW), which is less than the modelled effect of diurnal temperature gradient variations in summer at Schleswig (Fig. 4.12).

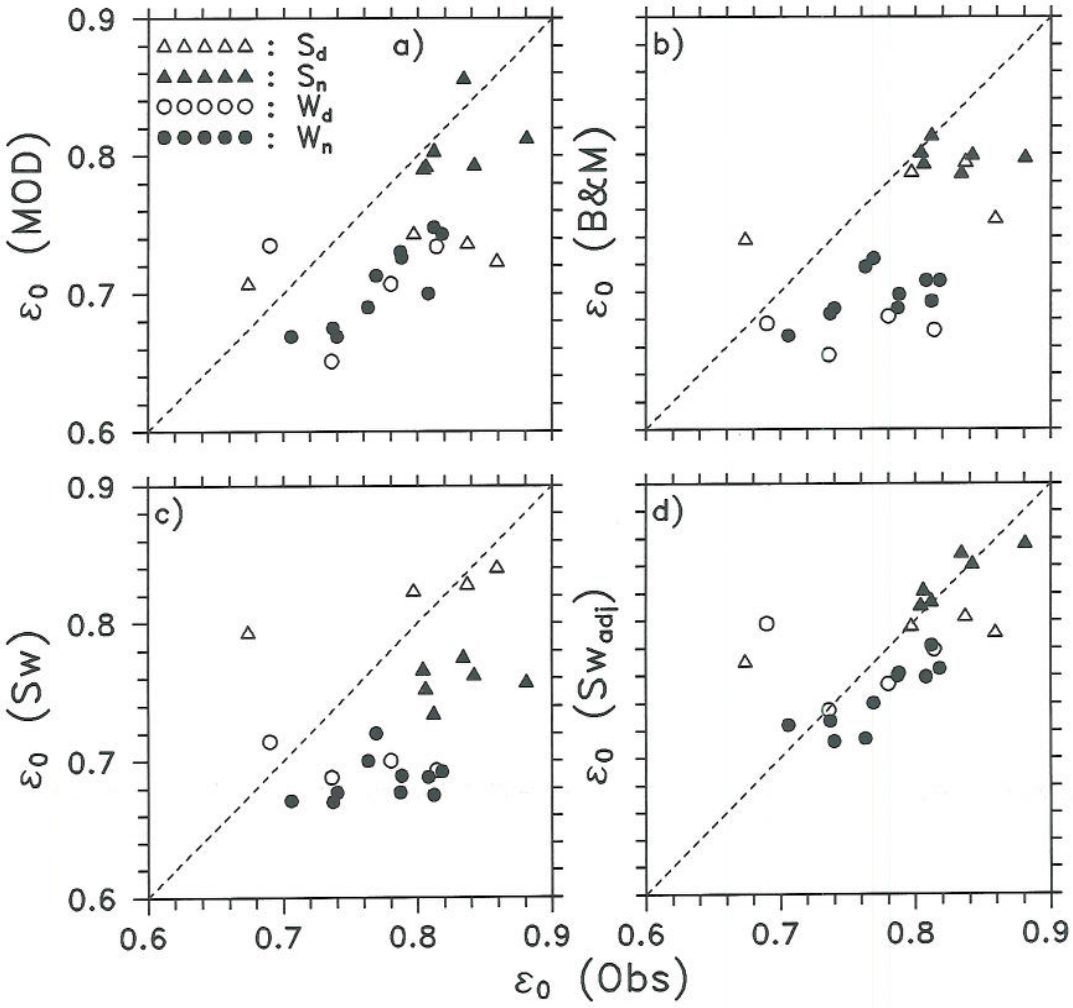

Fig. 4.14 Same Fig. 4.13, but: Emittances ϵ_0 predicted by MODTRAN, and by the Berdahl & Martin, the Swinbank, and the adjusted Swinbank formulae, plotted against observed ϵ_0.

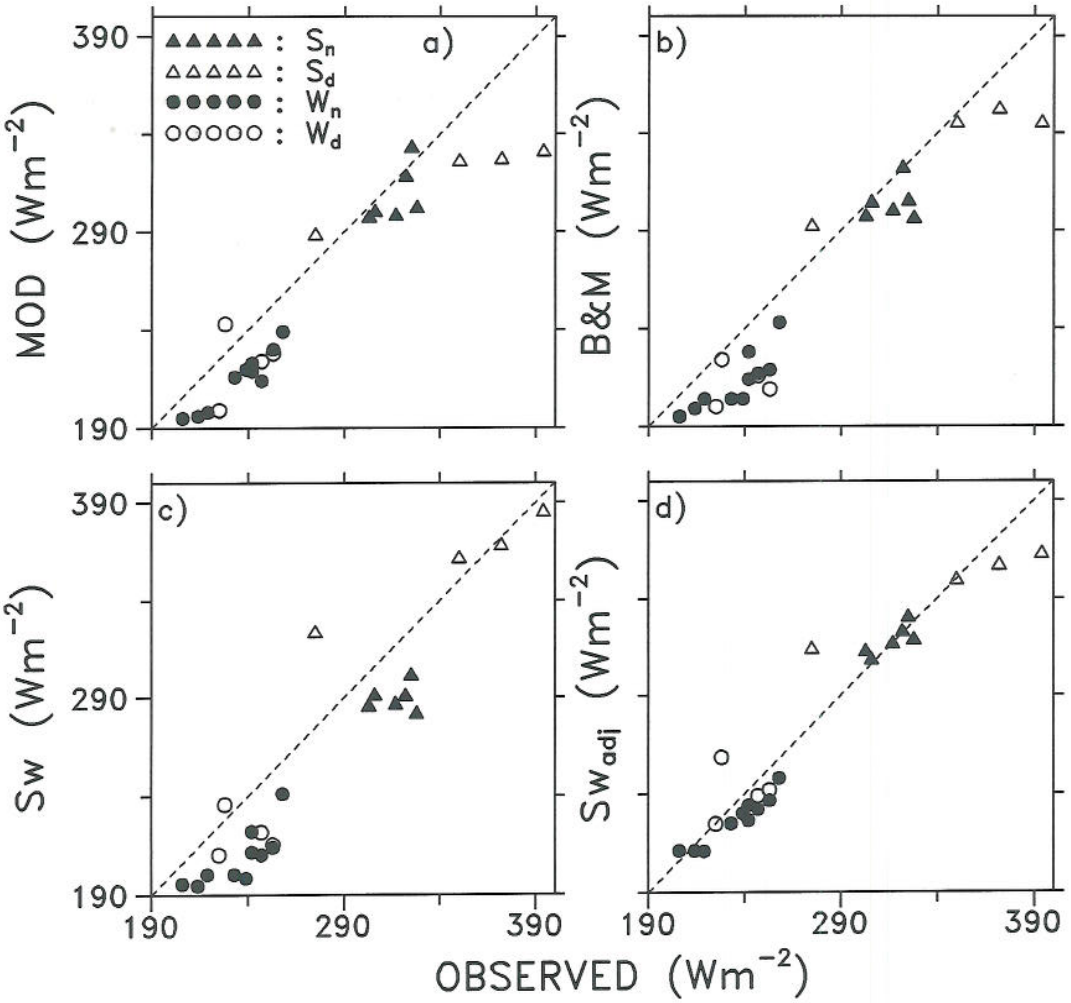

Fig. 4.15 Same as Fig. 4.13, but: Irradiances predicted by MODTRAN, and by the Berdahl & Martin, the Swinbank, and the adjusted Swinbank formulae, plotted against observations.

21 of 24 observed emittances in Fig. 4.13 are higher than the corresponding MODTRAN predictions. The mean differences are 29, 14, 8, and 20 Wm^{-2} for, respectively, summer days, winter days, summer nigths and winter nigths (Table 4.4). This observed excess exceeds the typical differences between MODTRAN and other profile-based formulae (Fig. 4.6a, note that MODTRAN exceeds the average of these models). The excess has therefore to be explained either by MODTRAN deficiencies shared by other profile-based models, or by faults of the cloudless data. The overall mean bias, 18 Wm^{-2}, was reduced to 8 Wm^{-2} by decreasing the surface visibility from 23 to 5 km in the rural aerosol below 2 km altitude (Table 4.4). That is, even such a heavy aerosol loading does not remove the observed excess. However, while aerosol particles of radius 0.1-1 μm are the optically most effective in the solar spectrum, particles of radius 1-10 μm are of greatest importance in the thermal infrared

spectral range (Houghton 1985). The observed excess may thus be due to the existence of more such large particles than implied by the MODTRAN aerosol model. Unnoticed cirrus clouds may be the reason, since the diagnosis "cloudless" is based on routine visual observations.

Table 4.4 Left: Observed cloudless irradiances (Wm^{-2}) at Schleswig, together with irradiances calculated by MODTRAN, the original and the adjusted (see text) Swinbank formula, and the Berdahl & Martin formula. Data are given as averages for summer days (S_d), summer nights (S_n), winter days (W_d), winter nights (W_n), and overall (Ave). Right: Calculated irradiances for the 6 standard atmospheres.

	Schleswig data					Standard atmospheres					
	S_d	S_n	W_d	W_n	Ave	Tr	MLS	MLW	SAS	SAW	US
Obs	348	317	238	235	275	-	-	-	-	-	-
MODTR	319	309	224	215	257	392	348	223	299	174	286
MODTR*	329	317	234	225	267	397	355	232	307	182	296
Sw	360	290	221	209	256	385	344	216	298	154	304
Sw_{adj}	347	319	243	227	272	381	346	219	297	165	300
B & M	335	305	212	213	256	397	351	213	297	157	286

* surface visibility 5 km

The relation between observed irradiances and MODTRAN predictions is studied also with more extensive data. Czeplak (1994, Tabs. 3.4a and 3.5a, Chapter 3 in this report) summarizes observations from cloudless winter and summer cases at 15 European and North American stations, 7 of which were equipped with Schulze radiometers and 8 with Eppley pyrgeometers. These data cannot be directly compared to MODTRAN predictions, however, since sounding data are not available for the vast majority of cases. Instead, we compare average observations under real atmospheres (15 stations) to average MODTRAN predictions under selected standard atmospheres, and we use each one of the simple formulae to correct for irradiance differences caused by differences between the real and the standard atmospheres:

$$(\Phi_{observed} - \Phi_{MODTRAN}) = (\Phi_{observed} - \Phi_{formula}) - (\Phi_{MODTRAN} - \Phi_{formual})$$
$$\approx (\Phi_{observed} - \Phi_{formula}) - (\Phi^*_{MODTRAN} - \Phi^*_{formula}) = (\Phi_{observed} - \Phi^*_{MODTRAN}) - (\Phi_{formula} - \Phi^*_{formula}) \quad (4.3)$$

$\phi_{observed}$ is observed irradiance, $\phi_{MODTRAN}$ is the MODTRAN prediction, and $\phi_{formula}$ is the prediction from one single simple formula (ϕ and ϕ^* are irradiances under the real and the standard atmospheres, respectively). Under the assumption $(\phi_{MODTRAN} - \phi_{formula}) \approx (\phi^*_{MODTRAN} - \phi^*_{formula})$ we thus obtain, for each simple formula, one estimate of the unknown difference $(\phi_{observed} - \phi_{MODTRAN})$ in terms of the two known differences

($\phi_{observed}$ - $\phi_{formula}$) and ($\phi^*_{MODTRAN}$ - $\phi^*_{formula}$). Reading these estimated ($\phi_{observed}$ - $\phi_{MODTRAN}$) as vertical distances between individual points and the 1:1 line in Fig. 4.16, we see that average observations appear to be some 10-15 Wm^{-2} higher relative to MODTRAN predictions in summer than in winter (independently of radiometer type).

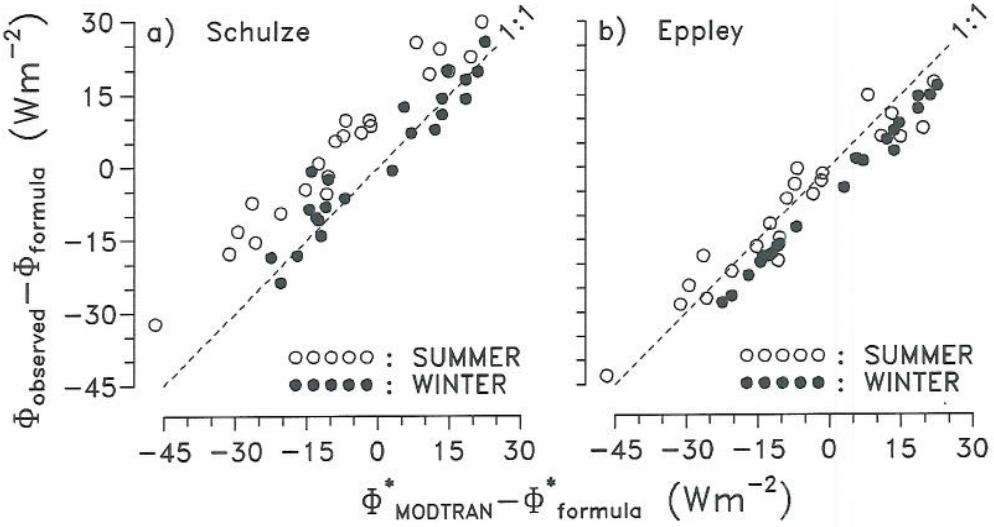

Fig. 4.16 Irradiance differences ($\phi_{observed}$ - $\phi_{formula}$) under real atmospheres plotted vs differences ($\phi^*_{MODTRAN}$ - $\phi^*_{formula}$) under standard atmospheres. $\phi_{observed}$ refers to Schulze radiometers and Eppley pyrgeometers under real winter and summer atmospheres. $\phi^*_{MODTRAN}$ refers to MODTRAN predictions averaged over the SAW and MLW atmospheres (winter) and over the four remaining standard atmospheres (summer). Each point refers to one single simple formula ($\phi_{formula}$).

The seasonal trend in Fig. 4.16, however, is not corroborated by the Schleswig data (Fig. 4.3), and may be an artifact arising from the assumption ($\phi_{MODTRAN}$ - $\phi_{formula}$) $\approx$ ($\phi^*_{MODTRAN}$ - $\phi^*_{formula}$). The accuracy of this approximation is affected differently in summer and winter, if the seasonal variation in boundary layer stratification differs between the real and the standard atmospheres. The potential effect of boundary layer temperature stratification may be exemplified with reference to the nomenclature of eqn (4.2): Given an inversion with T_s = 280K, ΔT_s = 8K and Δh = 0.1 - 0.3km, eqn (4.2) yields $\phi_{sw}(T_s,\Delta T_s,r_\Delta) \approx 1.13\ \phi_{sw}(T_s)$. While MODTRAN explicitly accounts for any boundary layer stratification, a simple formula which is adequate for "normally" stratified boundary layers, thus needs to be multiplied by 1.13 to account for this particular inversion case. Average nighttime (relative to daytime) and wintertime (relative to summertime) empirical correction factors of that order are in fact found at Braunschweig and Edmonton (Czeplak 1994, Table 3.6, Chapter 3 in this report). These examples are, however, extreme. The average (13 stations) night versus day empirical factor (1.05) is close to the factor 1.03-1.04 predicted by the Berdahl & Martin (1984) formula, and the average winter versus summer factor is 1.035. Finally, it should be noted that the above summer versus winter contrast is a small fraction of the corresponding solar irradiance difference, which in one way or the other is removed (with limited accuracy) from the recorded signal.

As a summer/winter average taken over the 22 simple models, the cloudless Schulze observations exceed MODTRAN predictions by only 8 Wm^{-2} (or less than half the average excess observed at Schleswig), while the cloudless Eppley observations are 1 Wm^{-2} lower than the MODTRAN predictions. Ignoring this moderate difference between radiometer types yields an overall average excess of 4 Wm^{-2} which is of the same order as the typical differences between MODTRAN and other profile-based models (Fig. 4.6a). It thus appears that average observed irradiances under cloudless skies are nicely corroborated by MODTRAN and other profile-based models.

Fig. 4.17 shows the same differences as Fig. 4.16, but averages are taken over summer/winter and over radiometer types. It is seen that the two temperature/humidity-dependent formulae (Berdahl & Fromberg, Frank & Püntener) which fit MODTRAN best over the entire climatic range of Figs 4.8-4.10, are also the formulae which are closest to the origin in Fig. 4.17. That is: On top of fitting MODTRAN best over an extremely wide range of "normally" stratified synthetic atmospheres, these two formulae are also closest to average observations as well as MODTRAN predictions at 15 European and North American stations. Also the two temperature-dependent formulae (Swinbank, Czeplak & Kasten) which fit MODTRAN well over a wide range of not too dry synthetic atmospheres (Fig. 4.7), are reasonably close to the origin in Fig. 4.17. Both empirical evidence as well as theoretical analysis thus strongly support these four formulae, and both rank the temperature/humidity-dependent formulae higher than the solely temperature-dependent formulae.

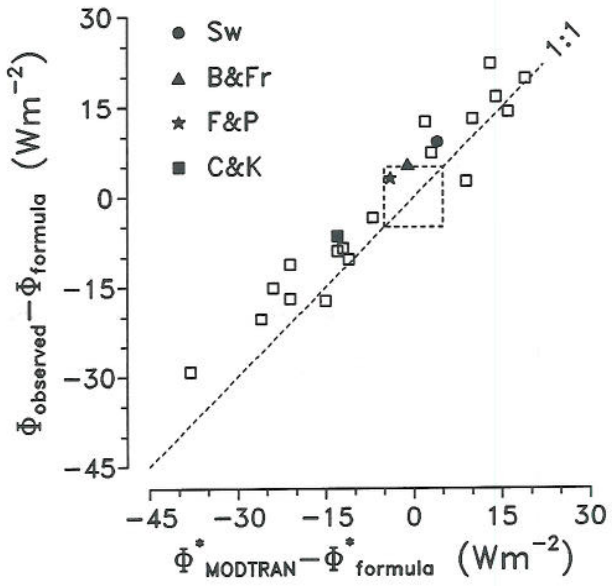

Fig. 4.17 Same as Fig. 4.16, but for differences averaged over summer/winter and over radiometer types. The square around origin indicates ±5 Wm^{-2} on both axes. The points corresponding to the formulae of Swinbank, Berdahl & Fromberg, Frank & Püntener, and Czeplak & Kasten are marked.

4.3.2 Cloudy sky

Clouds account for a major part of the variation in longwave atmospheric irradiance at the earth's surface. Air temperature normally decreases upwards and, compared to the cloudless atmosphere, clouds have a high emittance within the atmospheric spectral "window". Clouds therefore increase the atmospheric emittance ϵ beyond its cloudless value ϵ_0, sometimes even slightly beyond unity. The cloud formulae presented in Chapter 2 implicitly express this increase of emittance either as $(\epsilon - \epsilon_0)$, or as $(\epsilon - \epsilon_0)/\epsilon_0$ or as $(\epsilon - \epsilon_0)/(1 - \epsilon_0)$. Although any cloud formula is tuned to data in concert with a particular cloudless formula, the cloud formulae are compared to MODTRAN without reference to any cloudless formulae in this paper.

MODTRAN was run with unbroken cover of optically dense (black) clouds with bases at 0.66, 2.4, 5 and 10 km in each of the six standard atmospheres and in a modified SAW atmosphere. In the latter case, the relative humidity is preserved and the surface air temperature inversion is replaced by a gradient of -5K/km in order to separate the effect of low temperatures from the effect of the temperature gradient.

For the model of Ineichen et al. (1984), ϵ_0 was estimated by putting the beam solar irradiance $I_n = I_{n,max}$ in their eqn (4). Then the increase of the emittance under a cloudy sky was obtained from:

$$\epsilon - \epsilon_0 = \frac{\phi_*}{\sigma T^4}\left(1-\frac{I_n}{I_{n,\max}}\right) ; \; \phi_* = 58 \; Wm^{-2} \; for \; \frac{I_n}{I_{n,\max}} \geq 0.05 \; ,$$

$$\epsilon - \epsilon_0 = \frac{\phi_*}{\sigma T^4}\left(1-\frac{6I_n}{I_{n,\max}}\right) ; \; \phi_* = 78 \; Wm^{-2} \; for \; \frac{I_n}{I_{n,\max}} < 0.05 \; . \qquad (4.4)$$

Cole (1979) expressed the increase of emittance in terms of surface air temperature t_s (°C) and fractional cloud cover n:

$$\epsilon - \epsilon_0 = \frac{\phi_*}{\sigma T_s^4}\left(1+\frac{t_s}{t_*}\right) n \; ; \; \phi_* = 65 \; Wm^{-2} \; , \; t_* = 46.8°C \; . \qquad (4.5)$$

MODTRAN predicts that $(\epsilon - \epsilon_0)$ under unbroken black clouds decreases with increasing cloud base height (Fig. 4.18a). Since high clouds tend to be non-black, this trend is further strengthened in the real atmosphere. Mainly because the maximum increase ($\approx 1 - \epsilon_0$) declines with increasing temperature, $(\epsilon - \epsilon_0)$ decreases also with increasing temperature. By putting $I_n/I_{n,max} = 0$ in the Ineichen et al. formula (4.4), results reasonably close to MODTRAN predictions for low clouds are obtained. Moreover, $(\epsilon - \epsilon_0)$ decreases with increasing beam irradiance (increasing cloud altitude and decreasing cloud emittance) and becomes zero

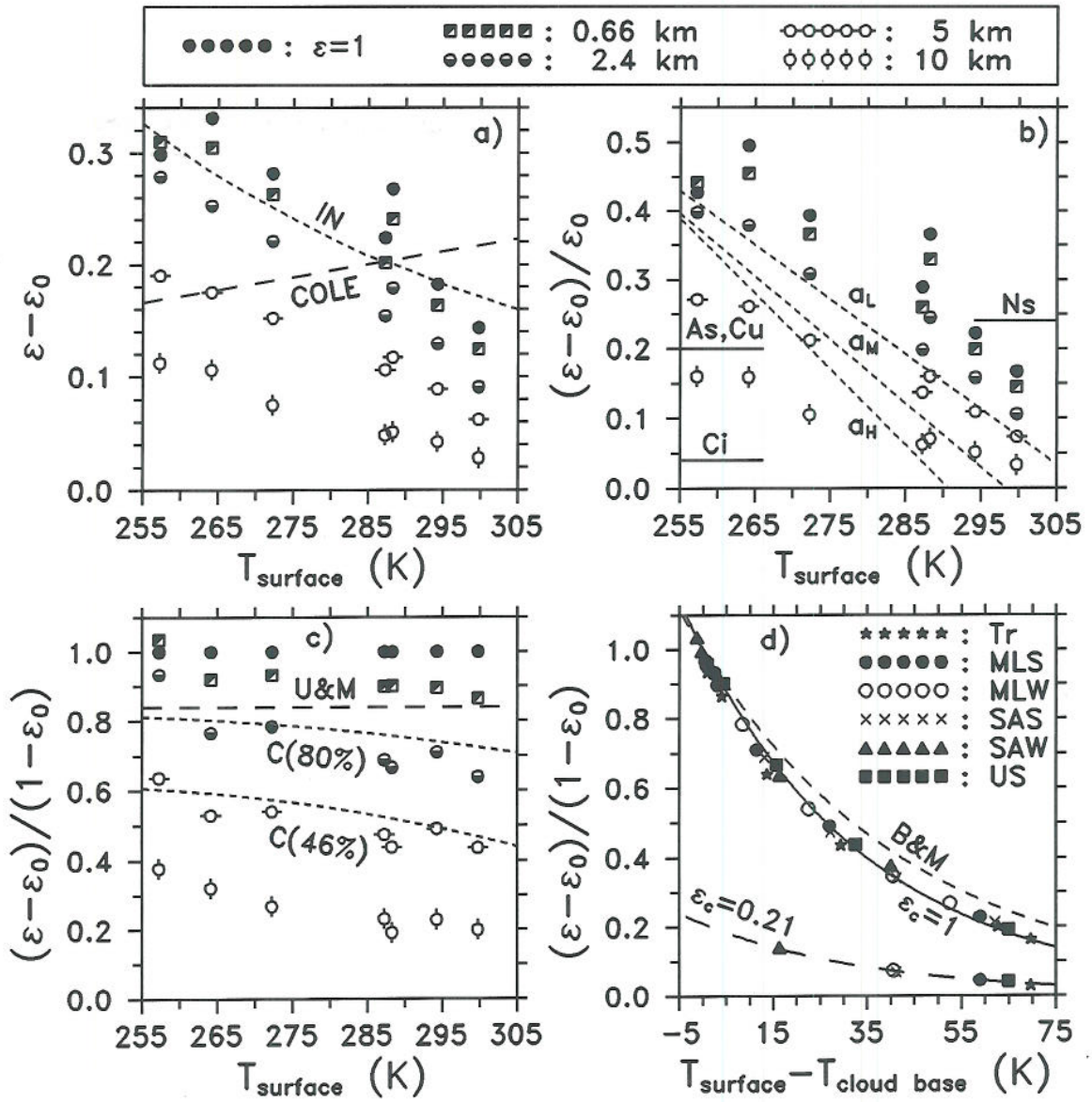

Fig. 4.18 Emittance differences of overcast and cloudless sky:
a-c) Symbols correspond to $\epsilon = 1$ and to MODTRAN predictions for black cloud bases at given heights (key at top) in 7 atmospheres (from left): SAW, modified SAW, MLW, US, SAS, MLS, and Tropical. The Ineichen (1984) formula , the Cole (1979) formula, the Bolz (1949) formula for different clouds (Ns, As, Cu, Ci), the Czeplak & Kasten (1987 and 1993) formula for low, medium high, and high clouds (a_L,a_M, a_H), the Unsworth & Monteith (1975) formula, and the Centeno (1982) formula for 46 and 80% relative humidity, are plotted as broken lines.
d) The MODTRAN predictions from a-c), together with MODTRAN predictions for some additional cloud levels and 6 cases with cloud flux emittance $\epsilon_c = 0.21$. The "host" atmospheres are specified by symbol key. Formula (4.10) is drawn for three pairs (ΔT_c, ϵ_c): (46K, 1; Martin & Berdahl 1984), (38K, 1), and (38K, 0.21).

for $I_n/I_{n,max} = 1$, in qualitatively the same way as indicated by the MODTRAN predictions. This formula thus appears to adequately reflect the physics of the overcast case. Cole's formula (4.5) is, however, independent of cloud base height, and it predicts an increase of (ϵ - ϵ_0) with increasing temperature. In fact, (ϵ - ϵ_0)

exceeds $(1 - \epsilon_0)$ beyond some 290K. We therefore recommend not to use formula (4.5) with other data, although it may fit the particular data which it was developed from.

Bolz (1949) expressed the increase of emittance in terms of cloud type and fractional cloud cover:

$$\frac{\epsilon - \epsilon_0}{\epsilon_0} = k\, n^2 \quad , \tag{4.6}$$

where k depends on cloud type only, as plotted in Fig. 4.18b.

Czeplak & Kasten (1987) and Czeplak (1993) generalized the Bolz formula by adjusting the cloud type factors and also allowing for clouds at different levels:

$$\begin{aligned} \frac{\epsilon - \epsilon_0}{\epsilon_0} = [1 &+ a_L\, n_L^{p_L} + a_M\,(1 - n_L)\, n_M^{p_M} \\ &+ a_H\,(1 - n_L)(1 - n_M)\, n_H^{p_H}\,] \quad , \end{aligned} \tag{4.7}$$

where the cloud type factors a_H, a_M, and a_L decrease with increasing temperature (Fig. 4.17b).

Since ϵ_0 increases with increasing surface air temperature, $(\epsilon - \epsilon_0)/\epsilon_0$ varies with temperature more than $(\epsilon - \epsilon_0)$ does (Fig. 4.18a-b). Allowing for non-black real cirrus clouds at 5 or 10 km altitude, the Bolz formula fits MODTRAN reasonably well at some 290K. Its lack of temperature dependency yields, however, too low (too high) emittance increase at lower (higher) temperatures. The Czeplak & Kasten formula yields the same cloud type and temperature dependency as MODTRAN does. However, even without the effect of non-black cirrus emittances, MODTRAN predicts a substantially greater difference between low and high clouds than the Czeplak & Kasten formula does. In particular, compared to MODTRAN, the Czeplak & Kasten formula underestimates the increase of emittance caused by low clouds at high temperatures while it overestimates the increase caused by high clouds at low temperatures.

Unsworth & Monteith (1975) expressed the increase of emittance in terms of fractional cloud cover:

$$\frac{\epsilon - \epsilon_0}{1 - \epsilon_0} = 0.84\, n \ . \tag{4.8}$$

This formula implies that any unbroken cloud cover compensates 84% of the cloudless radiation loss from a horizontal surface at air temperature. Similarly, Centeno (1982) expressed the emittance increase as a fraction of the difference between an average overcast emittance (ϵ_1) and the cloudless emittance (ϵ_0):

$$\frac{(\epsilon - \epsilon_0)}{(\epsilon_1 - \epsilon_0)} = n \ ,$$

$$\epsilon_1 = \left\{1 - \left[1 + \left(\frac{z_s}{z_*}\right)^{0.652}\right]\left(\frac{T_*}{T_s}\right)\left(\frac{RH_*}{RH_s}\right)^{1.5}\right\}^4 \ , \qquad (4.9)$$

where $z_* = 2.28$ km, $T_* = 3$K, and $RH_* = 100\%$.

MODTRAN indicates that $(\epsilon - \epsilon_0)/(1 - \epsilon_0)$ has not the pronounced temperature dependency of $(\epsilon - \epsilon_0)$ and $(\epsilon - \epsilon_0)/\epsilon_0$ (Figs 4.18a-c). Furthermore, the runs with the surface air temperature inversion removed from the SAW atmosphere indicate that most of the remaining weak temperature dependency derives from gradient differences rather than from temperature differences (Fig. 4.18c).

Except for the SAW atmosphere, the Unsworth & Monteith formula (4.8) yields an emittance increase reasonably well in accordance with MODTRAN predictions for black cloud bases at some 1 - 2 km altitude, which is probably a fairly adequate average for overcast cases. The temperature inversion in the SAW atmosphere causes low clouds to produce a slightly higher increase of emittance than that predicted by formula (4.8). Over the range of surface relative humidities encountered in the 6 MODTRAN atmospheres, the Centeno formula (4.9) is fairly consistent with MODTRAN predictions for black cloud bases at some 2 - 5 km altitude. The Centeno formula however, has a strong relative humidity dependency which yields overcast emittances below the cloudless ones for humidities below some 20%. This finding is markedly inconsistent with MODTRAN predictions and indicates that the Centeno formula does not adequately reflect the physics of the overcast case. Although it may fit the particular data from which it was developed, we recommend not to use formula (4.9) with other data.

Martin & Berdahl (1984) expressed the increase of emittance in terms of the fractional cloud cover n, the cloud emittance ϵ_c (10-12 μm), and the temperature difference $\Delta T_c = T_{surface} - T_{cloud\ base}$:

$$\frac{(\epsilon - \epsilon_0)}{(1 - \epsilon_0)} = n\ \epsilon_c \exp\left(-\frac{\Delta T_c}{\Delta T_0}\right) = n\ \epsilon_c \exp\left(\frac{\gamma z_c}{\Delta T_0}\right) , \qquad (4.10)$$

where $\Delta T_0 = 46$K, and $\Delta T_c = -\gamma z_c$ is given by the cloud base height z_c and the average subcloud temperature gradient γ (taken to be -5.6K/km by Martin & Berdahl). Moreover, Martin & Berdahl put ϵ_c equal to unity for low and medium high clouds, while cirrus emittance decreases with altitude according to an empirical linear relation.

Formula (4.10) convincingly fits the MODTRAN black cloud predictions over a wide range of surface air temperature and humidity, vertical temperature and humidity gradients, and cloud base height (Fig. 4.18d). Moreover, MODTRAN confirms that the emittance increase caused by non-black clouds is almost exactly proportional to ϵ_c (10-12 μm), as specified in (4.10). However, most probably because we used the more recent MODTRAN version, our runs fit formula (4.10) with $\Delta T_0 = 38$K rather than 46K as found by Martin & Berdahl who used an earlier LOWTRAN version.

Of the formulae discussed above, the Martin & Berdahl formula (4.10) is obviously the one which most explicitly reflects the physics of the overcast case. This means that phrasing the increase of emittance as $(\epsilon - \epsilon_0)/(1 - \epsilon_0)$ makes any input parameter irrelevant unless it implies information on ϵ_c and ΔT_c. The recommended strategy which ensures results with reasonable accuracy, is therefore to estimate ϵ_c and ΔT_c from cloud base height (from observations, climatology or empirical rules). Surface air temperature and humidity, which strongly affect ϵ_0, should be avoided as input parameters, since they imply site-specific information on ϵ_c and ΔT_c .

The above formulae imply that the increase of emittance, caused by a fractional cloud cover n, is proportional to n^α with α ranging from 1 to 3. MODTRAN cannot be used to test these α values since it has no option for partial cloudiness. From evidence presented by Czeplak & Kasten (1987) and others, it appears that α is in the range 2 - 3 rather than close to unity. However, since α is irrelevant for $n \approx 0$ and $n \approx 1$, which comprise the majority of all cases, the choice of α is not very critical.

4.4 CONCLUSIONS

Surface-based formulae for longwave atmospheric irradiance at the earth surface have often to be tuned to observations from a limited climatic range. In such cases, a profile-based model like MODTRAN may be used to evaluate formulae, or as a guide for designing formulae which may be used outside the climatic range they were developed for, with minimum probability of being greatly in error.

MODTRAN predictions nicely fit the average of 38 profile-based models, and the degree of consistency between such models is high. Indirect evidence, based on data from 15 European and North American stations, indicate that average observed irradiances and MODTRAN predictions agree within some 5 Wm^{-2} under cloudless sky with, if any, a slight tendency of observed irradiances exceeding MODTRAN predictions.

Both empirical evidence as well as theoretical analysis strongly suggest that four of the 23 simple formulae are particularly adequate in the case of "normally" stratified boundary layers: Over a wide range of temperatures, the Swinbank (1963) and Czeplak & Kasten (1987) formulae which express the emittance ϵ_0 as a quadratic function of dry bulb temperature, adequately reflect the radiation physics of cloudfree and not too dry atmospheres. Over a wide range of both tempertature and humidity, the Berdahl & Fromberg (1982) and Frank & Püntener (1986) formulae which express the emittance ϵ_0 as a linear function of dew point temperature, are even more adequate than the Swinbank and Czeplak & Kasten formulae.

Several empirical formulae apparently reflect frequent occurrence of temperature inversions at low temperatures. For "abnormally" stratified atmospheres, a correction to empirical formulae based on surface data is proposed. This correction requires summary information on the boundary layer temperature stratification.

Clouds increase the atmospheric emittance ϵ beyond its cloudless value ϵ_0, but at most slightly beyond unity. This increase of emittance is most adequately phrased as $(\epsilon - \epsilon_0)/(1 - \epsilon_0)$, i.e., as the fractional reduction of the longwave atmospheric radiation loss from a horizontal surface at ambient temperature (Martin & Berdahl, 1984). This fraction is governed by fractional cloud cover, cloud emittance, and the surface minus cloud base temperature difference. Given these parameters, MODTRAN runs indicate that temperature, humidity and cloud base height are irrelevant.

4.5 REFERENCES

Berdahl, P. and R. Fromberg, The thermal radiance of clear skies. Solar Energy **29**, 299-314 (1982).

Berdahl, P. and M. Martin, Emissivity of clear skies. Solar Energy **32**, 663-664 (1984).

Berk, A., L.S. Bernstein and D.C. Robertson, MODTRAN: A moderate resolution model for LOWTRAN7. GL-TR-89-0122. Geophysics Laboratory, Air Force Systems Command, Hanscom AFB, MA 0173 (1989).

Bolz, H.M., Die Abhängigkeit der infraroten Gegenstrahlung von der Bewölkung. Z. Meteor. **3**, 201-203 (1949).

Brunt, D., Notes on radiation in the atmosphere. Quart. J. Roy. Met. Soc. **58**, 389-418 (1932).

Brutsaert, W., On a derivable formula for long-wave radiation from clear skies. Water. Resour. Res. **11**, 742-744 (1975).

Budyko, M.I., Climate and life. International Geophysical Series 18. New York (1974).

Centeno, M., New formulae for the equivalent night sky emissivity. Solar Energy **28**, 489-498 (1982).

Clark, G. and C.P. Allen, The estimation of atmospheric radiation for clear and cloudy skies. Proc. Second Nat. Passive Solar Conf., Vol 2, p 676, Philadelphia (1978).

Cole, R.J., The longwave radiation incident upon inclined surfaces. Solar Energy **22**, 459-462 (1979).

Culf, A.D. and J.H.C. Gash, Longwave radiation from clear skies in Niger: A comparison of observations with simple formulas. J. Appl. Met. **32**, 539-547 (1993).

Czeplak, G. and F. Kasten, Parameterisierung der atmosphärischen Wärmestrahlung bei bewölktem Himmel. Met. Rundschau **6**, 184-187 (1987).

Czeplak, G., Personal communication (1993).

Czeplak, G., Comparison of parameterization formulae for atmospheric radiation. Draft Final Report IEA-SHCP, Subtask 17F. This report, Chapter 3 (1994).

Efimova, N.A., On methods of calculating monthly values of net-long-wave radiation. Meteorol. Gidrol. No. 10, 28-33 (1961).

Ellingson, R.G., J. Ellis and S. Fels, The intercomparison of radiation codes used in climate models: Long wave results. J. Geophys. Res. **96D5**, 8929-8953 (1991).

Feussner, in F. Möller: Einführung in die Meteorologie II, p. 53, Mannheim (1973).

Frank, T. and T.W. Püntener, Oberflächentemperaturen von besonnten Fensterglasscheiben und ihre Auswirkungen auf Raumklima und Komfort, NEFF-Projekt Nr. 266, (1986).

Houghton, H.G., Physical Meteorology, The MIT Press, Cambridge, London, 186 (1985).

Idso, S.B. and R.D. Jackson, Thermal radiation from the atmosphere. J. Geophys. Res. **74**, 5397-5403 (1969).

Idso, S.B., On the systematic nature of diurnal patterns of differences between calculations and measurements of clear sky atmospheric thermal radiation. Quart. J. Roy. Met. Soc. **107**, 737-741 (1981a).

Idso, S.B., A set of equations for full spectrum and 8 to 14 μm and 10.5 to 12.5 μm thermal radiation from cloudless skies. Water. Resour. Res. **17**, 295-304 (1981b).

Ineichen, P., J.M. Gremaud, O. Guisan and A. Mermoud, Infrared sky radiation in Geneva. Solar Energy, **32**, 537-545 (1984).

Kneizys, F.X., E.P. Shettle, L.W. Abreu, J.H. Chetwynd, G.P Anderson, W.O. Gallery, J.E.A. Selby and S.A. Clough, Users Guide to LOWTRAN7, AFGL-TR-88-0177, Air Force Geophysics Laboratory, Hanscom AFB, MA 01731 (1988).

Llebot, J.E. and J. Jorge, Some results of thermal atmospheric radiation measurements in Manresa (Spain). Solar Energy **32**, 473-477 (1984).

Martin, M. and P. Berdahl, Characteristics of infrared sky radiation in the United States. Solar Energy **33**, 321-336 (1984).

Paltridge, G.W. and C.M.R. Platt, Radiative Processes in Meteorology and Climatology. Elsevier Publishing Company, 318 pp (1976).

Schieldrup Paulsen, H., Some experiences with the calibration of radiation balance meters. Arch. Met. Geoph. Biokl., B, **15**, 156-174 (1967).

Staley, D.O. and G.M. Jurica, Effective atmospheric emissivity under clear skies. J. Appl. Met. **11**, 349-356 (1972).

Stamnes, K., S.C. Tsay, W. Wiscombe and K. Jayaweera, A numerically stable algorithm for discrete-ordinate-method radiative transfer in multiple scattering and emitting layered media, Appl. Optics, **27**, 2502-2509 (1988).

Swinbank, W.C., Long-wave radiation from clear skies. Quart. J. R. Met. Soc. **89**, 339-348 (1963).

Unsworth, M.H. and J.L. Monteith, Long-wave radiation at the ground - I. Angular distribution of incoming radiation. Quart. J. Roy. Met. Soc. **101**, 13-24 - II. Geometry of interception by slopes, solids, and obstructed planes. Quart. J. Roy. Met. Soc. **101**, 25-34 (1975).

Ångström, A., A study of the radiation of the atmosphere. Smithson. Inst. Misc. Coll., **65**(3), 1-159 (1915).

CHAPTER 5

A COMPARISON BETWEEN MODTRAN, SIMPLE SPECTRAL MODELS OF LONGWAVE RADIATION, AND SPECTRAL DATA FROM THE NEGEV DESERT

Arvid Skartveit and Jan Asle Olseth[1]

Geophysical Institute, University of Bergen,
Allégt. 70, N-5007 Bergen, NORWAY

Matthias Rommel

Fraunhofer-Institut für Solare Energiesysteme
Oltmannstrasse 5, D-79100 Freiburg, GERMANY

[1]Also at The Norwegian Meteorological Institute

5.1 INTRODUCTION

The spectral and angular distribution of atmospheric radiation affects radiative heating and cooling at the earth's surface. These distributions, governed by emission and absorption by a number of atmospheric constituents at all levels, can be modelled if extensive input data and a sophisticated model like MODTRAN (Kneizys et al 1988, Berk et al 1989) are available. Alternatively, the spectral distribution may be derived from more "user-friendly" models requiring only surface temperature and humidity as input.

The present paper compares spectral radiance data from the Negev desert with all wavelength irradiance data, and with predictions modelled by MODTRAN and by the simple models of Berger (1988) and Das & Iqbal (1987).

5.2 SITE DESCRIPTION AND DATA

5.2.1 Site description

Radiation data are available at three sites in the Negev desert in Israel (Fig. 5.1). Sede Boqer (30.8°N, 34.8°E, 500 m above m.s.l.) is a small village and university campus within a sandy desert area. Yotvata (29.8°N, 35.0°E, 50 m above m.s.l.) is a village situated within plantations in the Jordan valley, 40 km north of the Red Sea, while Newe Zohar (31.2°N, 35.3°E, 350 m below m.s.l.) lies directly at the southern shore of the Death Sea. The nearest radiosounding station is Bet Dagan (32.0°N, 34.5°E, 0-100 m above m.s.l.), 9 km from the Mediterranean coast.

5.2.2 The spectrometer data

The PC-controlled IR-spectrometer was developed and built at the Fraunhofer Institute for Solar Energy Systems (Brunold, 1989). As IR-detector a Golay-cell with chopper (7 Hz) was used. The wavelength-selective element was a stepper-motor-controlled filter-wheel with an edge-filter. The wavelength range extended from 4.25 to 15.86 μm, and the spectral resolution decreased slightly with increasing wavelength, ranging from 0.06 μm (at 4.25 μm) to 0.16 μm (at 15.86 μm). The wavelength uncertainty of the spectrometer is lower than 1.5%. Before the measurement of each spectrum, the spectrometer was automatically calibrated against a spectrally grey reference-IR-emitter

Fig. 5.1 Geographical map showing several sites in Israel.

of known emittance and temperature. The rectangular field of view of the spectrometer was 7° by 20° and was directed to the zenith. When a spectrum was taken the intensities were measured at 257 wavelengths and 4 times at each wavelength-stop. It takes approximately 10 minutes to measure one spectrum, and 43 spectrometer runs under cloudless sky after sunset, together with simultaneous pyrgeometer readings, are available from the three stations in the Negev desert.

5.2.3 Radiosoundings

Only surface temperatures are available from Sede Boqer, Yotvata and Newe Zohar, while Bet Dagan is the nearest radiosounding station. Contrary to the two other stations, there are no mountains between Bet Dagan and Sede Boqer. Therefore, Sede Boqer is regarded as the station being most comparable to Bet Dagan, and the comparability is supposedly best when both stations have cloudless sky. Among the available Bet Dagan soundings, gratefully received from A. Manes of the Israel Meteorological Service, we therefore selected those 8 cases with one octa or less cloud amount at Bet Dagan which deviated by less than one hour from a spectrometer run (under cloudless sky) at Sede Boqer.

It is, however, still difficult to obtain vertical temperature profiles over Sede Boqer (500 m above m.s.l. and 75 km from the coastline) from radiosoundings over Bet Dagan, being 125 km away (0-100 m above m.s.l. and 9 km from the coastline). Due to variable vertical subsidence, horizontal advection, and diabatic heating, depending upon e.g. atmospheric static stability, large scale wind speed/direction, and time of the year, the difference between the Bet Dagan and Sede Boqer vertical profiles certainly varies from day to day, even under cloudless sky. Given these problems, MODTRAN was run with the observed Bet Dagan profiles for reference. To yield an estimate of the corresponding temperature profiles over Sede Boqer, the following very simple adjustment to the Bet Dagan dew point and dry bulb temperature soundings were applied: The vertical extent of the dry bulb temperature inversion layer was found from the sounding at Bet Dagan. An equally thick surface inversion layer was assumed to exist at Sede Boqer, within which the temperatures were assumed to vary linearly between the observed surface (Sede Boqer) temperatures at the bottom level and the top level temperatures taken from the same altitude above sea level in the Bet Dagan sounding. The latter adoption of unmodified Bet Dagan temperatures was applied to all levels above the inversion top.

5.3 RESULTS

5.3.1 All-wave irradiances

Hemispherical all-wave irradiances were obtained from the 43 spectrometer runs under the following assumptions:

(1) Black body radiation at ambient air temperature outside the spectrometer's range (4.25 - 15.86 μm). MODTRAN runs (Kneizys et al 1988) indicate that, under cloudless sky at these altitudes, this assumption yields less than 1% too high hemispherical all-wave irradiances.

(2) Hemispherical all-wave irradiances ϕ are obtained by angular integration (Olseth & Skartveit, 1994, Chapter 4) of MODTRAN radiances, and related to zenith radiances $L_{\theta=0^\circ}$ as follows:

$$\phi = 1.064\ \pi\ L_{\theta=0^\circ}\ , \tag{5.1}$$

Here 1.064 is the average for the 8 selected cloudless cases at Sede Boqer. Actually, MODTRAN runs for the 8 estimated soundings at Sede Boqer, and for the 8 corresponding observed soundings at Bet Dagan, yielded 16 individual factors in the range 1.055 - 1.066. Fig. 5.2 shows modelled examples of the angular distribution of spectral radiance.

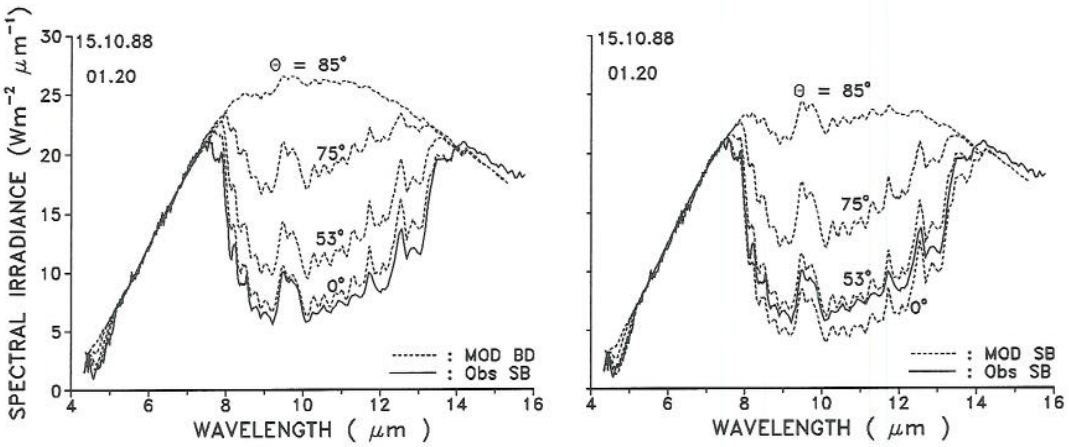

Fig. 5.2 Radiances (multiplied by π) at four zenith angles (θ), modelled by MODTRAN from one observed sounding at Bet Dagan (left) and from the estimated Sede Boqer profile (right). The corresponding observed zenith radiances at Sede Boqer are inserted for comparison, with the observed wavelengths increased by an amount corresponding to 8 cm^{-1}.

These spectrometer irradiances are compared to irradiances estimated from Sede Boqer profiles by MODTRAN, and from surface data by the Berdahl & Martin (1984) and Swinbank (1963) formulae (Fig. 5.3a-c), and also to the simultaneous pyrgeometer readings (Fig. 5.3d). It is noteworthy that less scatter is seen between pyrgeometer and spectrometer irradiances (Fig. 5.3d) than between spectrometer and modelled irradiances (Fig. 5.3a-c). This fact indicates that much of the scatter between observed and modelled irradiances (Fig. 5.3a-c) is due to real irradiance variations, being not picked up by the models, and is not due to e.g. random measurement errors.

The average spectrometer irradiance exceeds the average modelled irradiance by 14 - 16 Wm^{-2}. This observed excess is intermediate between the 18 Wm^{-2} average excess (Schulze radiometer minus MODTRAN) observed at Schleswig and the 4 Wm^{-2} average excess inferred from observations at 15 European and North American stations (Olseth & Skartveit 1994, Table 4.4 and Fig. 4.16, Chapter 4 in this report). This finding indicates that the spectrometer yields all-wave irradiances reasonably close to the readings of all-wave radiometers in question. It is, however, contradicted by the 18 Wm^{-2} average pyrgeometer vs. spectrometer deficit seen in Fig. 5.3d. The particular pyrgeometer applied in Israel was recalibrated by Deutscher Wetterdienst, Meteorologisches Observatorium Hamburg (Klaus Dehne, pers. comm.) in autumn 1993, and a responsivity 4.83 μV/Wm^{-2} (old : 4.61 μV/Wm^{-2}) was found. The new responsivity would reduce the above pyrgeometer vs. spectrometer deficit from 18 to 14 Wm^{-2}. Unfortunately, however, the thermopile signal was directly read during this recalibration, while the recorded signal in the field includes the voltage from the battery powered

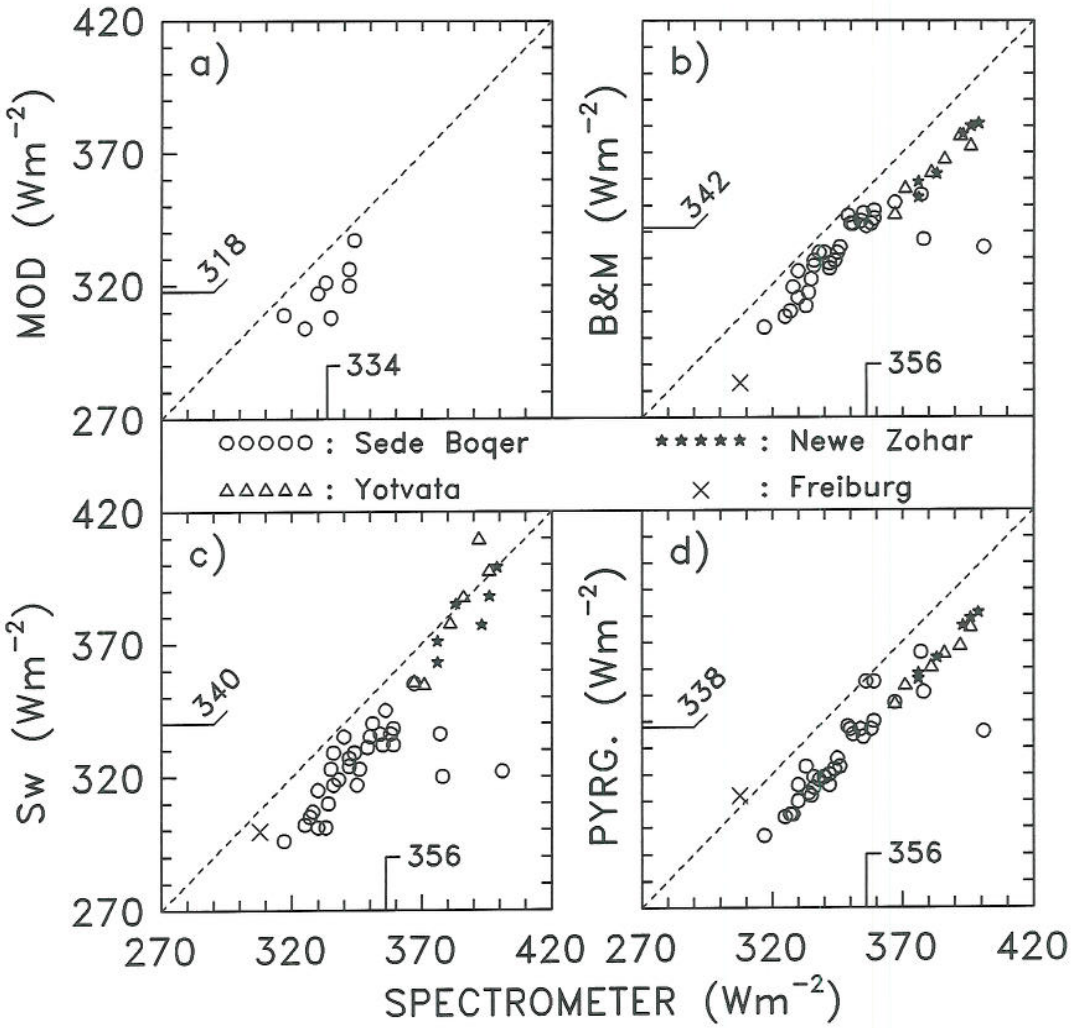

Fig. 5.3 Abscissa: All-wave hemispherical irradiances derived from spectral zenith radiances observed at Sede Boqer, Newe Zohar, Yotvata, and Freiburg.
Ordinate: Corresponding irradiances predicted by MODTRAN (a), the Berdahl & Martin formula (b), the Swinbank formula (c), and observed by pyrgeometer (d). The only outlier in Fig. 5.3d ("unknown problems" noted in the observation log) and the Freiburg case are omitted in the calculated averages given on the axes.

circuit which removes the substantial portion of the signal due to emission from the sensor surface. The recalibration is therefore hardly conclusive in our case, and we are left with the fact that one parallel run at Freiburg, Germany (Brunold 1989) of another pyrgeometer and the spectrometer did not show a deficit (Fig. 5.3d).

At Sede Boqer, the average surface air temperature drops from 18.4°C in the 4 evening cases to 14.4°C in the 4 midnight cases. This temperature drop causes the spectrometer and pyrgeometer irradiances to drop, on the average, by 4.3 and 2.4%, respectively, in reasonable agreement with the

corresponding 3.0% average drop of MODTRAN irradiance. The average Swinbank irradiance however, drops by as much as 7.8% since this formula neglects the fact that the evening to midnight temperature drop applies only to a shallow boundary layer, while the earth's surface receives irradiance from higher atmospheric layers which are less affected by surface cooling.

It is regarded as coincidental that the ratio 1.053 of average spectrometer and pyrgeometer irradiances is close to the factor 1.064 by which we multiply the spectrometer zenith radiances to obtain hemispherical irradiances in eqn (5.1).

5.3.2 Spectral zenith radiances

MODTRAN calculates molecular absorption in 1 cm^{-1} spectral bins. It turned out that scanning these MODTRAN spectra (Fig. 5.4a) with a triangular slit function of fixed half-width 0.06 μm yielded spectra with a similar resolution as that of the spectrometer (Fig. 5.4b). Moreover, a spectral shift between MODTRAN spectra and observed spectra (Fig. 5.4b), within the accuracy of the spectrometer wavelength determination, is removed (Fig. 5.5) by increasing the observed wavelengths by an amount corresponding to 8 cm^{-1} (0.02 μm at 5 μm and 0.2 μm at 16 μm). After this adjustment, the observed spectra (Fig. 5.5) show detailed spectral conformity with MODTRAN spectra, and they fall approximately between the spectra derived by MODTRAN from the observed Bet Dagan profiles and from the estimated Sede Boqer profiles, respectively.

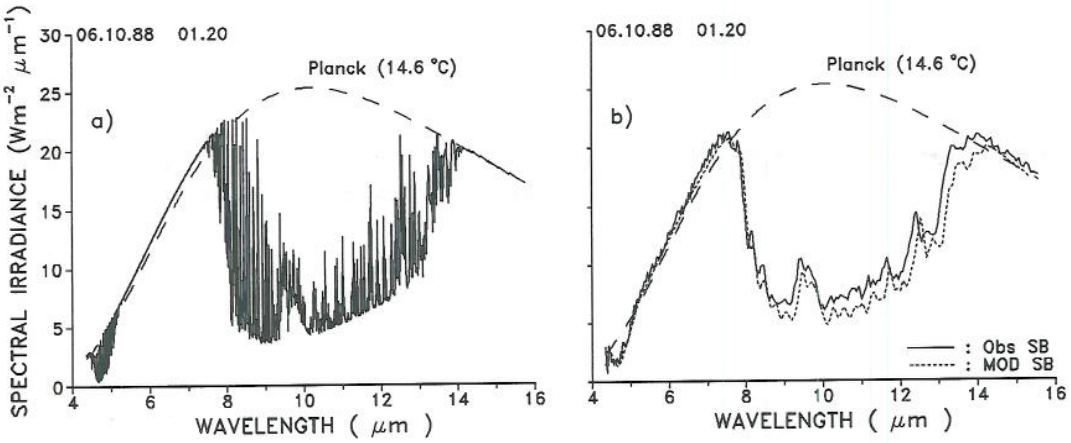

Fig. 5.4 Sede Boqer data at midnight, 6th October 1988:
a) Planck irradiance at air temperature and zenith MODTRAN radiances (multiplied by π) in 1 cm^{-1} bins.
b) The observed spectrum, and the MODTRAN spectrum scanned with a triangular slit function of fixed half-width 0.06 μm.

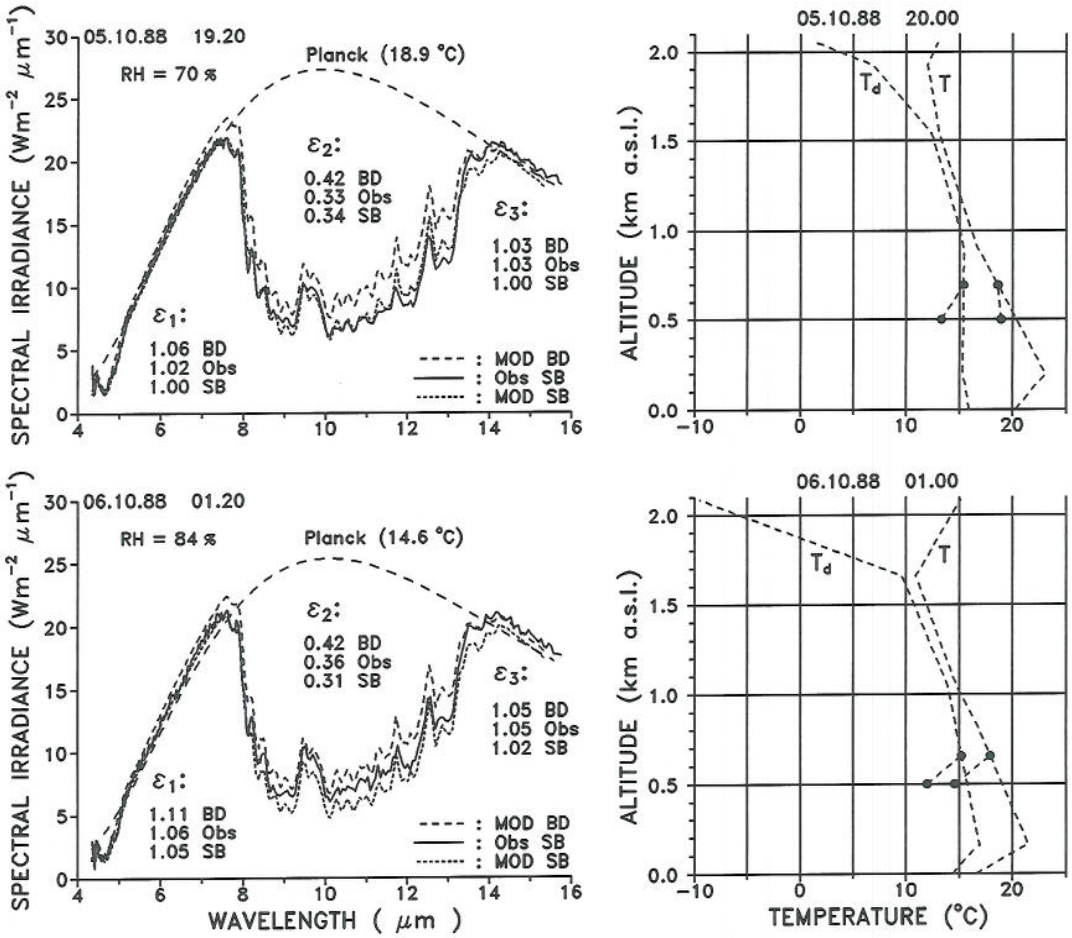

Fig. 5.5a) Left: Zenith spectral radiance (multiplied by π) observed at Sede Boqer (Obs), and modelled by MODTRAN from soundings observed at Bet Dagan (MOD BD) and estimated at Sede Boqer (MOD SB). Corresponding emittances are given within three spectral bands (ϵ_1, ϵ_2, ϵ_3 ; see text). Relative humidity (RH) and Planck irradiance at surface air temperature are given for Sede Boqer. Data for the evening (upper figures) and night (lower figures) between October 5th and 6th 1988. Note that the observed wavelengths are increased by an amount corresponding to 8 cm^{-1}.
Right: Temperature (T) and dew point (T_d) profiles in the lowest 2 km above m.s.l. at Bet Dagan (observed) and Sede Boqer (● - - - - ● estimated, see Chapter 5.2.2).

Within the opaque bands, 5.5-7.5 μm and 14.5-15.5 μm, the atmospheric zenith emittances ϵ_1 and ϵ_3, respectively, are significantly affected by the boundary layer temperature stratification. In particular, a temperature inversion may produce zenith radiances in excess of the black body radiance at surface air temperature, i.e. the zenith emittances exceed unity.

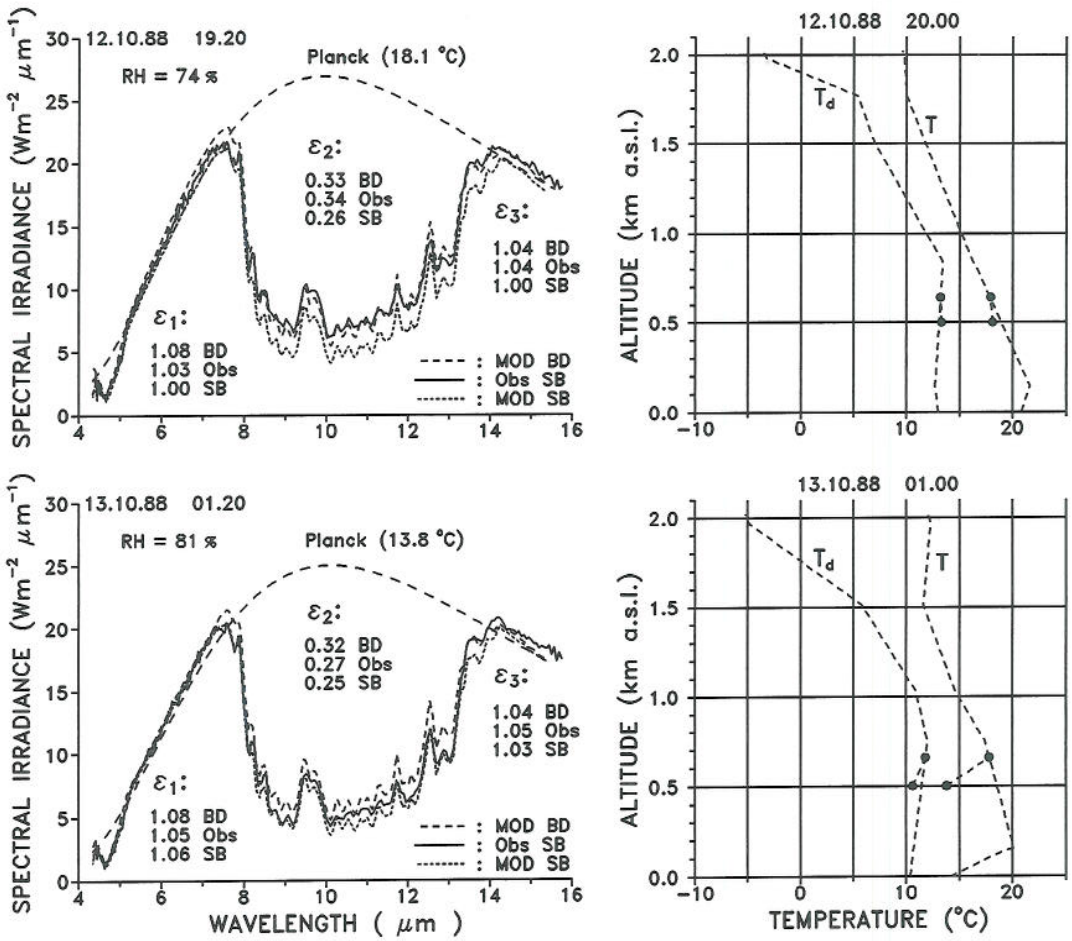

Fig. 5.5b) Same as Fig. 5.5a, but in the evening and night between October 12th and 13th 1988.

The observed inversion strength (temperature difference between inversion top and surface) at Bet Dagan ranges from 0.2 to 2.8K in the evening and from 4.9 to 6.7K at midnight. The estimated inversion strength at Sede Boqer, which ranges from -0.6 to 0.6K in the evening and from 2.6 to 5.3K at midnight, is slightly weaker than that observed at Bet Dagan. However, since the dry desert surface favours the formation of surface inversions, the inversions at Sede Boqer are probably stronger than those at Bet Dagan. The discrepancy between estimates and expectations indicates that our Sede Boqer temperature profiles may be slightly too low aloft. This assumption is corroborated by the fact that the observed opaque band emittances slightly exceed those modelled from Sede Boqer profiles.

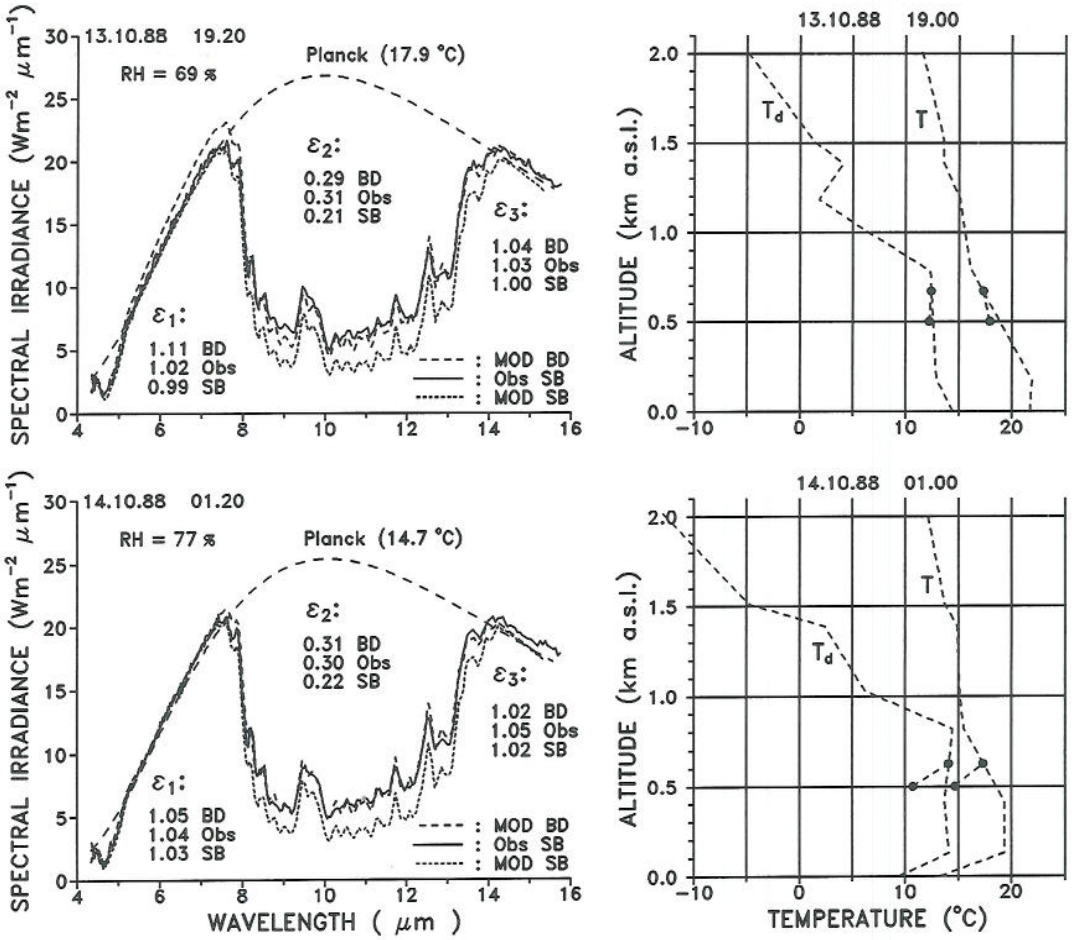

Fig. 5.5c) Same as Fig. 5.5a, but in the evening and night between October 13th and 14th 1988.

Since the average estimated inversion strength at Sede Boqer increases from -0.1K in the evening to 3.8K at midnight, the average, from Sede Boqer profiles modelled opaque band emittance increases from 1.00 in the evening to 1.04 at midnight. This modelled increase reasonably well fits, but slightly exceeds the average observed emittance increase (from 1.03 in the evening to 1.05 at midnight). The window emittances ϵ_2 (8.5 - 13 μm), depending more heavily on deeper atmospheric layers than the opaque band emittances, are more variable. The average observed window emittance is 0.32 and exceeds the average 0.27 yielded by MODTRAN from the estimated Sede Boqer profiles (Fig. 5.5).

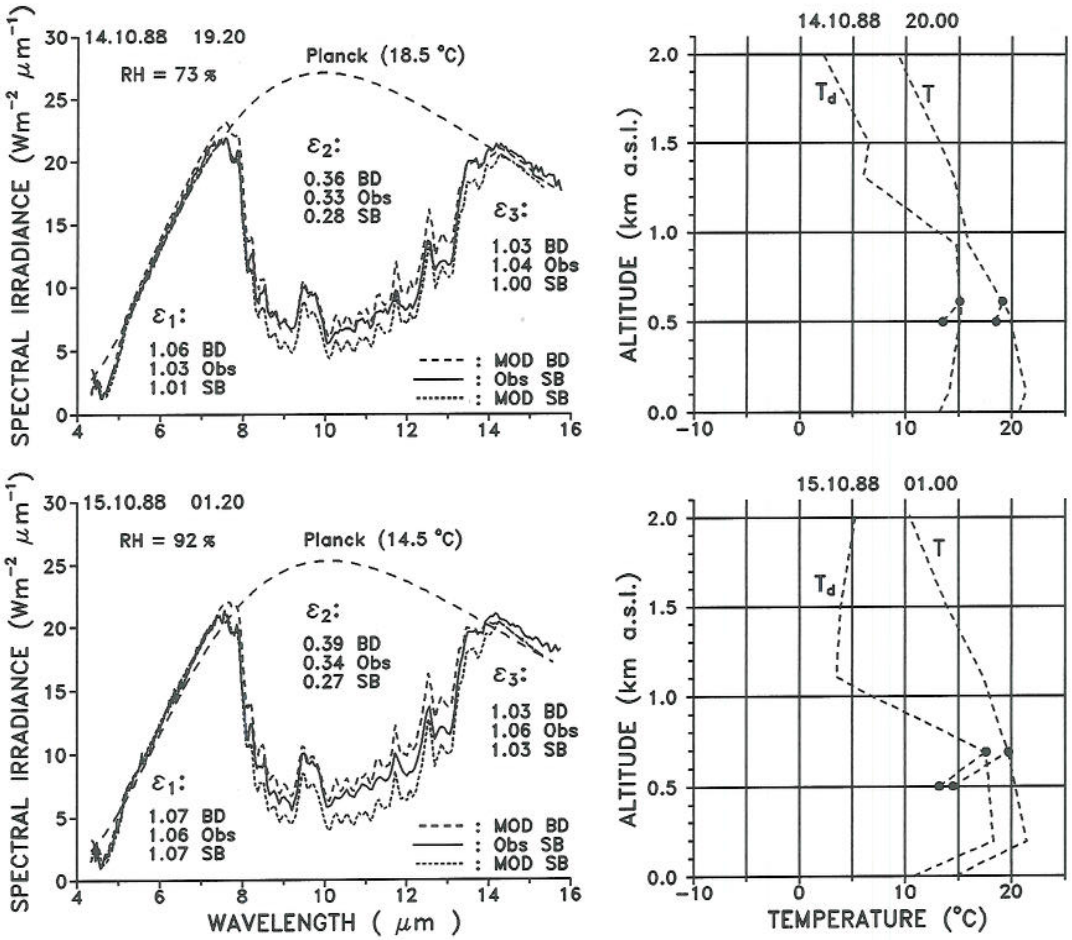

Fig. 5.5d) Same as Fig. 5.5a, but in the evening and night between October 14th and 15th 1988.

It thus appears that the 5% spectrometer vs. MODTRAN excess seen in Fig. 5.3a originates from the entire spectrum, with the major part originating from the atmospheric window band.

5.3.3 Spectral irradiances

The spectrometer data were also compared to the spectral irradiance models of Das & Iqbal (1987) and Berger (1988), both based on surface data. The Das & Iqbal model is based on the rigourous model of Ramsey et al (1982), while the Berger model is based on an earlier version of MODTRAN, namely LOWTRAN6. Since eqn (5.1) is restricted to the all-wave case, spectral hemispherical irradiances were obtained from the observed spectral zenith radiances $L_{\lambda,\theta=0°}$ as follows:

$$\phi_\lambda = \pi\, L_{\lambda,\theta=53°} = \pi\, \frac{L_{\lambda,\theta=53°}}{L_{\lambda,\theta=0°}}\, L_{\lambda,\theta=0°}\,, \tag{5.2}$$

where the ratio $L_{\lambda,\theta=53°} / L_{\lambda,\theta=0°}$ is obtained from MODTRAN runs applied to the respective Sede Boqer temperature profiles (Fig. 5.6).

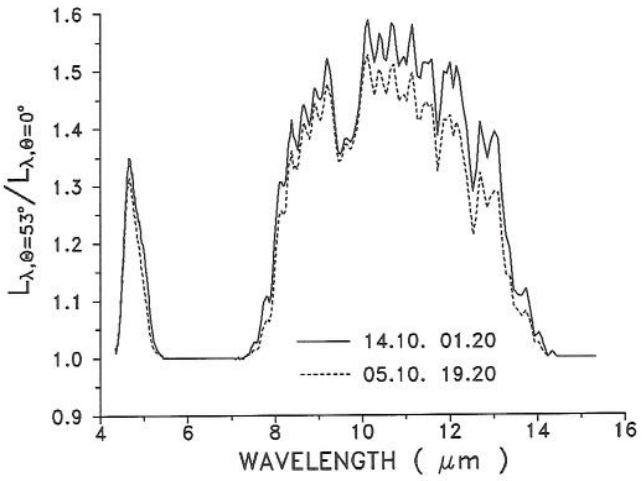

Fig. 5.6 Ratios $L_{\lambda,\theta=53°} / L_{\lambda,\theta=0°}$ of spectral radiances at zenith angles 53° and 0°. The ratios are modelled from estimated temperature profiles at Sede Boqer, and only the extreme ratios among the 8 cases in Fig. 5.5 are shown.

Fig. 5.7 shows that, except for a small observed excess and a coarser spectral resolution, the Berger model nicely fits the observed spectrum, while the Das & Iqbal model, within parts of the atmospheric window, yields spectral irradiances which are less than half of the observed ones.

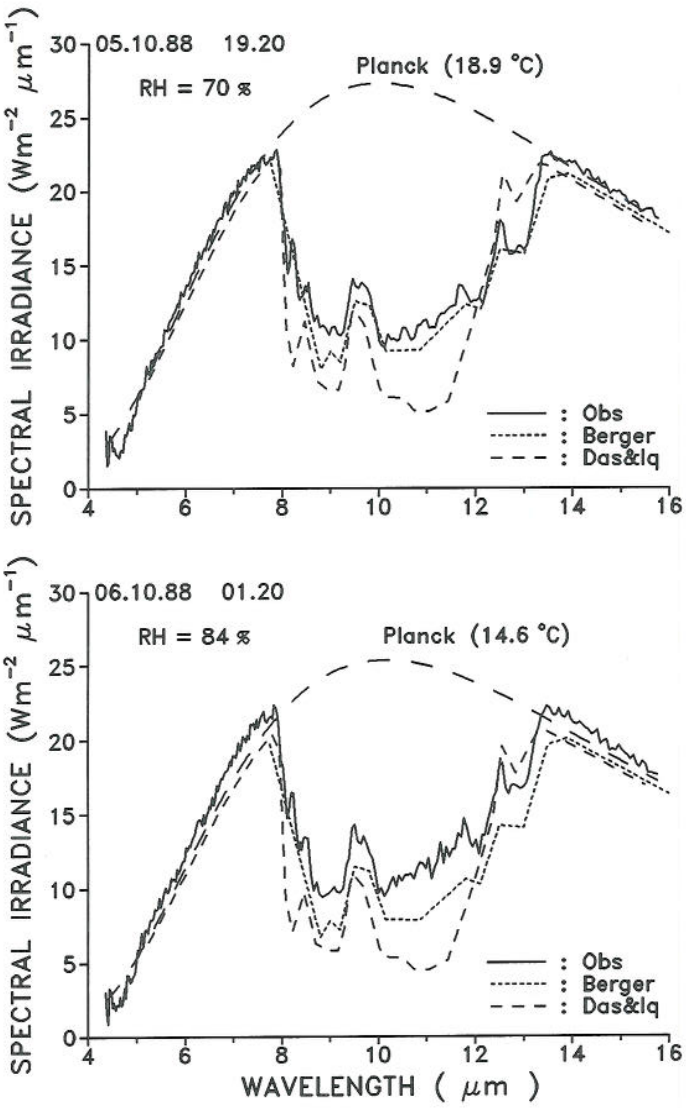

Fig. 5.7a) Spectral irradiances derived from observed zenith radiances (Obs), together with irradiances predicted by the models of Berger (1988) and Das & Iqbal (1987). Relative humidity (RH) and Planck irradiance at air temperature are given. Observations from Sede Boqer in the evening (upper figure) and night (lower figure) between October 5th and 6th 1988.

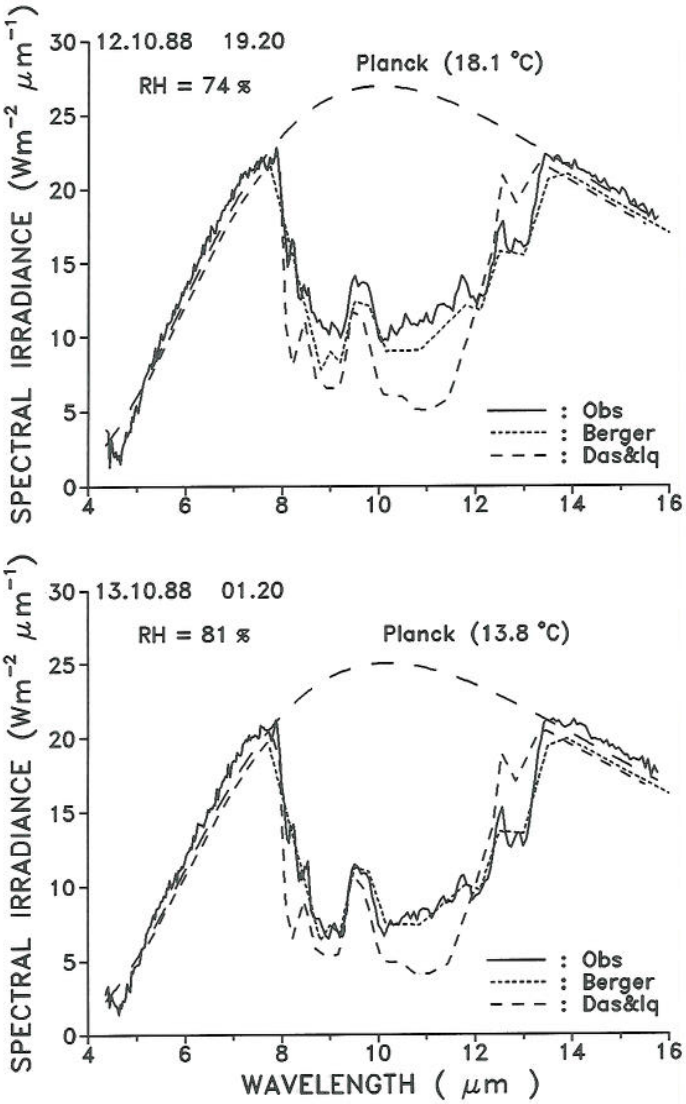

Fig. 5.7b) Same as Fig. 5.7a, but in the evening and night between October 12th and 13th 1988.

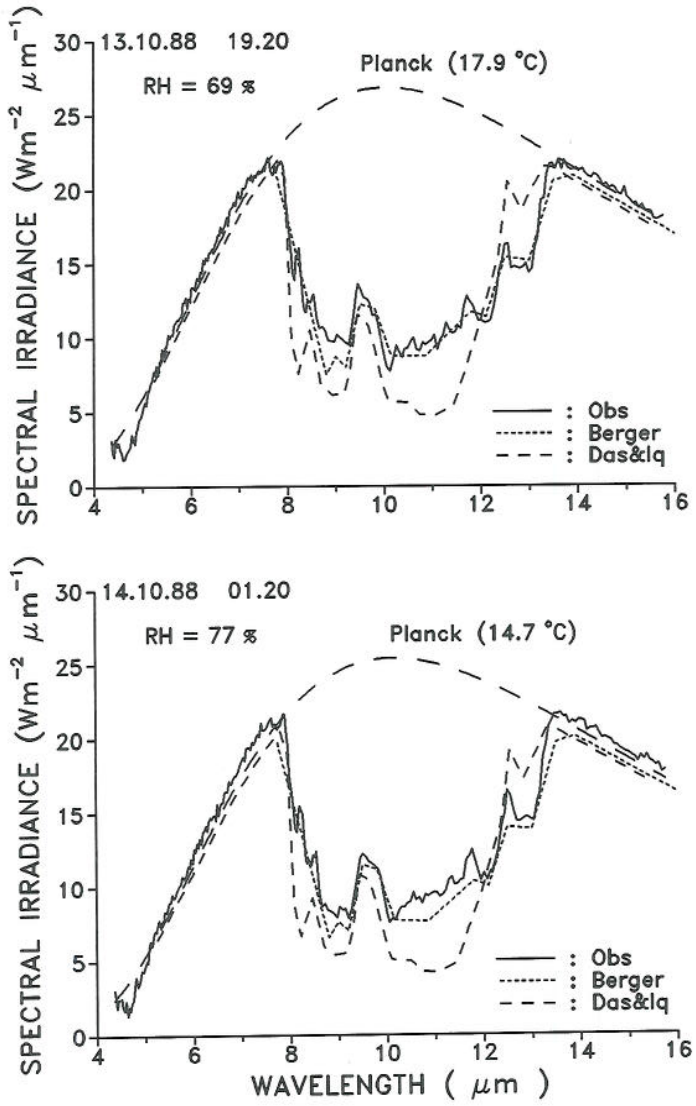

Fig. 5.7c) Same as Fig. 5.7a, but in the evening and night between October 13th and 14th 1988.

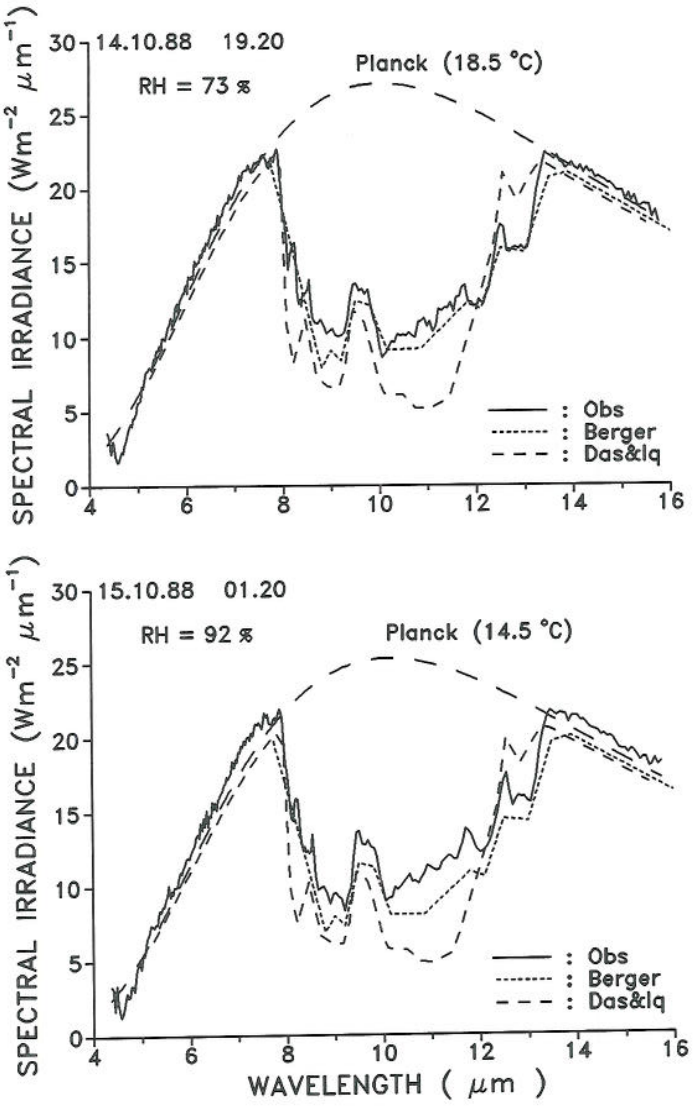

Fig. 5.7d) Same as Fig. 5.7a, but in the evening and night between October 14th and 15th 1988.

5.4 CONCLUSIONS

Hemispherical all-wave irradiances obtained from spectral zenith radiances are some 15 Wm^{-2} higher than those computed from temperature soundings by MODTRAN. The excess is in qualitative agreement with the corresponding excess obtained from the readings of all-wave radiometers (Olseth and Skartveit, 1994, Chapter 4.3.1 in this report). This finding is, however, not consistent with the fact that the particular pyrgeometer applied in Isreal yielded irradiances some 5% below those inferred

from the spectrometer. The inconsistency may be due to moderate calibration or sampling errors of this particular pyrgeometer.

The observed spectral variation of zenith radiance agrees quite well with that modelled from temperature soundings by MODTRAN. Slight variations of opaque band emittances are in accordance with modelled (MODTRAN) effects of variations in boundary layer temperature gradients. The observed window emittances slightly exceed the MODTRAN emittances; the excess may explain a major fraction of the all-wave excess reported above.

Spectral irradiances derived from observed spectral zenith radiances conform with the model of Berger (1988), while the model of Das & Iqbal (1987), within parts of the atmospheric window, yields spectral irradiances which are less than half of the observed ones.

5.5 REFERENCES

Berdahl, P. and M. Martin, Emissivity of clear skies. Solar Energy **29**, 663-664 (1984).

Berger, X., A simple model for computing the spectral radiance of clear skies. Solar Energy **40**, 321-333 (1988).

Berk, A., L.S. Bernstein and D.C. Robertson, MODTRAN: A moderate resolution model for LOWTRAN7. GL-TR-89-0122. Geophysics Laboratory, Air Force Systems Command, Hanscom AFB, MA 0173 (1989).

Brunold, S., Untersuchung zum Potential der Strahlungskühlung in ariden Klimazonen. Diplomarbeit, Fraunhofer Institut für Solare Energiesysteme, D-79106 Freiburg, Germany (1989).

Das, A.K. and M. Iqbal, A simplified technique to compute spectral atmospheric radiation. Solar Energy **39**, 143-155 (1987).

Kneizys, F.X., E.P. Shettle, L.W. Abreu, J.H. Chetwynd, G.P Anderson, W.O. Gallery, J.E.A. Selby and S.A. Clough, Users Guide to LOWTRAN7, AFGL-TR-88-0177, Air Force Geophysics Laboratory, Hanscom AFB, MA 01731 (1988).

Olseth, J.A. and A. Skartveit, A comparison between longwave atmospheric irradiance formulae and MODTRAN over a wide range of climates. Draft Final Report IEA-SHCP, Subtask 17F. This Report, Chapter 4 (1994).

Ramsey, J.W., H.D. Chiang and R.J. Goldstein, A study of incoming longwave radiation from a clear sky. J. Appl. Meteor. **21**, 566-578 (1982).

Swinbank, W.C., Long-wave radiation from clear skies. Quart. J. R. Met. Soc. **89**, 339-348 (1963).